NASA TECHNICAL MEMORANDUM

NASA TM X-3160

NASA TM X-3160

EXPERIMENTAL AND THEORETICAL LOW-SPEED AERODYNAMIC CHARACTERISTICS OF THE NACA 65_1-213, a = 0.50, AIRFOIL

William D. Beasley and Robert J. McGhee

Langley Research Center
Hampton, Va. 23665

NATIONAL AERONAUTICS AND SPACE ADMINISTRATION • WASHINGTON, D. C. • FEBRUARY 1975

1. Report No.	2. Government Accession No.	3. Recipient's Catalog No.
NASA TM X-3160		

4. Title and Subtitle	5. Report Date
EXPERIMENTAL AND THEORETICAL LOW-SPEED AERODYNAMIC CHARACTERISTICS OF THE NACA 65_1-213, a = 0.50, AIRFOIL	February 1975
	6. Performing Organization Code

7. Author(s)	8. Performing Organization Report No.
William D. Beasley and Robert J. McGhee	L-9773
	10. Work Unit No.
	505-06-31-01
9. Performing Organization Name and Address	11. Contract or Grant No.
NASA Langley Research Center Hampton, Va. 23665	
	13. Type of Report and Period Covered
12. Sponsoring Agency Name and Address	Technical Memorandum
National Aeronautics and Space Administration Washington, D.C. 20546	14. Sponsoring Agency Code

15. Supplementary Notes

16. Abstract

Low-speed wind-tunnel tests have been conducted to determine the two-dimensional aerodynamic characteristics of the NACA 65_1-213, a = 0.50, airfoil. The results were compared with data from another low-speed wind tunnel and also with theoretical predictions obtained by using a viscous subsonic method. The tests were conducted over a Mach number range from 0.10 to 0.36. Reynolds numbers based on the airfoil chord varied from about 3.0×10^6 to 23.0×10^6.

17. Key Words (Suggested by Author(s))	18. Distribution Statement
Low-speed airfoil data Reynolds number effects Experimental-theoretical comparison	Unclassified – Unlimited STAR Category 01

19. Security Classif. (of this report)	20. Security Classif. (of this page)	21. No. of Pages	22. Price*
Unclassified	Unclassified	74	$4.25

*For sale by the National Technical Information Service, Springfield, Virginia 22151

EXPERIMENTAL AND THEORETICAL LOW-SPEED AERODYNAMIC CHARACTERISTICS OF THE NACA 65_1-213, a = 0.50, AIRFOIL

By William D. Beasley and Robert J. McGhee
Langley Research Center

SUMMARY

An investigation was conducted in the Langley low-turbulence pressure tunnel to determine the low-speed two-dimensional aerodynamic characteristics of the NACA 65_1-213, a = 0.50, airfoil. The results are compared with data from another low-speed wind tunnel and also with theoretical predictions obtained by using a subsonic viscous method. The tests were conducted over a Mach number range from 0.10 to 0.36 and an angle-of-attack range from -10° to 20°. Reynolds numbers, based on the airfoil chord, were varied from about 3.0×10^6 to 23.0×10^6.

The results of the investigation showed that the maximum section lift coefficient at a constant Mach number of 0.22 increased rapidly as Reynolds number increased from about 3.0×10^6 to 9.0×10^6 and attained a value of about 1.7 at 9.0×10^6; further increases in Reynolds number had only small effects on the maximum section lift coefficient. The stall was abrupt below Reynolds numbers of about 9.0×10^6 and gradual at higher Reynolds numbers. The application of a narrow roughness strip near the leading edge resulted in only small effects on the lift characteristics at a Reynolds number of about 6.0×10^6, whereas extensive roughness wrapped around the leading edge forward of 5-percent chord resulted in a decrease in maximum section lift coefficient of about 13 percent. Increasing the Mach number at a constant Reynolds number of about 6.0×10^6 was found to have large effects on the maximum section lift coefficient as a result of the flow over the airfoil becoming supercritical and the maximum section lift coefficient decreased about 30 percent when the Mach number was increased from 0.10 to 0.36. Section lift and pitching-moment coefficients obtained at low Reynolds numbers for the smooth airfoil were in good agreement with results from another low-speed wind tunnel; however, there were differences in drag coefficients in the lift coefficient range where the laminar bucket would be expected. Comparisons of experimental section lift coefficients, pitching-moment coefficients, and chordwise pressure distributions with those calculated from a viscous flow theoretical method were good as long as no boundary-layer flow separation was present; however, the theoretically calculated drag coefficients were generally less than the experimental drag coefficients.

INTRODUCTION

Research on both advanced technology and conventional airfoils has received considerable attention over the last several years at the Langley Research Center. Particular emphasis has been placed on obtaining data at high Reynolds numbers to study the shock-wave boundary-layer interaction phenomena and to compare results measured in various ground test facilities. The present investigation was conducted to obtain the basic low-speed two-dimensional aerodynamic characteristics of the NACA 65_1-213 airfoil over a broad range of Reynolds numbers. In addition, the experimental results have been compared with theoretical data obtained by using a viscous subsonic prediction method. The NACA 65_1-213 airfoil was selected to be representative of conventional airfoils because of the existence of flight data and wind-tunnel data obtained in various research facilities.

The investigation was performed in the Langley low-turbulence pressure tunnel over a Mach number range from 0.10 to 0.36. The Reynolds number, based on airfoil chord, varied from about 3.0×10^6 to 23.0×10^6. The geometrical angle of attack varied from about -10° to 20°. The operational characteristics and a new calibration of the tunnel are presented in an appendix.

SYMBOLS

Values are given in both SI and the U.S. Customary Units. The measurements and calculations were made in the U.S. Customary Units.

a mean-line designation

C_p pressure coefficient, $\dfrac{p_L - p_\infty}{q_\infty}$

$C_{p,critical}$ critical pressure coefficient equivalent to a local Mach number of unity

c airfoil chord, cm (in.)

c_c section chord-force coefficient, $\displaystyle\int_{Forward(t/c)_{max}} C_p \, d\left(\frac{z}{c}\right) - \int_{Aft(t/c)_{max}} C_p \, d\left(\frac{z}{c}\right)$

c_d section profile-drag coefficient, $\displaystyle\int_{Wake} c_d' \, d\left(\frac{h}{c}\right)$

c_d' point drag coefficient, $\displaystyle 2\left(\frac{\rho_1}{\rho_2}\right)^{1/2}\left(\frac{q_1}{q_\infty}\right)^{1/2}\left[\left(\frac{\rho_2}{\rho_\infty}\right)^{1/2} - \left(\frac{q_2}{q_\infty}\right)^{1/2}\right]$

c_l section lift coefficient, $c_n \cos \alpha - c_c \sin \alpha$

c_m section pitching-moment coefficient about quarter-chord point $\int_{l.s.} C_p\left(0.25 - \frac{x}{c}\right) d\left(\frac{x}{c}\right) - \int_{u.s.} C_p\left(0.25 - \frac{x}{c}\right) d\left(\frac{x}{c}\right)$

c_n section normal-force coefficient, $\int_{l.s.} C_p \, d\left(\frac{x}{c}\right) - \int_{u.s.} C_p \, d\left(\frac{x}{c}\right)$

h vertical distance in wake profile, cm (in.)

M free-stream Mach number

p static pressure, N/m^2 (lb/ft^2)

q dynamic pressure, N/m^2 (lb/ft^2)

R Reynolds number based on free-stream conditions and airfoil chord

t airfoil thickness, cm (in.)

x airfoil abscissa (see fig. 1), cm (in.)

z airfoil ordinate (see fig. 1), cm (in.)

α geometric angle of attack, deg

ρ density, kg/m^3 ($slugs/ft^3$)

Subscripts:

L local point on airfoil

max maximum

min minimum

1 tunnel station 1 chord length downstream of model

2 tunnel station downstream of model where static pressure is equal to free-stream static pressure and total pressure is assumed equal to total pressure at station 1

∞ undisturbed stream conditions

Abbreviations:

l.s. lower surface

u.s. upper surface

MODEL, APPARATUS, AND PROCEDURE

Model

The development of the NACA 6 series airfoils is discussed in detail in reference 1. The NACA 65_1-213, a = 0.50, section was obtained by linearly increasing the basic thickness distribution of the NACA 65_1-012 airfoil and combining this thickness distribution with the a = 0.50 mean camber line for a design lift coefficient of 0.20. The nose radius was increased as the square of the thickness ratio. The airfoil section shape is shown in figure 1, and table I presents the measured airfoil coordinates.

The airfoil model was machined from an aluminum billet and had a chord of 60.63 cm (23.87 in.) and a span of 91.44 cm (36 in.). The model was equipped with both upper and lower surface midspan orifices located at the chord stations indicated in table II. Grooves were machined in the surface of the aluminum model and pressure tubing was routed in the grooves to desired orifice locations. The tubes were potted in place with a plastic resin and orifices were drilled through the plastic into the tubing. The plastic was then machined to reform to the original surface and the airfoil surface was hand polished in the chordwise direction with number 400 silicon carbide paper to provide a smooth aerodynamic finish.

Wind Tunnel

The Langley low-turbulence pressure tunnel (ref. 2) is a closed-throat, single-return tunnel which can be operated at stagnation pressures from 1 to 10 atmospheres with tunnel-empty test-section Mach numbers up to 0.42 and 0.22, respectively. The maximum unit Reynolds number is about 49×10^6 per meter (15×10^6 per foot) at a Mach number of about 0.22. The tunnel test section is 91.44 cm (3 ft) wide by 228.6 cm (7.5 ft) high. Operational characteristics and results of a new calibration of the tunnel are included in the appendix.

Hydraulically powered circular plates provided positioning and attachment for the two-dimensional model. The plates are 101.60 cm (40 in.) in diameter, rotate with the airfoil, and are flush with the tunnel wall. The airfoil ends were attached to rectangular model attachment plates (fig. 2) and the airfoil was mounted so that the center of rotation of the circular plates was at 0.25c on the model chord line. The air gaps at the tunnel walls between the rectangular plates and circular plates were sealed with flexible sliding metal seals, shown in figure 2.

Wake Survey Rake

A fixed wake survey rake (fig. 3) at the model midspan was cantilever mounted from the tunnel sidewall and located 1 chord length behind the trailing edge of the airfoil. The wake rake utilized 91 total-pressure tubes, 0.1524 cm (0.060 in.) in diameter, and five static-pressure tubes, 0.3175 cm (0.125 in.) in diameter. The total-pressure tubes were flattened to 0.1016 cm (0.040 in.) for 0.6096 cm (0.24 in.) from the tip of the tube. The static-pressure tubes each had four flush orifices drilled 90° apart and located 8 tube diameters from the tip of the tube and in the measurement plane of the total-pressure tubes.

Instrumentation

Measurements of the static pressures on the airfoil surfaces and the wake rake pressures were made by an automatic pressure-scanning system utilizing variable-capacitance-type precision transducers. Basic tunnel pressures were measured with precision quartz manometers. Angle of attack was measured with a calibrated digital shaft encoder operated by a pinion gear and rack attached to the circular plates. Data were obtained by a high-speed data-acquisition system and recorded on magnetic tape.

TESTS AND METHODS

The airfoil was tested at Mach numbers from 0.10 to 0.36 over an angle-of-attack range from about -10° to 20°. Reynolds number based on the airfoil chord was varied from about 3.0×10^6 to 23.0×10^6.

Most of the roughness data were obtained with standard NASA type strips located at $x/c = 0.05$ on both upper and lower surfaces. The strips were 0.25 cm (0.10 in.) wide over the airfoil span and the carborundum grains were sparsely spaced and attached to the airfoil surface with clear lacquer. The roughness was sized according to reference 3 and the size required for each Reynolds number is listed in table III. A limited comparison of roughness techniques was made for the selected test condition of $M = 0.15$ and $R = 5.9 \times 10^6$ by utilizing a sparse distribution of number 60 grains in

the forms of a strip and extensive roughness wrapped around the leading edge. The strips were 0.25 cm (0.10 in.) wide and located at $x/c = 0.04$, whereas the wraparound extended from the leading edge to $x/c = 0.04$ over both surfaces.

For several test runs oil was spread over the airfoil upper and lower surfaces to determine whether any local flow separation was present. Tufts were attached to the airfoil and tunnel sidewalls with plastic tape to determine stall patterns on both the airfoil and adjacent tunnel sidewalls.

The static-pressure measurements at the airfoil surface were reduced to standard pressure coefficients and machine integrated (based on the trapezoidal method) to obtain section normal-force and chord-force coefficients and section pitching-moment coefficients about the quarter chord. Section profile-drag coefficient was computed from the wake-rake total and static pressures by the method reported in reference 4 and machine integrated by use of the trapezoidal method.

An estimate of the standard low-speed wind-tunnel boundary corrections (ref. 5) amounted to about 2 percent of the measured coefficients and these corrections have not been applied to the data.

PRESENTATION OF RESULTS

The results of this investigation are presented in the following figures:

DISCUSSION OF RESULTS

Experimental Results

Wind-tunnel sidewall effects.- The stall characteristics, and hence $c_{l,max}$, of any airfoil are generally a function of Reynolds number, Mach number, and airfoil surface conditions (roughness). In addition, the maximum lift of an airfoil may be limited in wind tunnels by the interaction of the airfoil upper surface pressure gradients and the airfoil boundary layer with the wind-tunnel sidewall boundary layer. This interaction may induce sidewall boundary-layer separation and hence premature airfoil stall. Detailed examination of the pressure data and tuft pictures obtained on the NACA 65_1-213 airfoil indicated no evidence of any wind-tunnel sidewall boundary-layer effects severe enough to induce premature stall. Selected tuft pictures are shown in figure 4(a) to illustrate the flow field on both the wind-tunnel sidewall and airfoil upper surface at several Reynolds numbers. Flow-field disturbances were confined to a small region at the airfoil sidewall intersection.

Reynolds number effects (model smooth; $M = 0.22$).- The angle of attack for zero lift coefficient was unaffected by Reynolds number. (See fig. 5.) The lift-curve slope (measured between $\alpha = +4^\circ$ and $\alpha = -4^\circ$ and uncorrected for wall boundary effects) showed a modest increase as Reynolds number increased up to about $R = 9.0 \times 10^6$ and attained a value of about 0.12 per degree. The maximum lift coefficient (fig. 9) increased rapidly as Reynolds number increased from $R = 3.0 \times 10^6$ to $R = 9.0 \times 10^6$ and attained a value of about 1.7 at $R = 9.0 \times 10^6$; further increases in Reynolds number had only small effects on $c_{l,max}$. The stall (fig. 5) was abrupt (generally, a laminar leading-edge type) below Reynolds numbers of about $R = 9.0 \times 10^6$ and gradual (turbulent trailing-edge type) at higher Reynolds numbers. Oil-flow photographs obtained at $R = 3.0 \times 10^6$ (fig. 4(b)) illustrate a laminar bubble near the leading edge on the airfoil upper surface. The Reynolds number range was obtained at a Mach number of 0.22, the maximum Reynolds number capability of the wind tunnel, and figure 6 indicates that local compressibility effects may have been present for Reynolds numbers larger than about $R = 6.0 \times 10^6$ ($C_{p,min}$ approaches $C_{p,critical}$ near $c_{l,max}$).

The pitching-moment data (fig. 5) were generally insensitive to Reynolds number except near stall. Abrupt negative increments in c_m (figs. 5(a) and 5(b)) occurred near stall for Reynolds numbers less than about $R = 9.0 \times 10^6$.

The "laminar bucket" near the design c_l of 0.20 is illustrated at $R = 3.0 \times 10^6$ in figure 5(a). Increasing the Reynolds number to $R = 5.9 \times 10^6$ (fig. 5(b)), however, resulted in a less distinct bucket and above $R = 9.0 \times 10^6$ the bucket was no longer apparent. The elimination of the bucket would not be expected to occur until somewhat higher Reynolds numbers as indicated by the 6-series airfoil data of reference 1. However, reference 1 reports that wind-tunnel tests of 6-series airfoils indicated that airfoil surface conditions had a marked influence on maintaining laminar flow. The model surface orifices for the NACA 65_1-213 airfoil of this test were located at the center span of the model, which was also the span station where the profile drag measurements were made, whereas the airfoil models used in reference 1 had no orifices. Surface roughness effects may have resulted from the presence of the orifices despite the care taken during installation. Variation of $c_{d,min}$ with Reynolds number is shown in figure 10. The increase in c_d as a result of increasing the Reynolds number from $R = 3.0 \times 10^6$ to $R = 9.0 \times 10^6$ for the model without fixed transition is largely the result of the forward movement of the natural transition point on the airfoil. Above $R = 9.0 \times 10^6$, the decrease in $c_{d,min}$ with increasing Reynolds number is associated with the decrease in the growth rate of the turbulent boundary-layer thickness and corresponding reduction in skin-friction drag.

Roughness effects.- The effects of applying a standard roughness at $x/c = 0.05$ are shown in figure 5 for various Reynolds numbers. Roughness had no measurable effect on the lift and pitch data except near the angle of attack for maximum lift. Figure 9 indicates that below Reynolds numbers of about $R = 9.0 \times 10^6$, a slightly higher value of $c_{l,max}$ was obtained with roughness. This favorable effect on $c_{l,max}$ at the lower Reynolds numbers is believed to be the result of a reduction of the extent of laminar separation near the airfoil leading edge. Applying roughness resulted in the expected increase in c_d compared with the smooth model results (fig. 5) with essentially full-chord turbulent flow obtained over the airfoil and the effects of Reynolds number on $c_{d,min}$ are shown in figure 10. Increasing the Reynolds number from $R = 3.0 \times 10^6$ to $R = 23.0 \times 10^6$ resulted in a decrease in $c_{d,min}$ of about 0.0022. The effects on the section characteristics of applying various grit sizes varying from number 60 to number 180 are shown in figure 7 for $R = 5.9 \times 10^6$. The largest value of $c_{l,max}$ was obtained by using number 120 grit, the recommended size for this Reynolds number. (See table III.) Figure 7(b) indicates that grit number 180 was sufficient to cause boundary-layer transition at this Reynolds number. Increasing the grit size generally resulted in increases in c_d at moderate lift coefficients. This result is to be expected because of the thickening of the turbulent boundary layer.

A comparison of the section data obtained with a roughness strip and with extensive roughness wrapped around the leading edge is shown in figure 8. A decrease in the angle of attack for $c_{l,max}$ of about 2° and a decrease of about 13 percent in $c_{l,max}$ is shown in figure 8(a) for the wraparound roughness. Comparison of the drag data (fig. 8(b)) indicates small increases in c_d near design lift and rather large increases at the higher lift coefficients for the wraparound roughness. A comparison of the lift data obtained with a narrow roughness strip at $x/c = 0.05$ (fig. 7(a)) and $x/c = 0.04$ (fig. 8(a)) at $R \approx 6 \times 10^6$ indicates that the nature of the stall changed from abrupt to gradual when the strip was positioned at the most forward chordwise location.

Mach number effects.- The effects of Mach number on the airfoil characteristics at a Reynolds number of $R = 5.9 \times 10^6$ with a NASA standard roughness are shown in figures 11 and 12. The expected Prandtl-Glauert increase in lift-curve slope is indicated by increasing the Mach number from 0.10 to 0.36. Large Mach number effects are indicated on both the stall characteristics and $c_{l,max}$ above $M \approx 0.22$. Increasing the Mach number from 0.10 to 0.36 resulted in the stall changing from abrupt to gradual, the stall angle of attack decreased about 7°, and $c_{l,max}$ decreased about 30 percent. These pronounced Mach number effects are a result of supercritical flow occurring on the airfoil. Figure 12 indicates that above a Mach number of about $M = 0.22$, the flow on the airfoil upper surface exceeded sonic velocities; that is, $C_{p,min}$ exceeded $C_{p,critical}$ near $c_{l,max}$. Similar compressibility effects are discussed in detail in reference 6.

The effects of Mach number on the chordwise pressure data at $\alpha = 12^{\circ}$ are illustrated in figure 11(c). At subcritical flow conditions ($M < 0.28$), compressibility effects on the chordwise pressure data are small. However, for supercritical flow conditions ($M \geq 0.28$), the chordwise pressure coefficient is significantly reduced and the extent of trailing-edge separation on the upper surface is increased. The resulting loss in lift coefficient (fig. 11(a)) is therefore attributed to the presence of local supersonic flow on the airfoil upper surface near the leading edge at Mach numbers equal to or greater than 0.28.

Increasing the Mach number had no effect on c_m up to about $\alpha = 8^{\circ}$ (fig. 11(a)); however, at higher angles of attack a positive increment in c_m occurred and the break occurred earlier. The drag data (fig. 11(b)) also indicate large increases at high lift coefficients due to Mach number effects.

Comparison with other airfoil data.- Comparisons of the section data obtained in this test (model smooth) with data obtained in another low-speed wind tunnel on another NACA 65_1-213 airfoil (ref. 7) and with data on the NACA 65_1-212 airfoil (ref. 1) are shown in figure 13. Reasonable agreement in the lift and pitch data (fig. 13(a)) obtained in the two wind tunnels is indicated for the two NACA 65_1-213 airfoils. The drag data

for the NACA 65_1-213 airfoil of reference 7 (fig. 13(a)) indicate the absence of the "laminar bucket." Reference 7 attributes this result to model surface-roughness effects. The data for the NACA 65_1-212 airfoil indicate about a 0.10 higher value of $c_{l,max}$ at $R = 3.0 \times 10^6$ (fig. 13(a)) and about a 0.15 lower value at $R = 6.0 \times 10^6$ (fig. 13(b)), compared with the NACA 65_1-213 data. Comparison of the drag data between the NACA 65_1-212 (ref. 1) and the present NACA 65_1-213 airfoil at $R = 3.0 \times 10^6$ (fig. 13(a)) and at $R = 6.0 \times 10^6$ (fig. 13(b)) indicates that the extent of laminar flow was considerably less for the NACA 65_1-213 airfoil, especially at $R = 6.0 \times 10^6$.

Pressure distributions.- The chordwise pressure data of figure 14 illustrate the effects of angle of attack at a Reynolds number of $R = 5.9 \times 10^6$ and a Mach number of $M = 0.22$ for the smooth model. The data in figure 14(c) $\left(\alpha = 0.6^\circ;\ c_l = 0.20\right)$ indicate the favorable pressure gradients extending to about $x/c = 0.50$ on both surfaces of the airfoil at design lift. These pressure distributions are typical of the NACA 6-series airfoils designed to have long regions of laminar flow. Figure 14(d) shows the pressure data $\left(\alpha = 2.1^\circ;\ c_l = 0.40\right)$ near the limit of the low-drag or laminar-flow region. Some upper surface trailing-edge separation is indicated by the change in pressure recovery over the aft region of the airfoil at about $\alpha = 8^\circ$. (See fig. 14(f).) The extent of the separated region progressed forward with further increase of angle of attack and the relatively flat pressure distribution over the aft region at $c_{l,max}$ (fig. 14(h)) indicated separation extended from about $x/c = 0.65$ to the trailing edge. The lift-curve slope decreased as the chordwise extent of separation increased (fig. 5(b)) and became zero at stall. The stall was of the abrupt trailing-edge type as indicated by figure 14(i) at $\alpha = 16.2^\circ$.

Comparison of Experimental and Theoretical Data

Examples of the chordwise pressure distributions calculated by the viscous flow method of reference 8 are compared with the experimental pressure data of the present investigation in figure 14 for free transition (model smooth) at $R = 5.9 \times 10^6$. The agreement between experiment and theory is good over most of the airfoil chord, as long as no boundary-layer flow separation is present. For example, figures 14(f) and 14(g) illustrate the discrepancies between experiment and theory near the trailing edge of the airfoil caused by boundary-layer separation.

Comparisons of the experimental lift and pitching-moment data with theory for Reynolds numbers from 3.0×10^6 to 22.8×10^6 with free transition (model smooth) are shown in figure 15. The theoretical method satisfactorily predicts the lift and pitching-moment data for angles of attack where no significant boundary-layer flow separation is present. For example, at $R = 5.9 \times 10^6$ (fig. 15(b)), good agreement is shown up to about $\alpha = 12^\circ$. The discrepancy in c_l and c_m at the higher angles of attack is as

expected, since the theoretical method is only applicable for airfoils with attached boundary layers. Figure 15(e) shows the same results for $R = 5.9 \times 10^6$ with transition fixed at 0.05c.

The viscous-flow theoretical method of reference 8 was developed to calculate the surface pressures for viscous, subsonic flows on airfoils composed of one or more elements. An evaluation of the airfoil profile drag was not in the scope of the technical effort. However, an approximate calculation of drag coefficient was included which consisted of the integration of the airfoil pressure drag and the addition of skin-friction drag based on flat-plate calculations. Reference 9 indicated that the resulting drag coefficients were greatly in excess of the measured values. An attempt to improve the agreement between experimental and theoretical drag coefficients was made by modifying the pressure drag integration procedure and doubling the chord Reynolds number. Comparison of the modified drag coefficients with experiment in figure 15, however, indicates that for either free or fixed transition, the theory now generally underpredicts the drag coefficients. Further improvement in the theoretical drag prediction is therefore needed even when no boundary-layer separation occurs.

SUMMARY OF RESULTS

Low-speed wind-tunnel tests have been conducted to determine the two-dimensional aerodynamic characteristics of the NACA 65_1-213, a = 0.50, airfoil section. The results have been compared with data from another low-speed wind tunnel and also with theoretical predictions obtained from a subsonic viscous-flow method. The tests were conducted over a Mach number range from 0.10 to 0.36. Reynolds number, based on the airfoil chord, was varied from about 3.0×10^6 to 23.0×10^6. The following results were determined from this investigation:

1. Maximum section lift coefficients at a constant Mach number of 0.22 increased rapidly with Reynolds number from about 3.0×10^6 to 9.0×10^6 and attained a value of about 1.7.

2. Stall was abrupt below a Reynolds number of about 9.0×10^6 and changed to gradual at higher Reynolds numbers.

3. The application of a narrow roughness strip near the leading edge at a Reynolds number of about 6.0×10^6 resulted in small effects on lift whereas extensive roughness around the leading edge resulted in a decrease in the maximum section lift coefficient of about 13 percent.

4. Increasing Mach number at a constant Reynolds number of about 6.0×10^6 showed large effects on the maximum section lift coefficient as a result of the flow over the

airfoil becoming supercritical. The maximum section lift coefficient decreased about 30 percent for an increase in Mach number from 0.10 to 0.36.

5. Section lift and pitching-moment coefficients at low Reynolds numbers for the smooth airfoil were in good agreement with results from another low-speed wind tunnel. However, there were differences in the drag coefficients within the lift coefficient range where the laminar bucket would be expected.

6. Comparisons of experimental section lift coefficients, pitching-moment coefficients, and chordwise pressure distributions with those calculated from a viscous-flow theoretical method were good as long as no boundary-layer flow separation was present; however, the theoretically calculated drag coefficients were less than the experimental drag coefficients.

Langley Research Center,
National Aeronautics and Space Administration,
Hampton, Va., December 7, 1974.

APPENDIX

CALIBRATION OF THE LANGLEY LOW-TURBULENCE PRESSURE TUNNEL

A calibration of the Langley low-turbulence pressure tunnel has been performed using a long survey probe alined with the longitudinal center line of the test section. The nose of the probe contained a total-pressure tube and static-pressure orifices were installed flush with the probe surface at fixed interval distances over the probe length. These were used to measure the probe total-pressure and probe static-pressure distribution of the airstream. A photograph of the probe is shown in figure 16 and a sketch of the calibration arrangement, relative to the wind tunnel at various longitudinal stations x cm (in.), is shown in figure 17. Also shown in figure 17 are the reference total-pressure tubes on the floor of the wind tunnel and the tunnel sidewall reference static-pressure orifices from which the tunnel test conditions are calculated.

Some typical Mach number distributions at various tunnel total pressures (that is, Reynolds numbers) are shown in figure 18. The Mach number distributions show that the flow is uniform with negligible deviations between $x = -101.6$ cm (-40 in.) and $x = 101.6$ cm (40 in.). Figure 19(a) shows the results of the calibration in terms of a calibration factor (C.F.) against average probe Mach number, and figure 19(b) shows the present operational boundaries of the tunnel. The calibration factor is shown to vary by less than 1 percent over the entire operational Mach number and Reynolds number range of the tunnel, and no specific trends of variation of the calibration factor with either Mach number or Reynolds number could be identified. The dashed line in figure 19(a) indicates the root-mean-square value (rms value) of all the data (C.F. = 1.006), which therefore is defined as the calibration factor for the tunnel. This calibration factor is in good agreement with a previously used but unpublished value (1.005). The symbols used in the calibration of the tunnel (see figs. 16 to 19) are as follows:

C.F. calibration factor, $\frac{p_{t,p} - p_p}{p_{t,ref} - p_{ref}}$, averaged from $x = -30.48$ cm (-12 in.) to $x = 60.96$ cm (24 in.)

M free-stream Mach number

M_{av} longitudinal average of probe Mach number between $x = -30.48$ cm (-12 in.) and $x = 60.96$ cm (24 in.)

M_p probe Mach number (computed from p_p and $p_{t,p}$)

p_p probe static pressure, kN/m^2 (lb/in^2)

p_{ref} tunnel sidewall static pressure, kN/m^2 (lb/in^2)

$p_{t,p}$ probe total pressure, kN/m^2 (lb/in^2)

$p_{t,ref}$ tunnel total pressure, kN/m^2 (lb/in^2)

q dynamic pressure, kN/m^2 (lb/in^2)

R unit Reynolds number per m (per ft), based on stagnation temperature 300 K (540^o R)

x longitudinal station, cm (in.); x = 0 coincides with axis through center of rotation of sidewall circular plates

REFERENCES

1. Abbott, Ira H.; Von Doenhoff, Albert E.; and Stivers, Louis S., Jr.: Summary of Airfoil Data. NACA Rep. 824, 1945. (Supersedes NACA WR L-560.)

2. Von Doenhoff, Albert E.; and Abbott, Frank T., Jr.: The Langley Two-Dimensional Low-Turbulence Pressure Tunnel. NACA TN 1283, 1947.

3. Braslow, Albert L.; and Knox, Eugene C.: Simplified Method for Determination of Critical Height of Distributed Roughness Particles for Boundary-Layer Transition at Mach Numbers From 0 to 5. NACA TN 4363, 1958.

4. Baals, Donald D.; and Mourhess, Mary J.: Numerical Evaluation of the Wake-Survey Equations for Subsonic Flow Including the Effect of Energy Addition. NACA WR L-5, 1945. (Formerly NACA ARR L5H27.)

5. Allen, H. Julian; and Vincenti, Walter G.: Wall Interference in a Two-Dimensional-Flow Wind Tunnel, With Consideration of the Effect of Compressibility. NACA Rep. 782, 1944. (Supersedes NACA WR A-63.)

6. Wootton, L. R.: The Effect of Compressibility on the Maximum Lift Coefficient of Aerofoils at Subsonic Airspeeds. J. Roy. Aeronaut. Soc., vol. 71, July 1967, pp. 476-486.

7. Englar, R. J.; and Ottensoser, J.: Calibration of Some Subsonic Wind Tunnel Inserts for Two Dimensional Airfoil Experiments. TN-AL-275, Naval Ship Res. & Develop. Center, Sept. 1972. (Available from DDC as AD 913 412L.)

8. Stevens, W. A.; Goradia, S. H.; and Braden, J. A.: Mathematical Model for Two-Dimensional Multi-Component Airfoils in Viscous Flow. NASA CR-1843, 1971.

9. McGhee, Robert J.; and Beasley, William D.: Low-Speed Aerodynamic Characteristics of a 17-Percent-Thick Airfoil Section Designed for General Aviation Applications. NASA TN D-7428, 1973.

TABLE I.- NACA 65_1-213, a = 0.50, MEASURED AIRFOIL COORDINATES

[c = 60.63 cm (23.87 in.)]

Upper surface		Lower surface	
x/c	z/c	x/c	z/c
0.00000	0.00000		
.00014	.00297	0.00021	-0.00096
.00042	.00431	.00054	-.00215
.00080	.00551	.00098	-.00327
.00127	.00669	.00152	-.00431
.00132	.00775	.00214	-.00533
		.00285	-.00626
.00244	.00880	.00362	-.00717
.00313	.00981	.00444	-.00797
.00386	.01074	.00530	-.00871
.00624	.01311	.00619	-.00943
		.00884	-.01114
.01111	.01656	.01403	-.01363
.02348	.02298	.02680	-.01788
.04840	.03281	.05214	-.02404
.07345	.04052	.07737	-.02868
.09858	.04703	.10252	-.03256
.14893	.05750	.15271	-.03858
.19939	.06550	.20279	-.04308
.24993	.07153	.25280	-.04640
.30052	.07604	.30275	-.04872
.35115	.07897	.35267	-.05016
.40182	.08031	.40254	-.05065
.45254	.07990	.45238	-.04999
.50339	.07749	.50207	-.04811
.55416	.07291	.55185	-.04504
.60462	.06665	.60193	-.04106
.65493	.05918	.65216	-.03625
.70513	.05066	.70251	-.03086
.75522	.04151	.75297	-.02504
.80526	.03201	.80347	-.01899
.85525	.02250	.85403	-.01298
.90527	.01329	.90456	-.00729
.95532	.00520	.95506	-.00250
.99999	.00015	1.0	-.00013

TABLE II.- AIRFOIL ORIFICE LOCATIONS

[c = 60.63 cm (23.87 in.)]

Upper surface		Lower surface	
x/c	z/c	x/c	z/c
0.0	0.0		
.00281	.00933	0.00515	-0.00862
.00715	.01388		
.01031	.01619	.01010	-.01183
.01273	.01753		
.01759	.02017		
.02012	.02144	.02008	-.01588
.02520	.02378		
.03009	.02589		
.05024	.03344	.05045	-.02372
.07538	.04107		
.10044	.04750	.10087	-.03235
.15078	.05786	.15130	-.03843
.20105	.06574	.20129	-.04296
.25178	.07180	.25162	-.04636
.30180	.07615	.30189	-.04870
.35211	.07902	.35204	-.05016
.37729	.07987		
.40264	.08032	.40231	-.05065
.42775	.08033		
.45293	.07990	.45260	-.04999
.47781	.07898		
.50319	.07752	.50304	-.04806
.52811	.07551		
.54077	.07432		
.55334	.07302	.55337	-.04497
.56607	.07159		
.57843	.07009		
.59116	.06848		
.60342	.06685	.60374	-.04090
.62863	.06324		
.65391	.05934	.65377	-.03609
.70407	.05087	.70375	-.03074
.75419	.04173	.75459	-.02485
.80482	.03210	.80490	-.01879
.85509	.02252	.85513	-.01286
.90484	.01336	.90504	-.00722
.95530	.00519	.95543	-.00248

TABLE III.- NOMINAL ROUGHNESS PARTICLE HEIGHTS

[Grit located at x/c = 0.05]

R	Grit number	Nominal particle height, cm (in.)
3.0×10^6	80	0.021 (0.0083)
5.9	120	.012 (.0049)
9.0	180	.0089 (.0035)
11.8	220	.0074 (.0029)
14.5	220	.0074 (.0029)
17.4	220	.0074 (.0029)
22.8	220	.0074 (.0029)

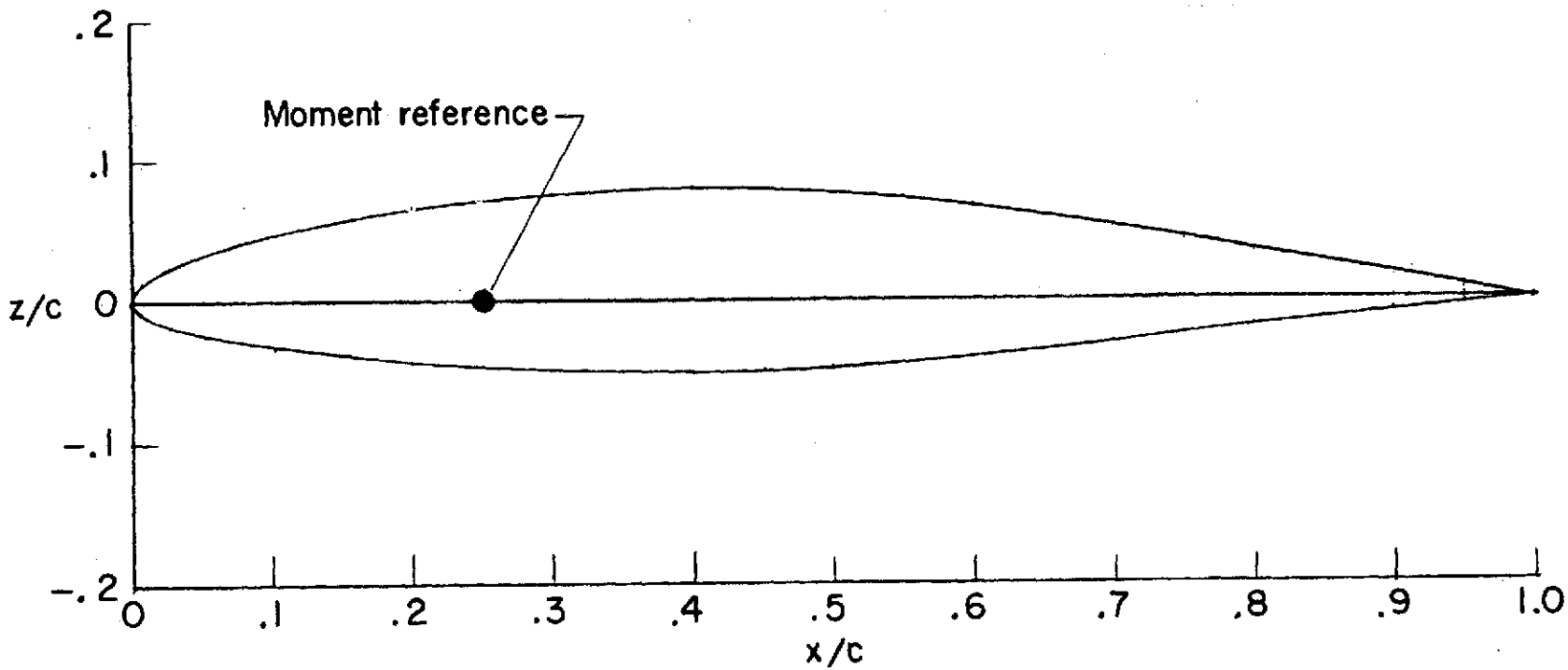

Figure 1.- Section shape for NACA 65_1-213, a = 0.50, airfoil.

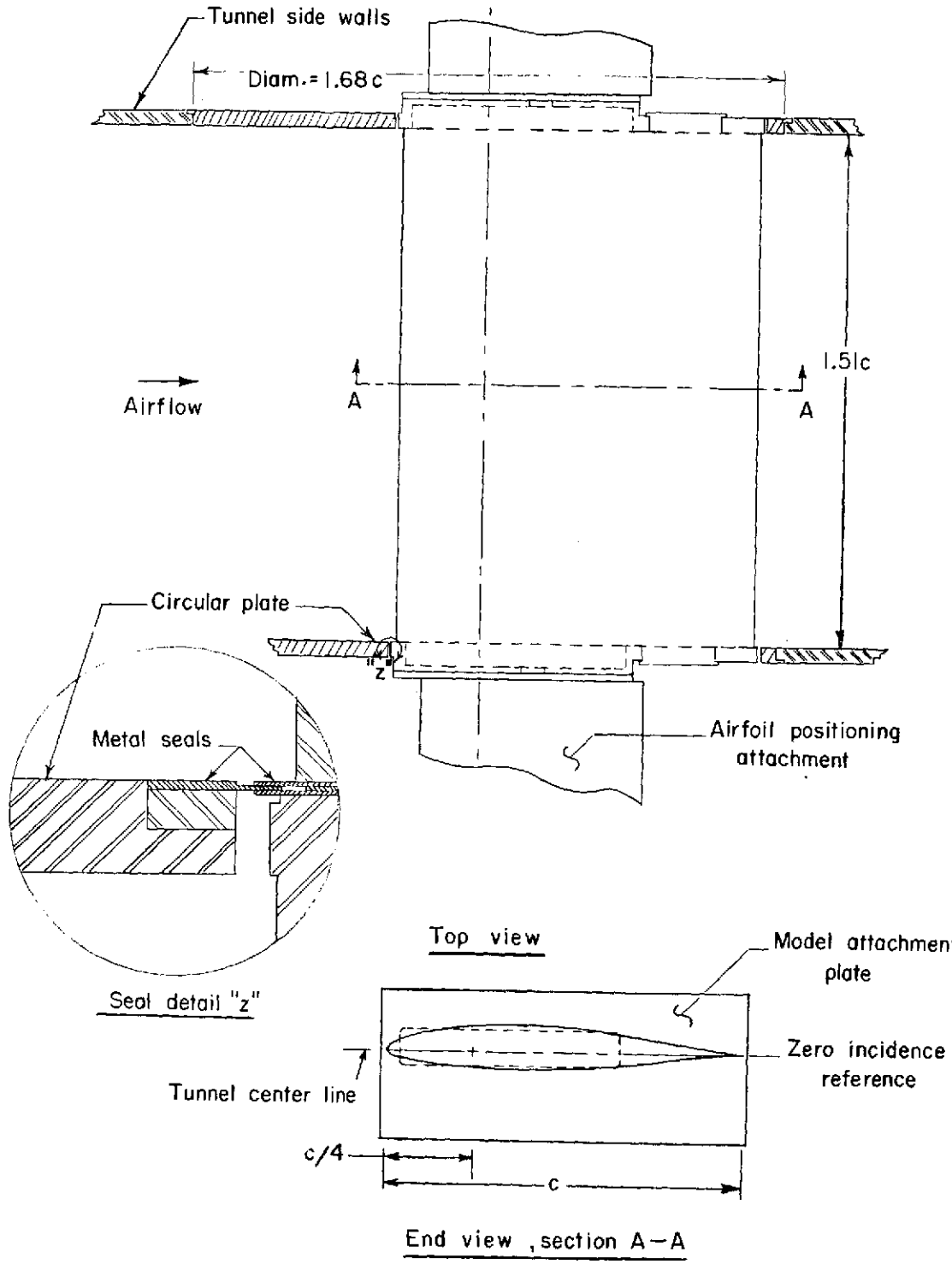

Figure 2.- Airfoil mounted in wind tunnel. All dimensions are in terms of airfoil chord c = 60.63 cm (23.87 in.).

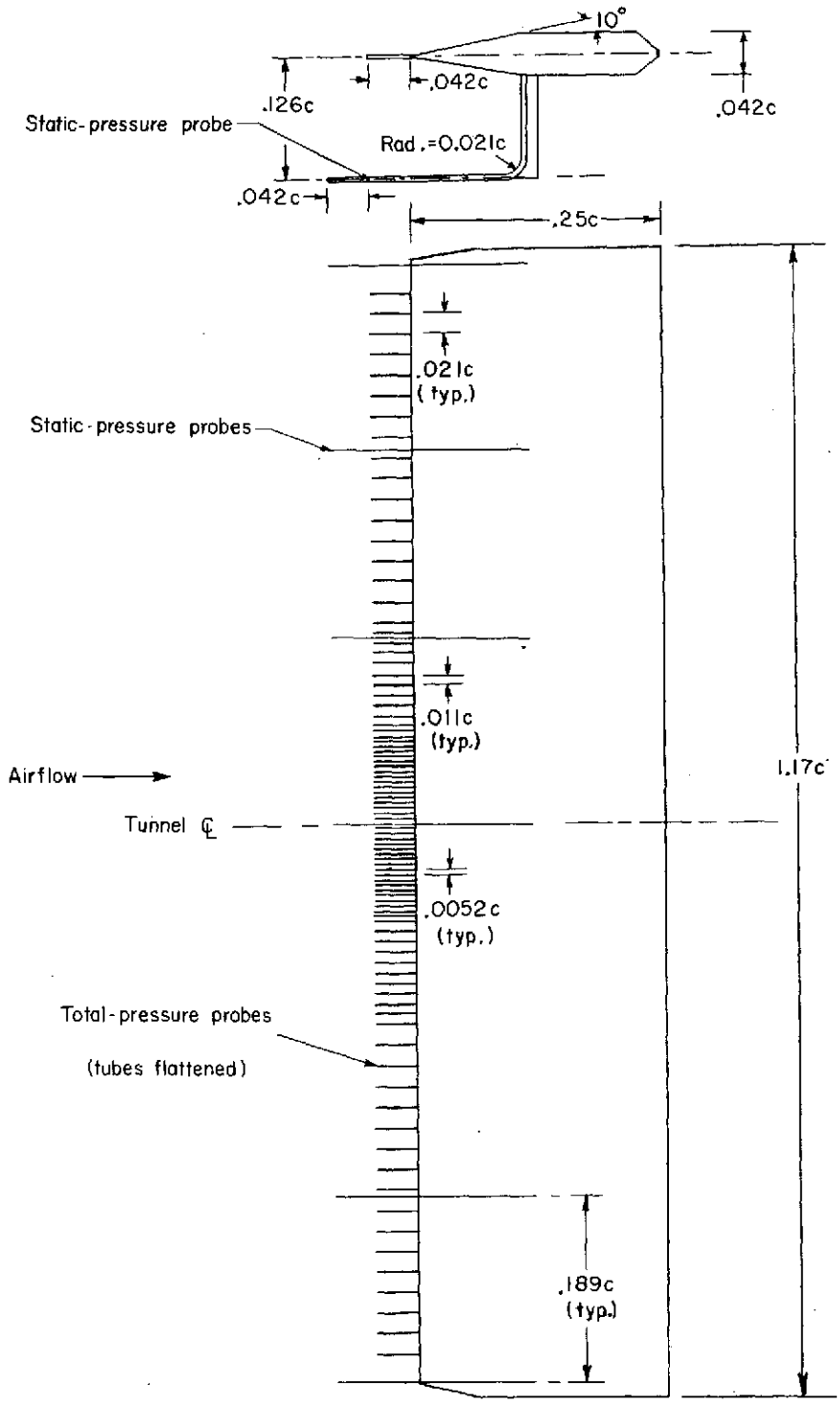

Figure 3.- Drawing of wake rake. All dimensions are in terms of airfoil chord. c = 60.63 cm (23.87 in.).

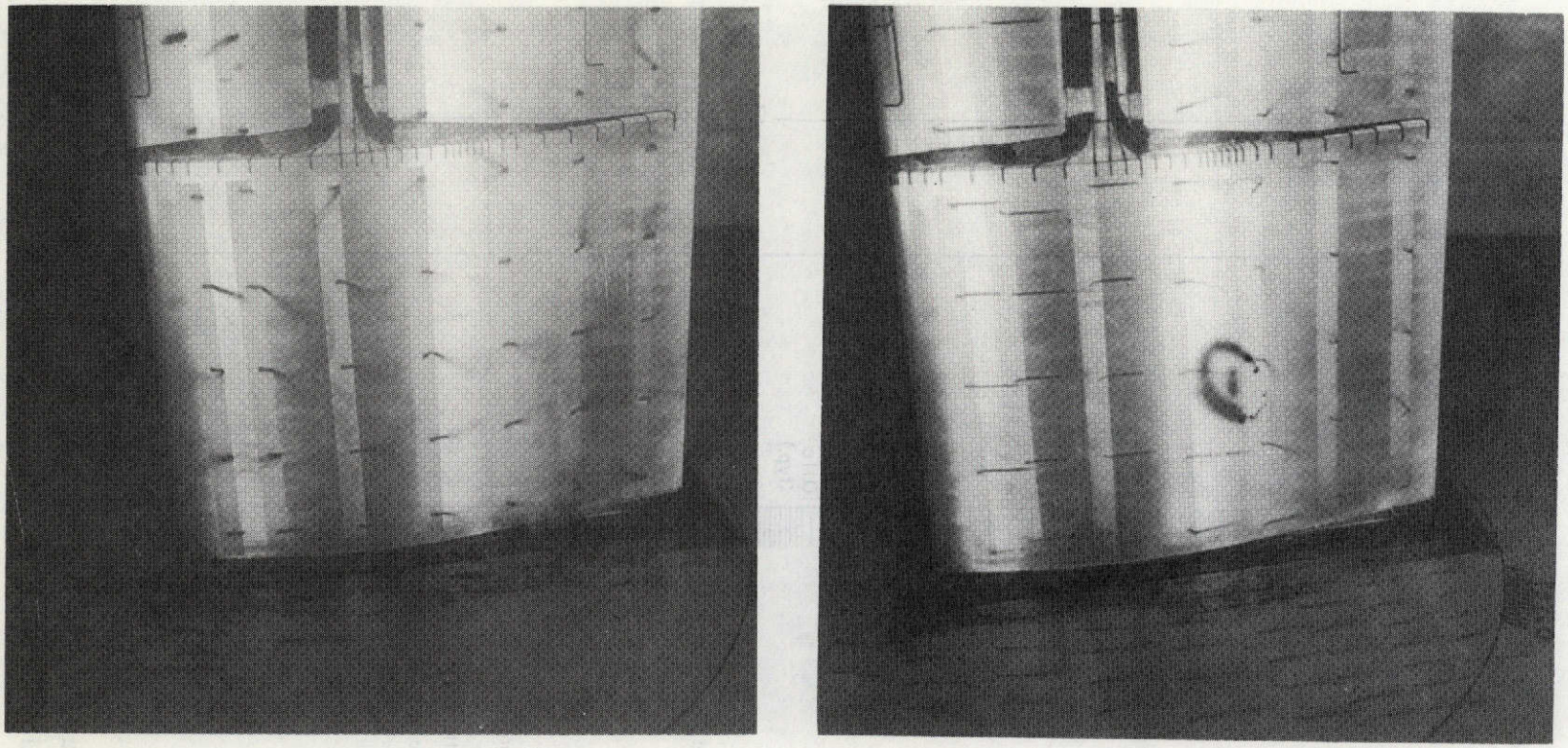

$\alpha = 15^{o}$; $R = 3.0 \times 10^{6}$
Stall

$\alpha = 16^{o}$; $R = 6.0 \times 10^{6}$
$c_{l,max}$

(a) Tufts.

L-74-8543

Figure 4.- Flow-visualization photographs for NACA 65_1-213 airfoil. M = 0.22; model smooth.

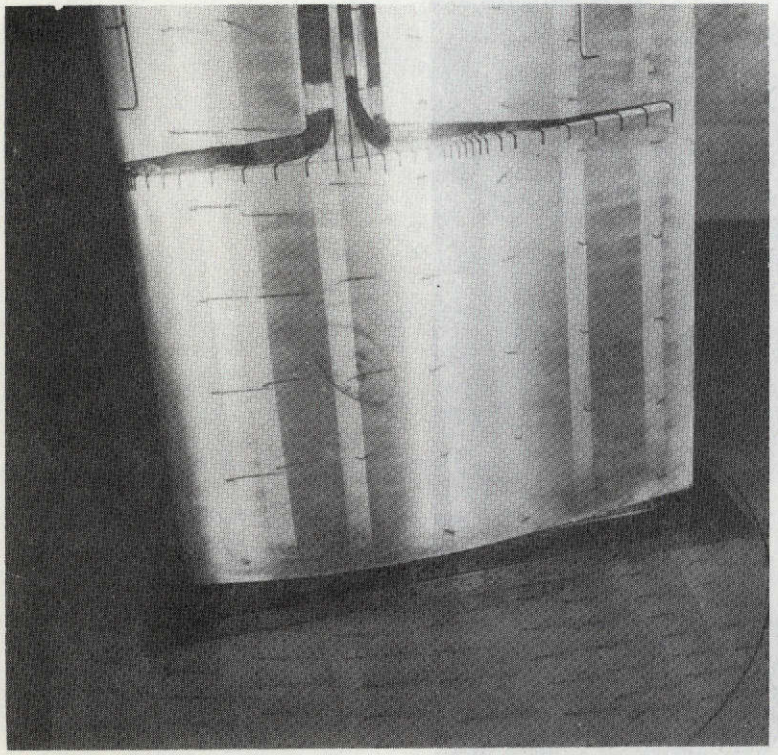

$\alpha = 17^{o}$; R = 12.0×10^{6}
Stall

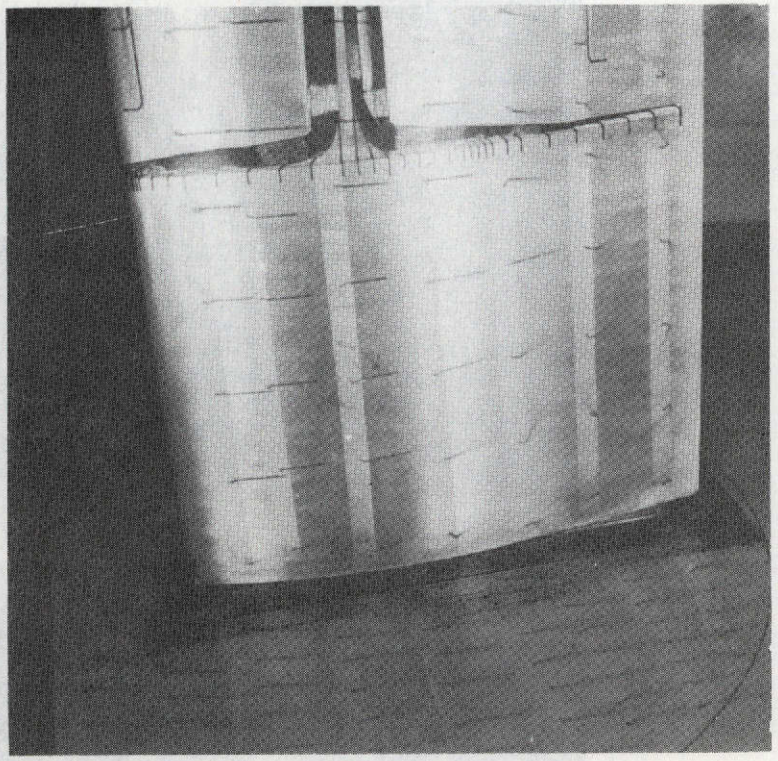

$\alpha = 16^{o}$; R = 18.0×10^{6}
Stall

(a) Tufts. Concluded.

L-74-8544

Figure 4.- Continued.

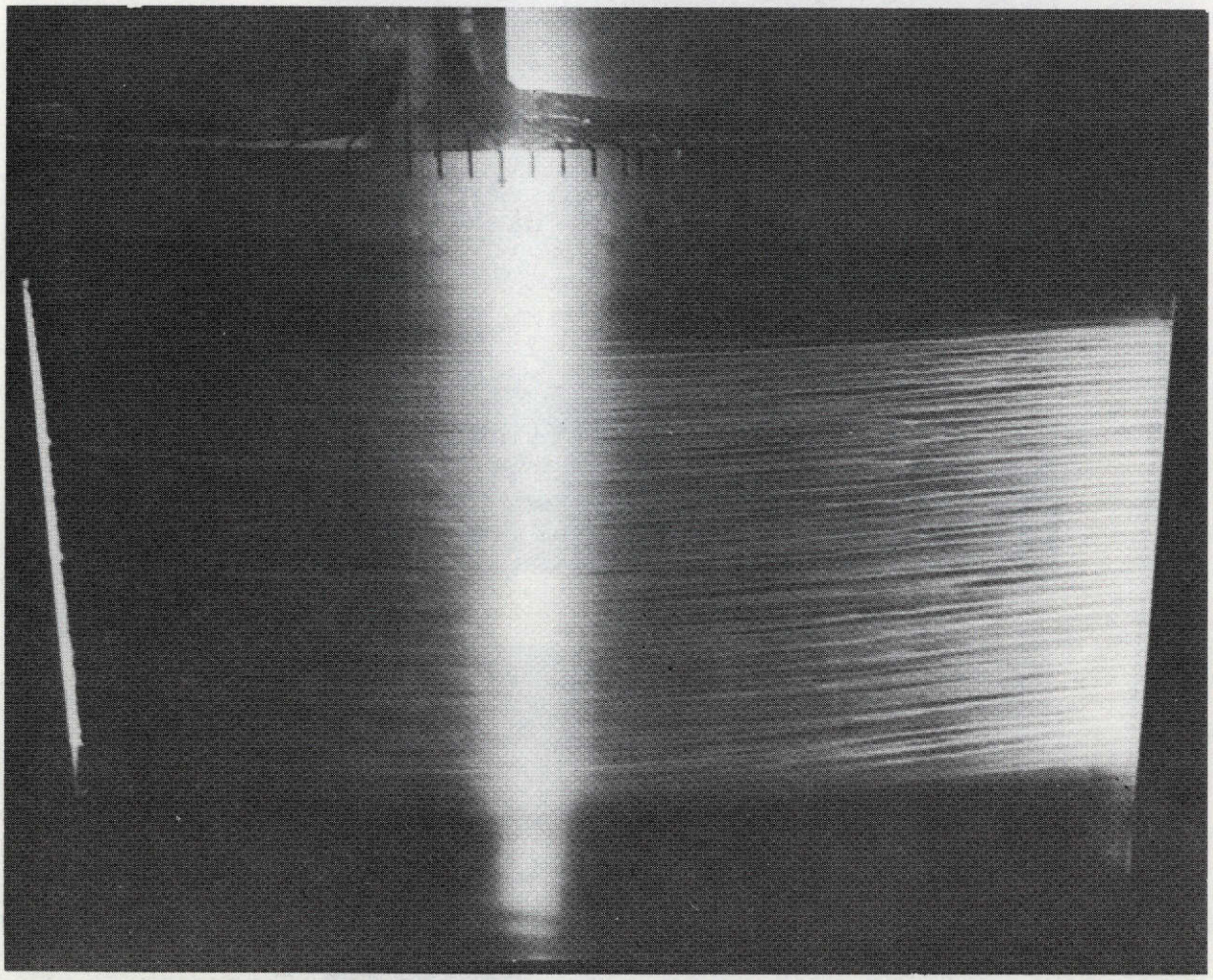

$\alpha = 5^{o}$; $R = 3.0 \times 10^{6}$. L-74-8545

(b) Oil flow.

Figure 4.- Concluded.

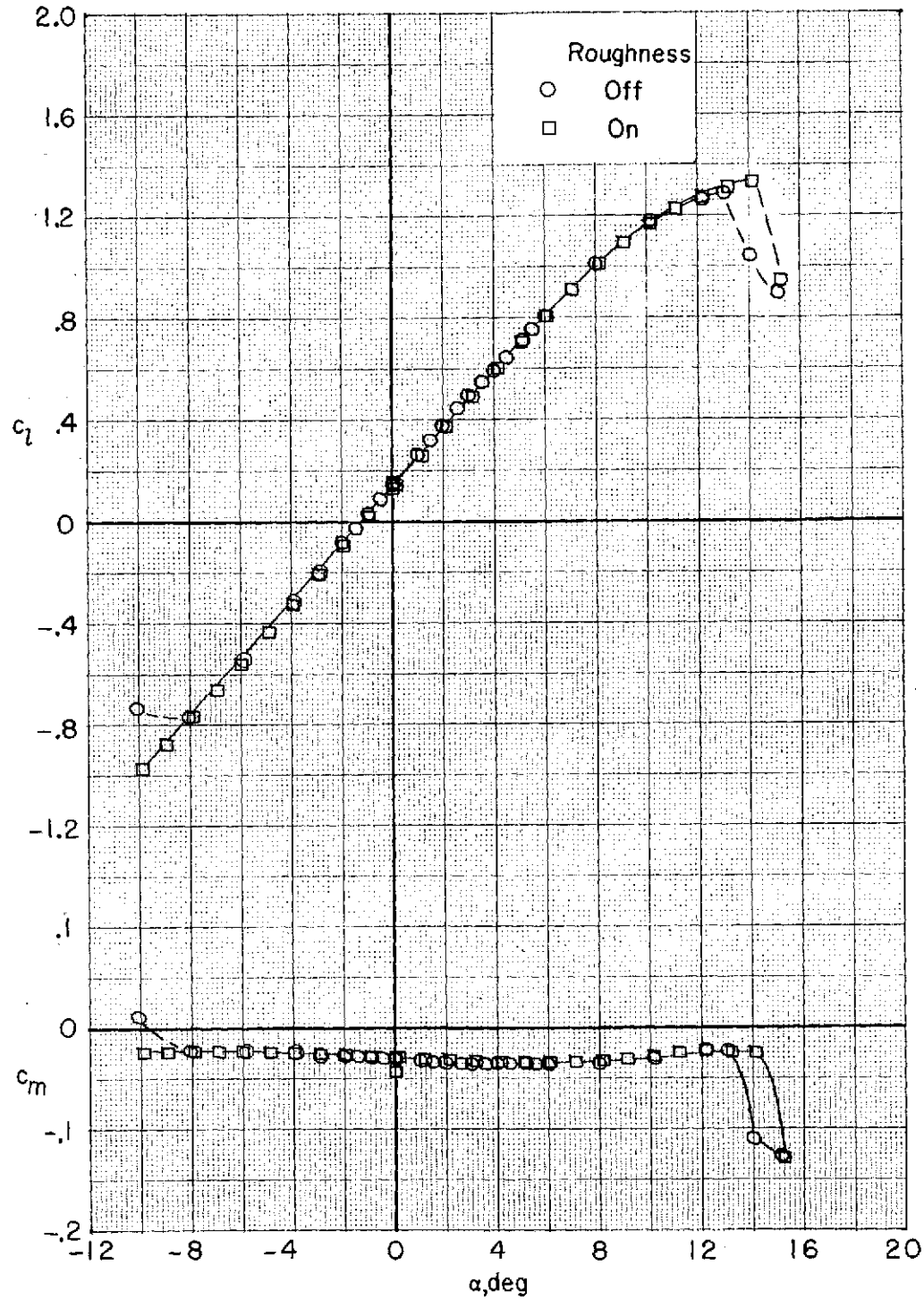

(a) $R = 3.0 \times 10^6$.

Figure 5.- Effect of Reynolds number on section characteristics. M = 0.22.

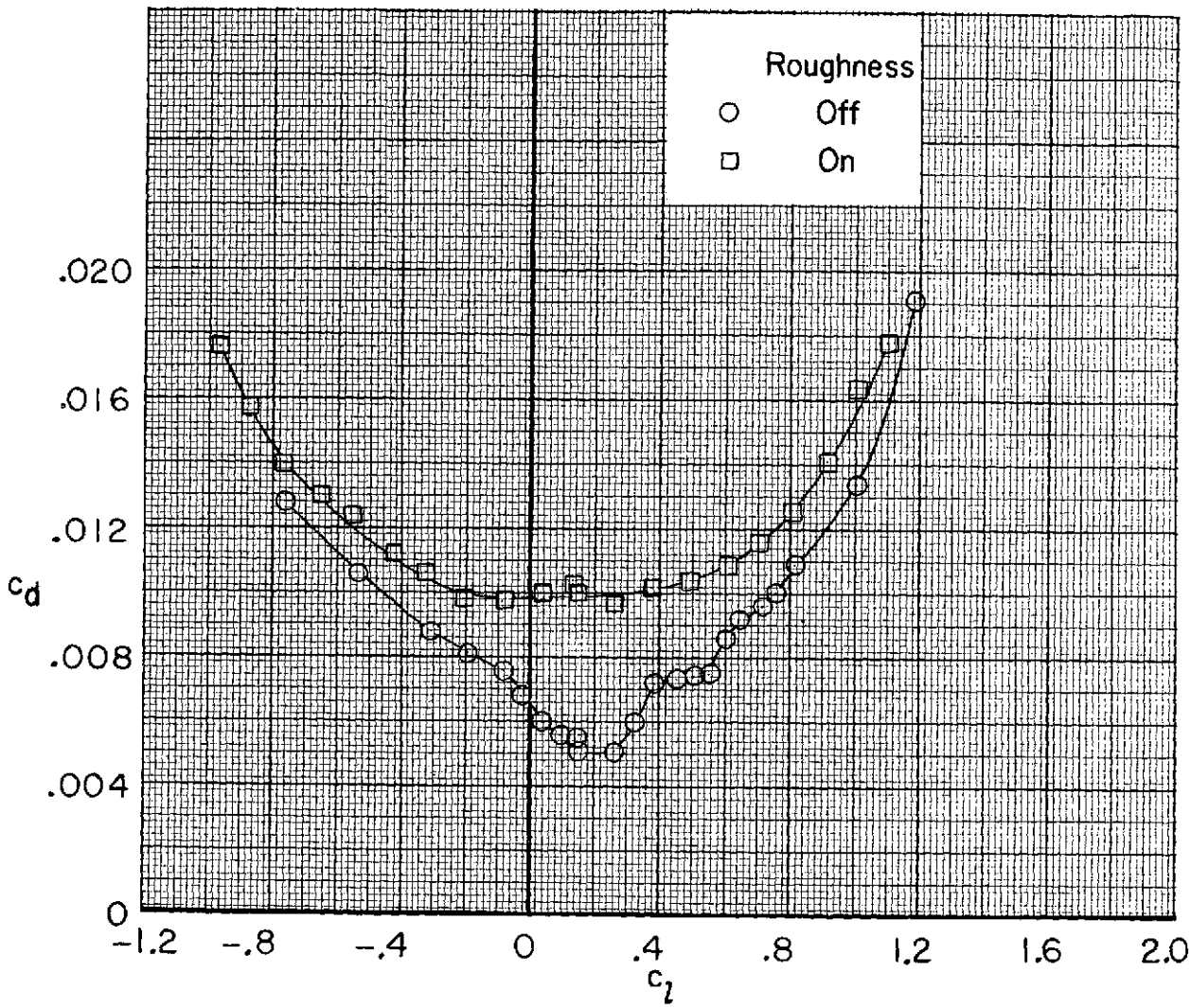

(a) $R = 3.0 \times 10^6$. Concluded.

Figure 5.- Continued.

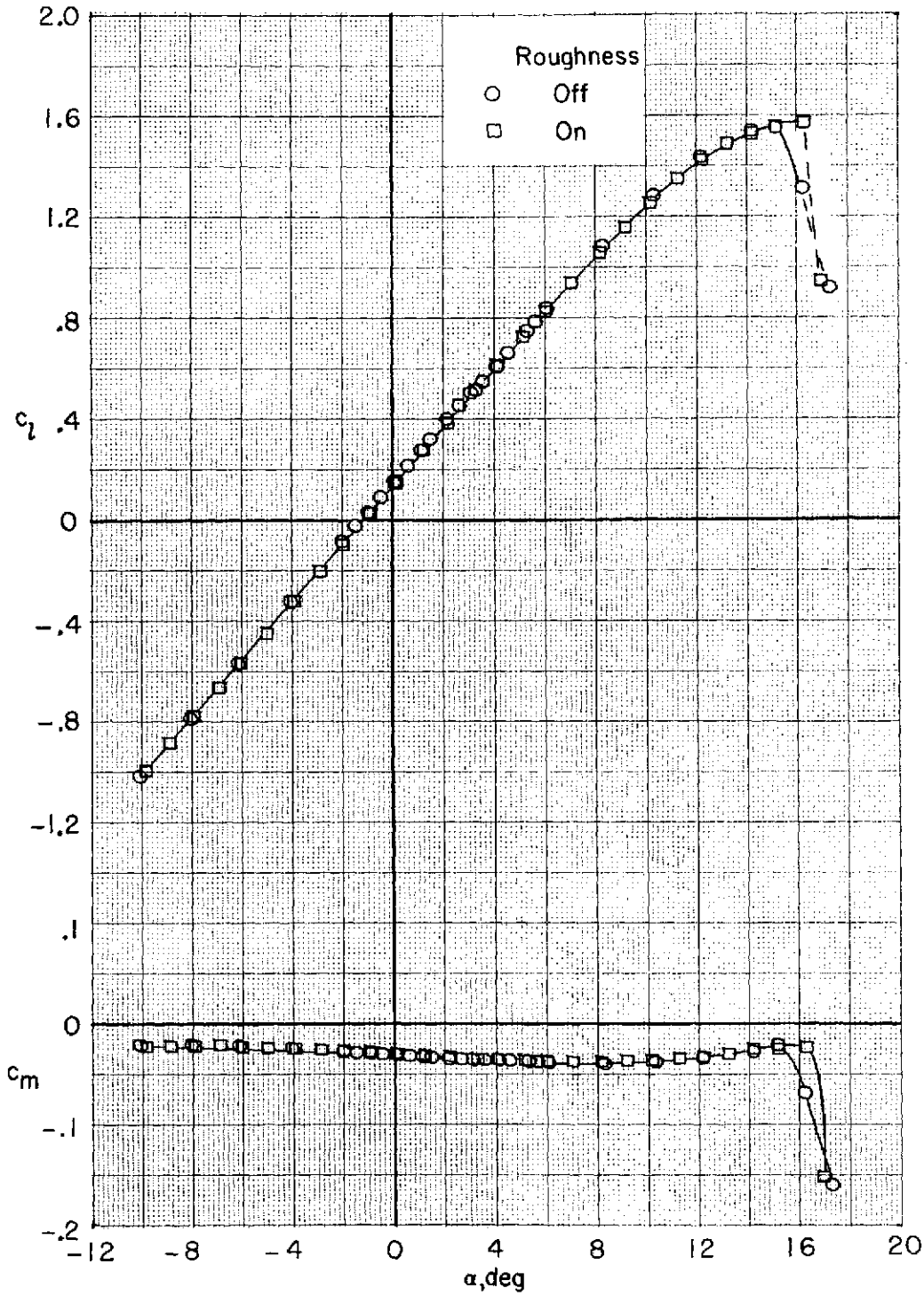

(b) $R = 5.9 \times 10^6$.

Figure 5.- Continued.

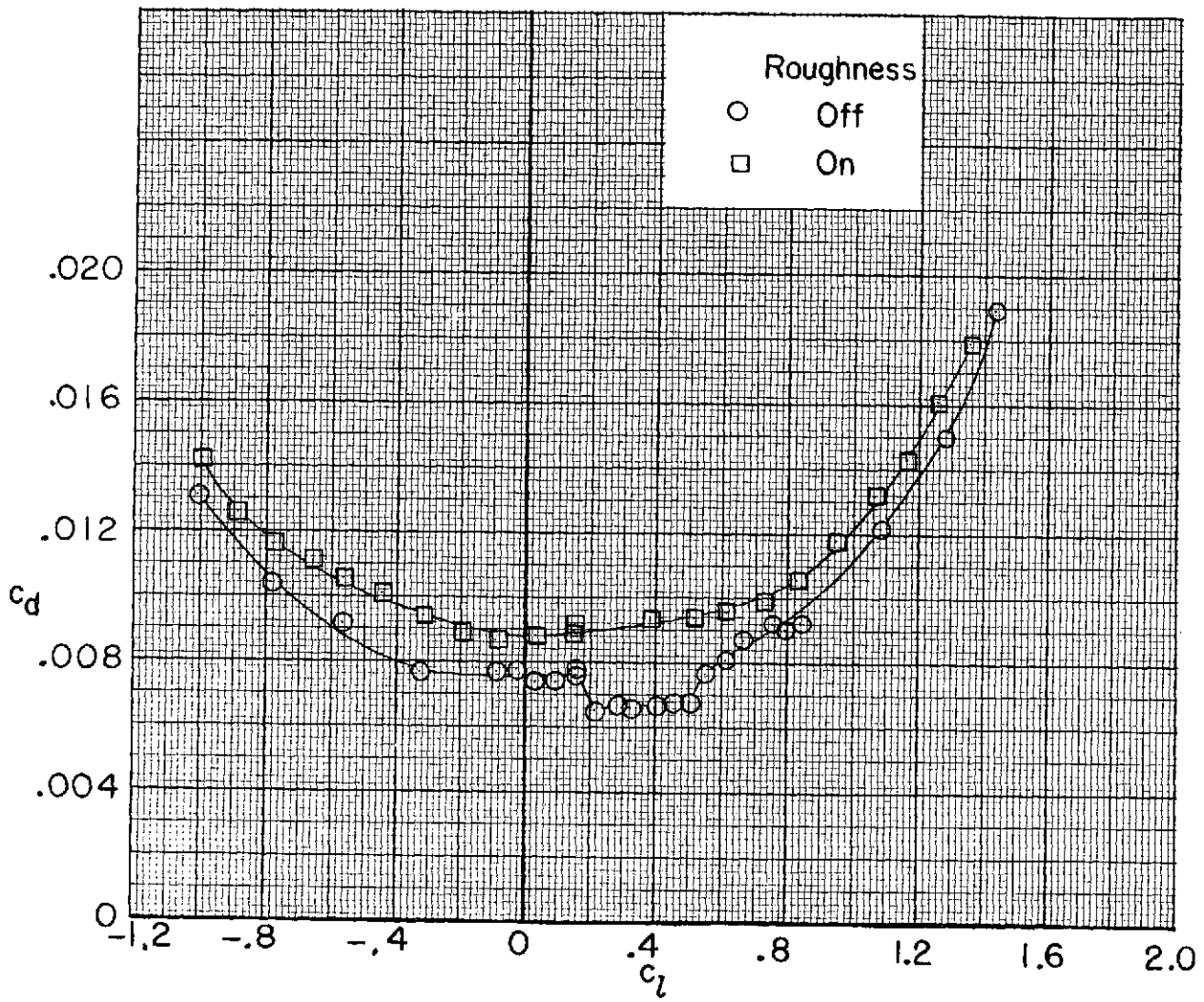

(b) R = 5.9×10^6. Concluded.

Figure 5.- Continued.

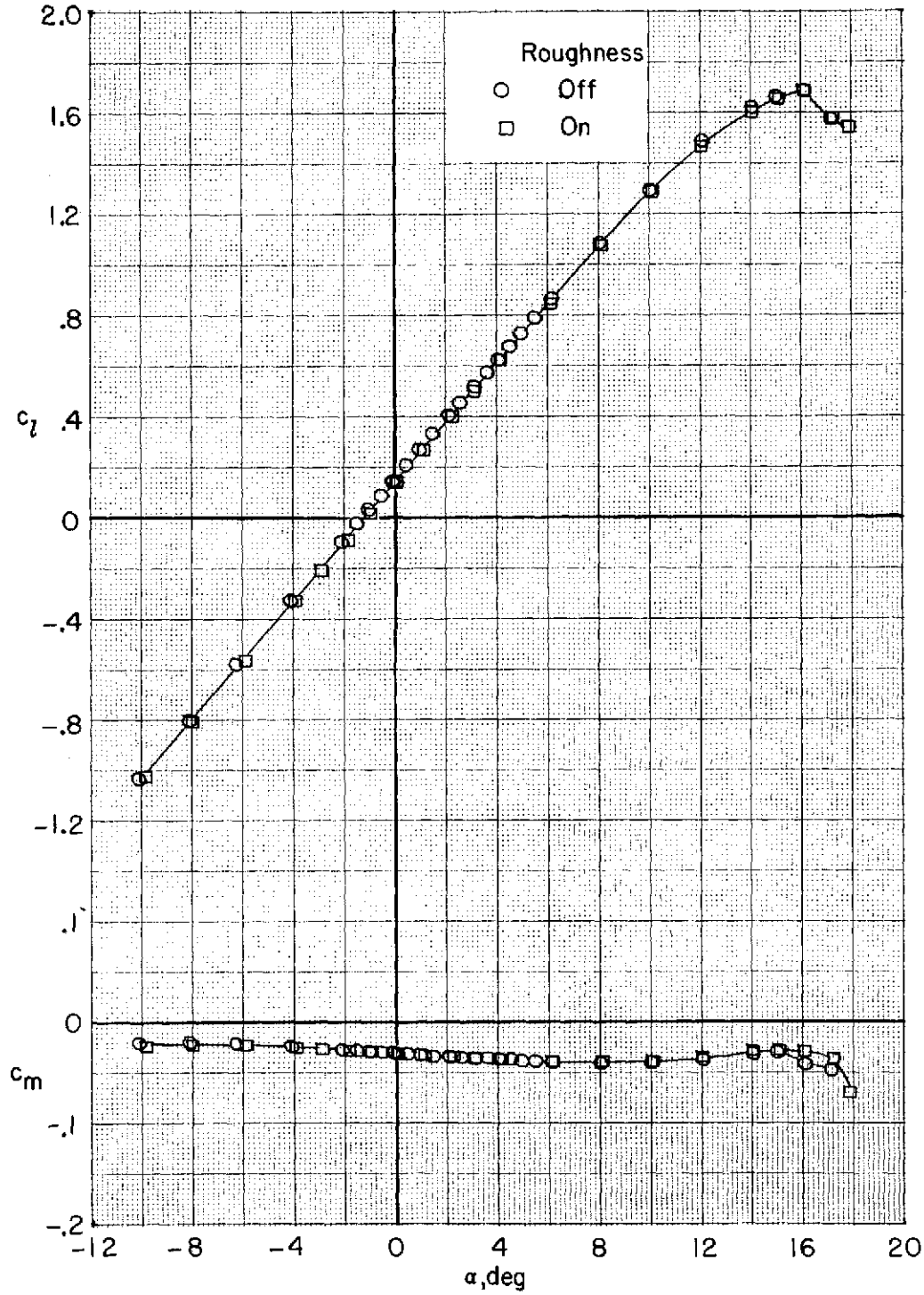

(c) $R = 9.0 \times 10^6$.

Figure 5.- Continued.

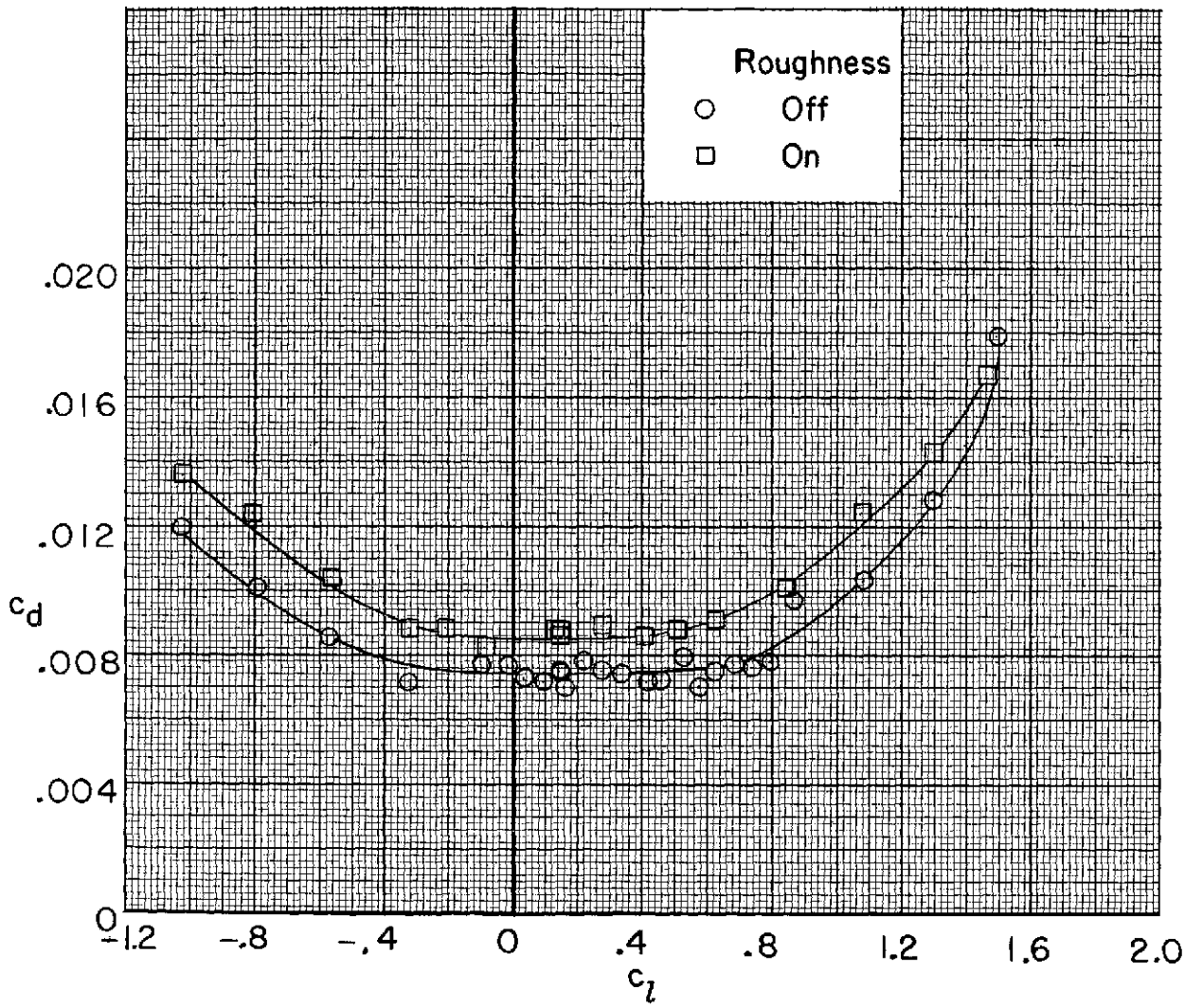

(c) R = 9.0×10^6. Concluded.

Figure 5.- Continued.

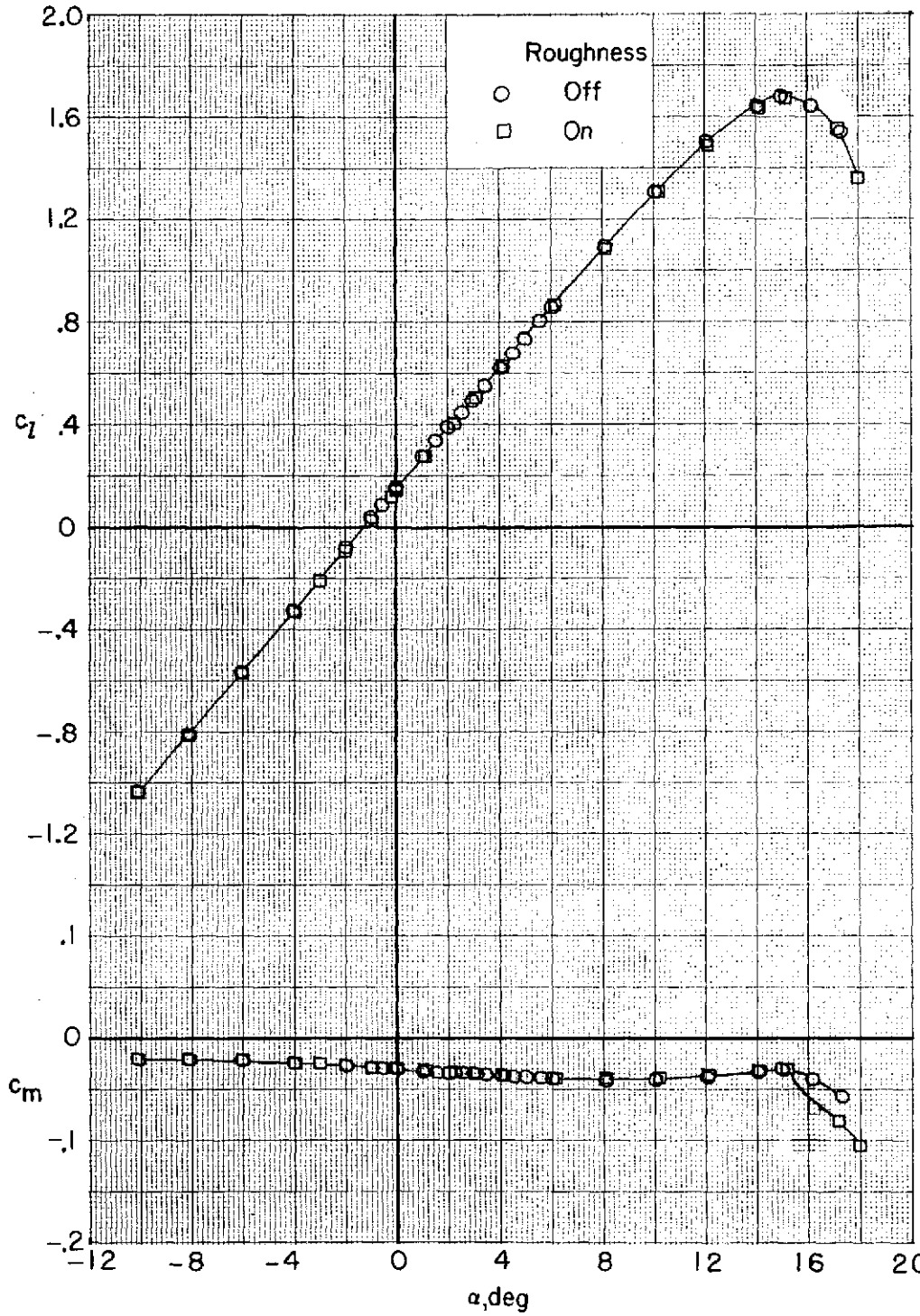

(d) $R = 11.8 \times 10^6$.

Figure 5.- Continued.

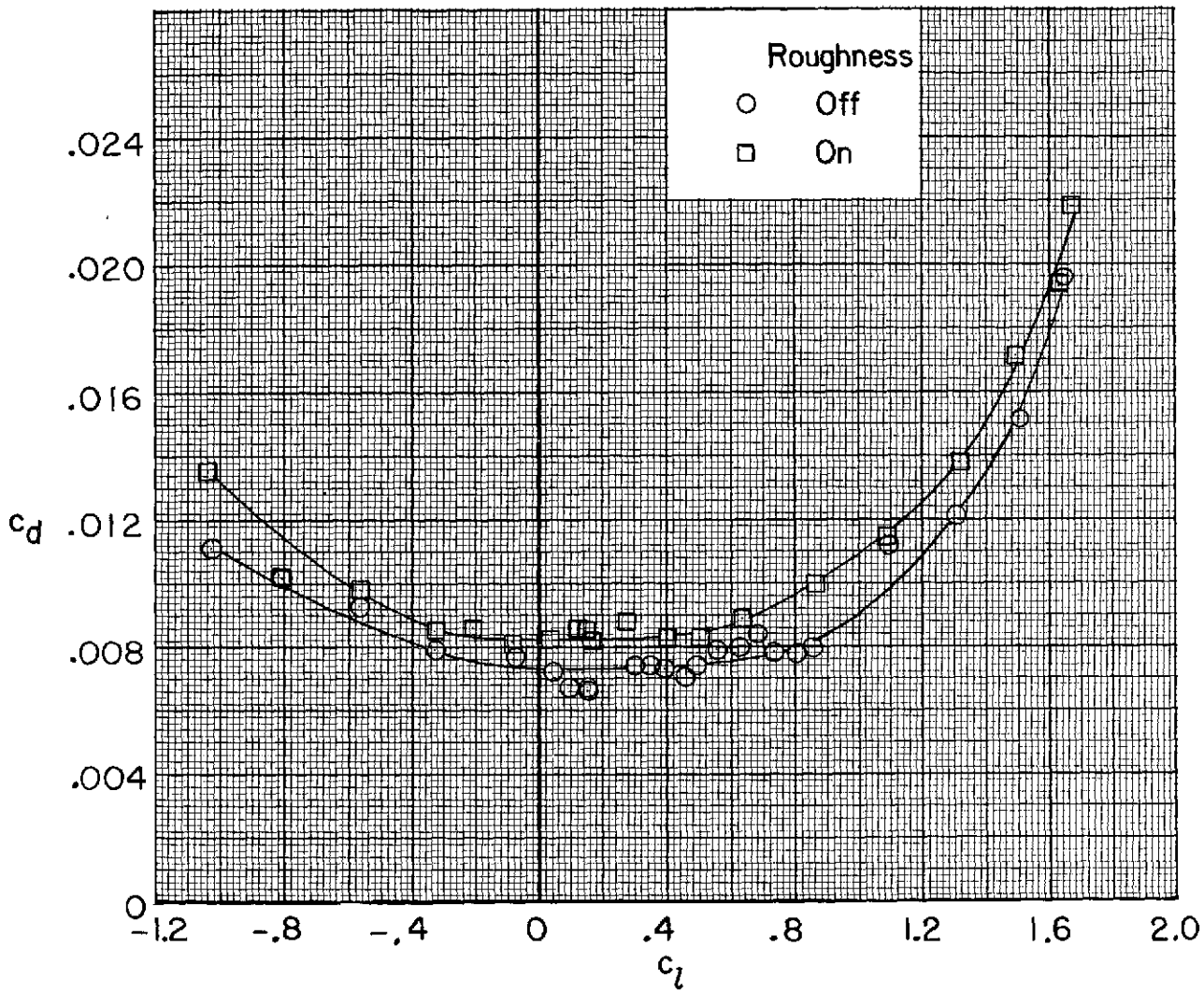

(d) R = 11.8×10^6. Concluded.

Figure 5.- Continued.

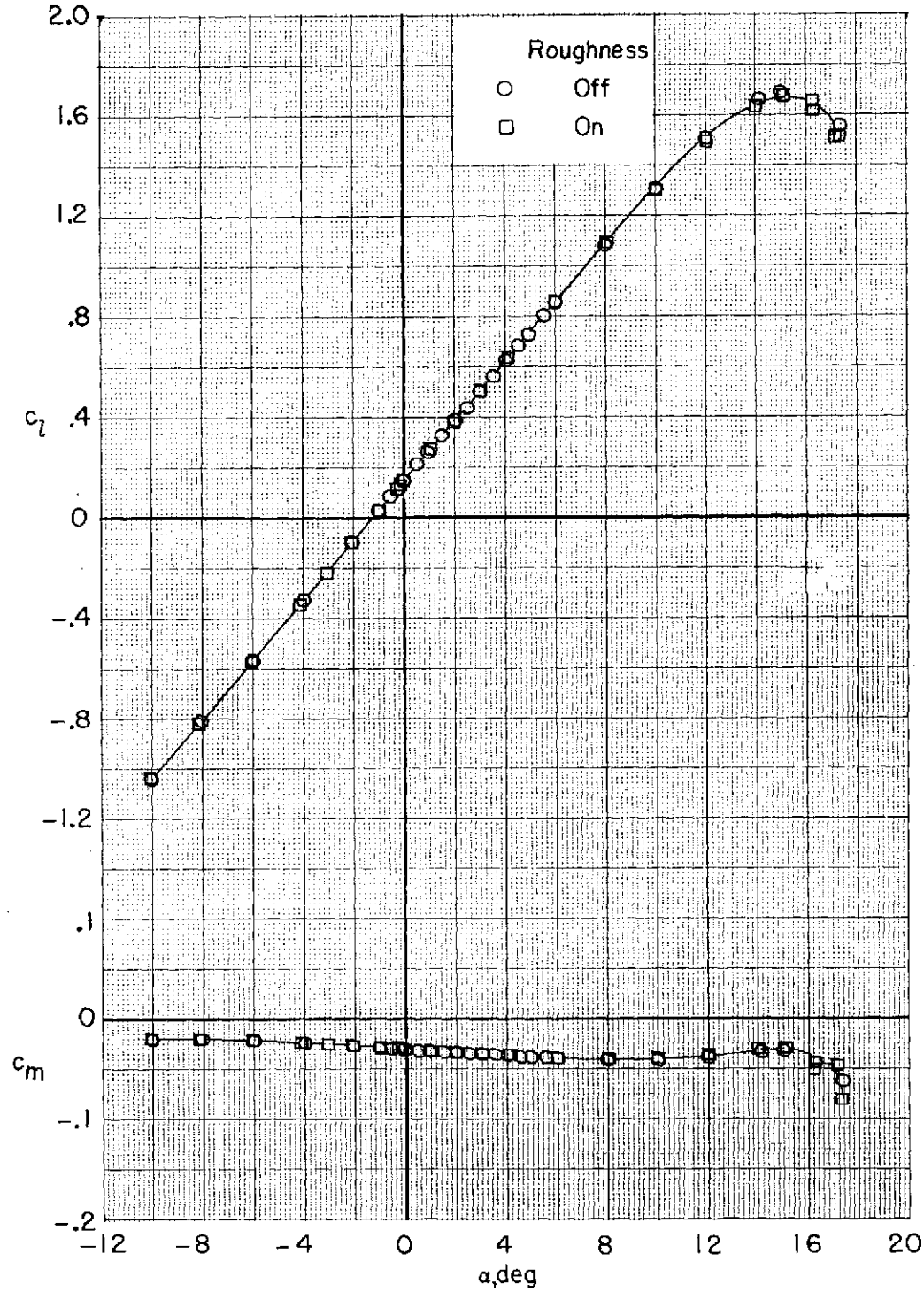

(e) $R = 14.5 \times 10^6$.

Figure 5.- Continued.

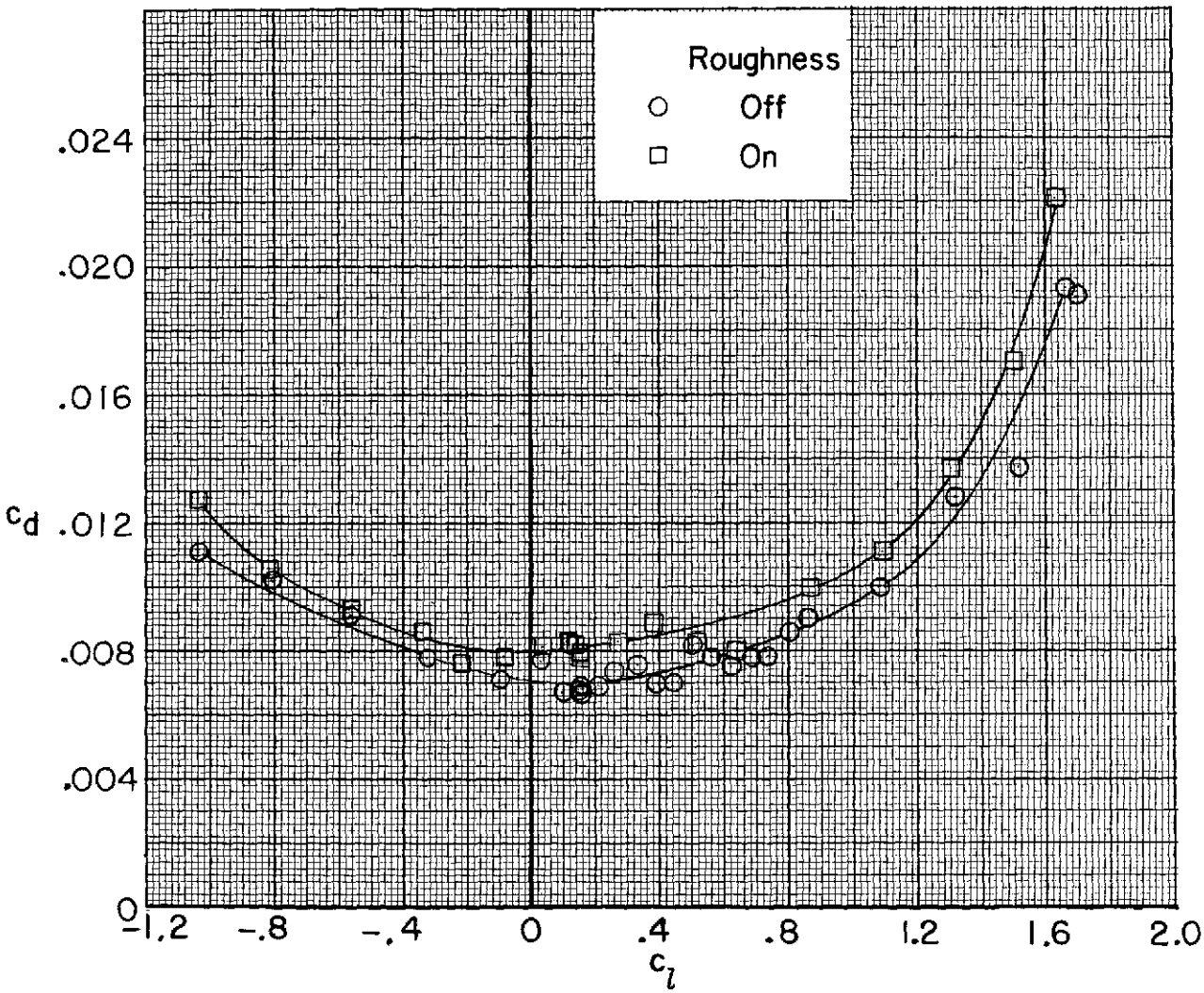

(e) R = 14.5×10^6. Concluded.

Figure 5.- Continued.

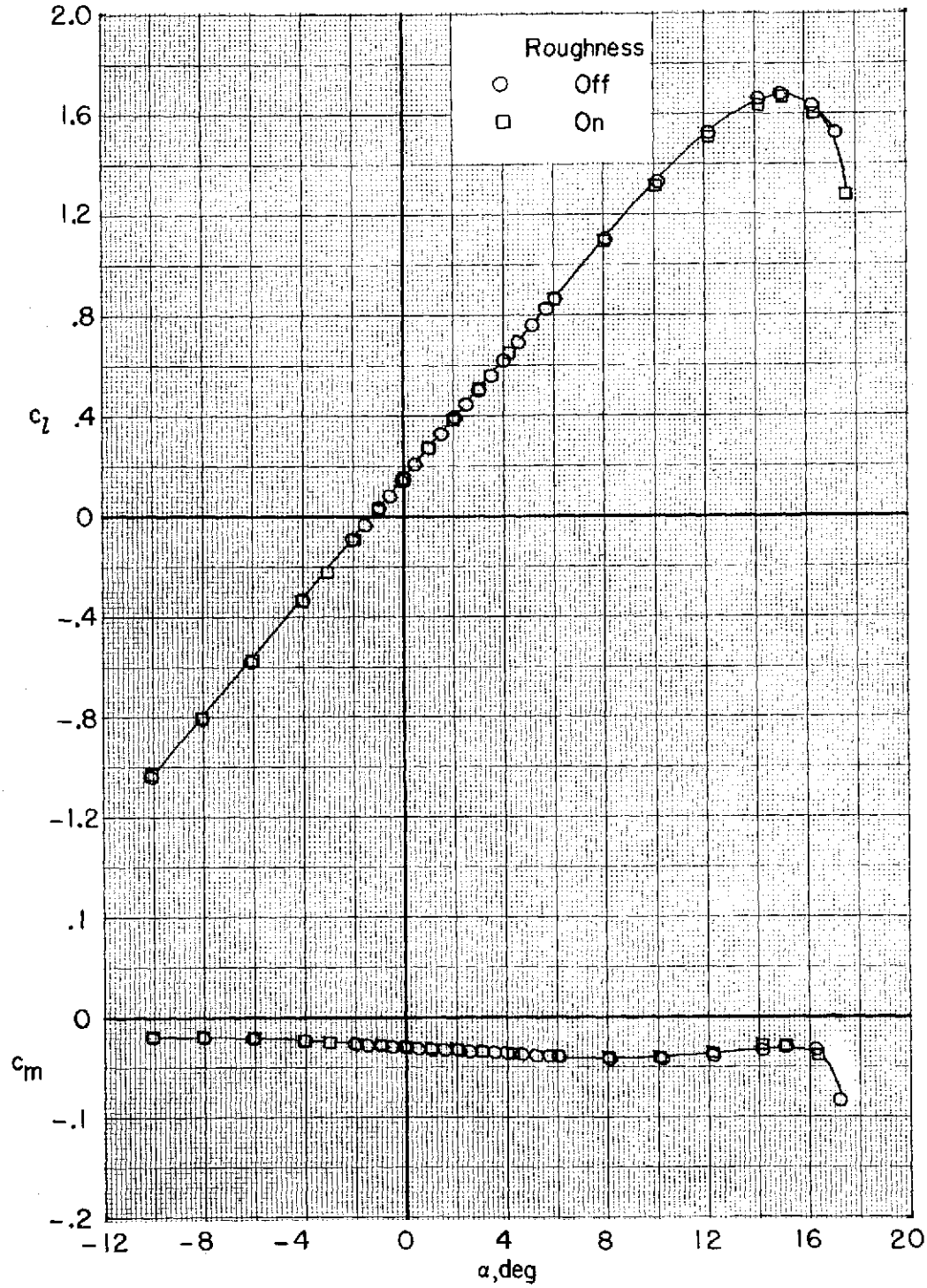

(f) $R = 17.4 \times 10^6$.

Figure 5.- Continued.

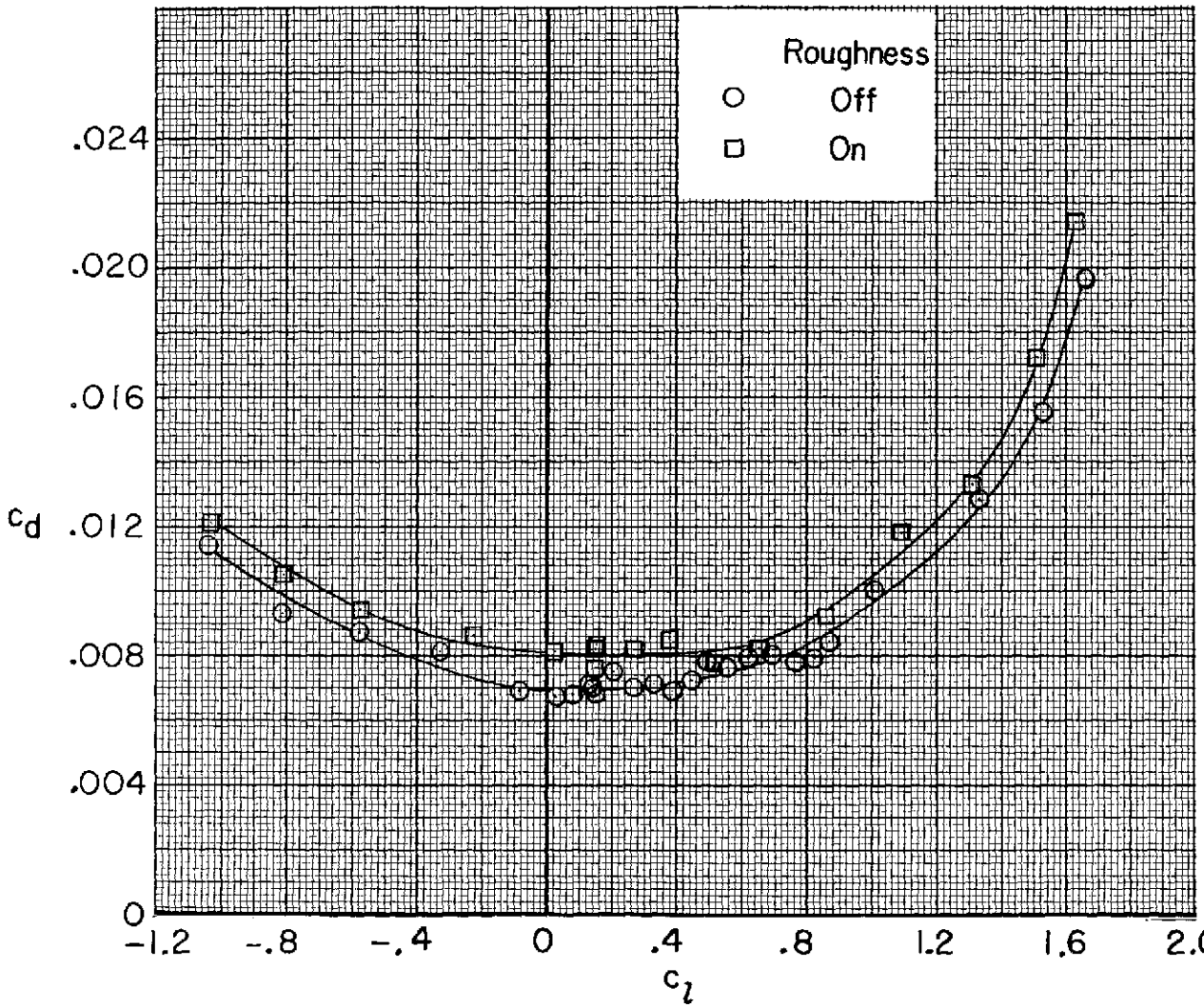

(f) R = 17.4×10^6. Concluded.

Figure 5.- Continued.

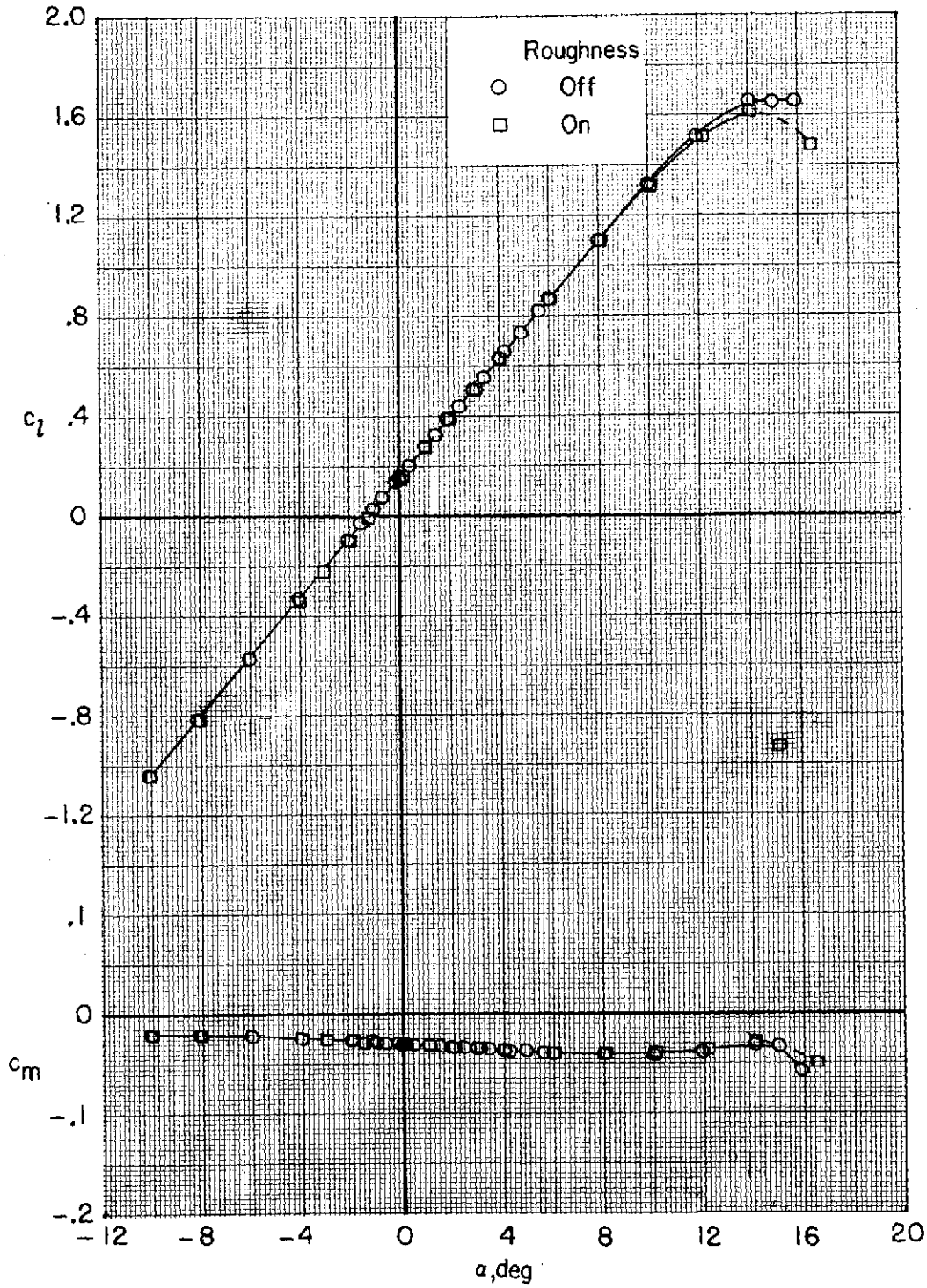

(g) $R = 22.8 \times 10^6$.

Figure 5.- Continued.

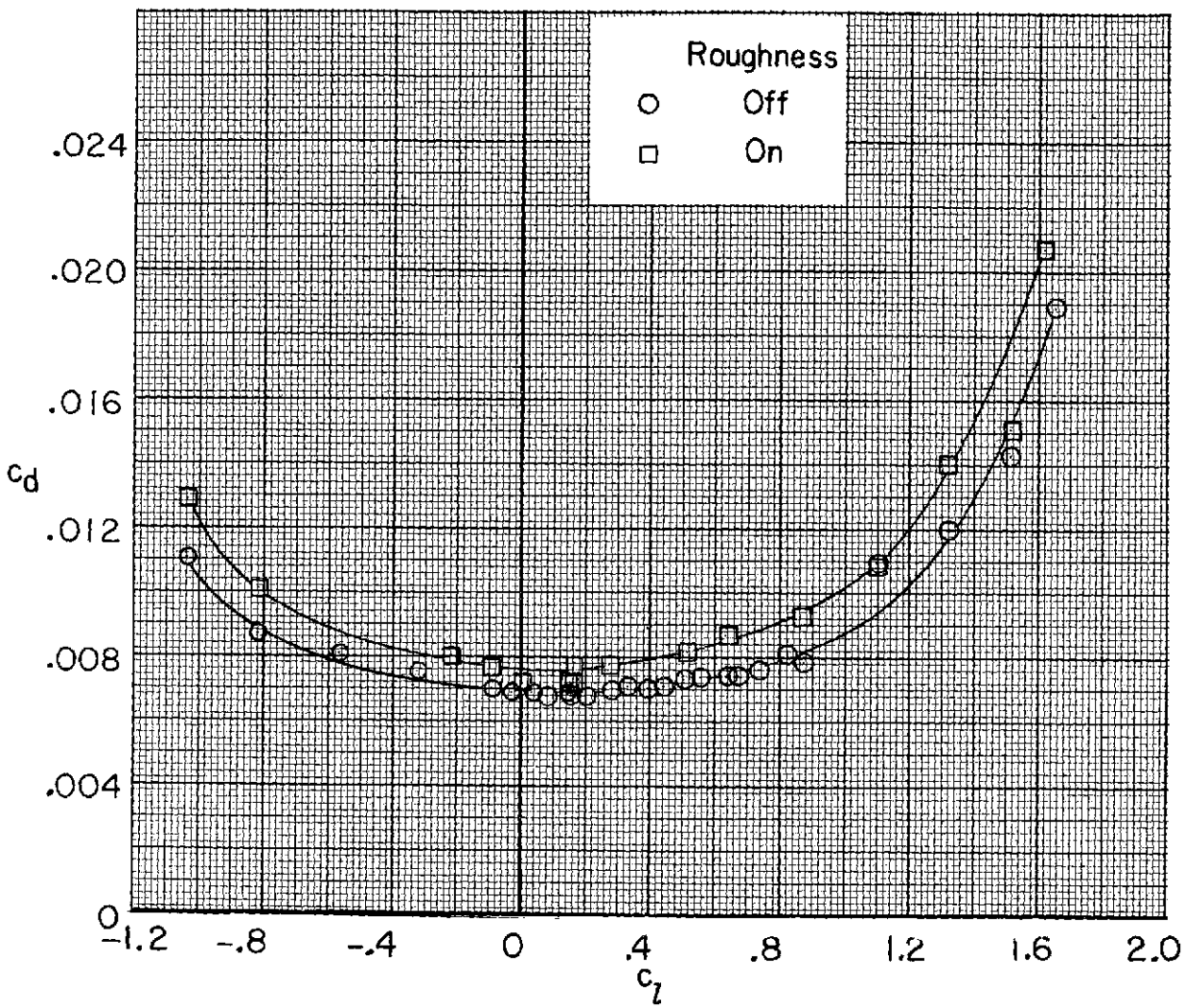

(g) $R = 22.8 \times 10^6$. Concluded.

Figure 5.- Concluded.

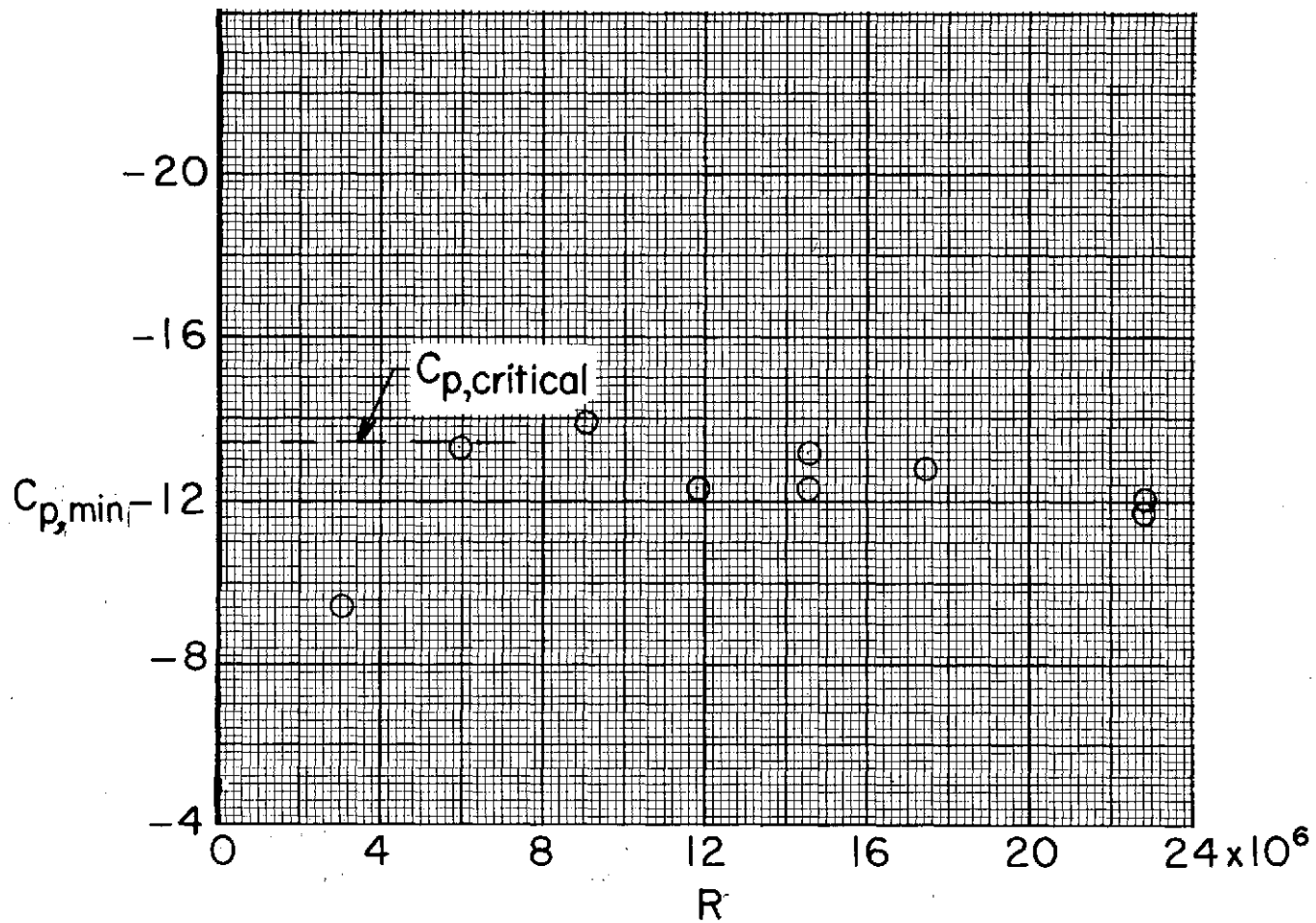

Figure 6.- Variation of airfoil minimum upper surface pressure coefficient with Reynolds numbers. M = 0.22; transition fixed at x/c = 0.05.

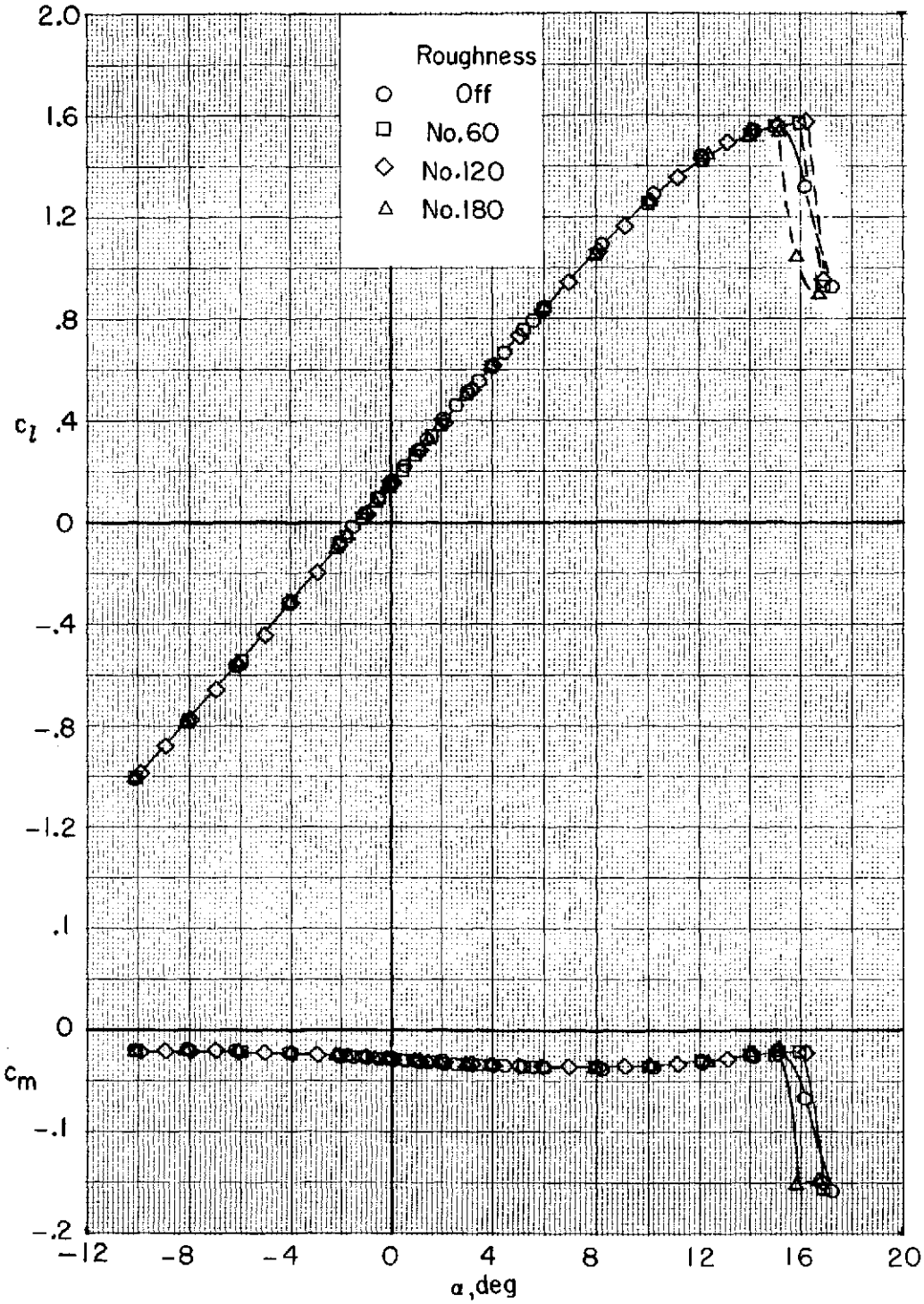

(a) Lift and moment data.

Figure 7.- Effect of various grit sizes on section characteristics. M = 0.22; R = 5.9×10^6; transition fixed at x/c = 0.05.

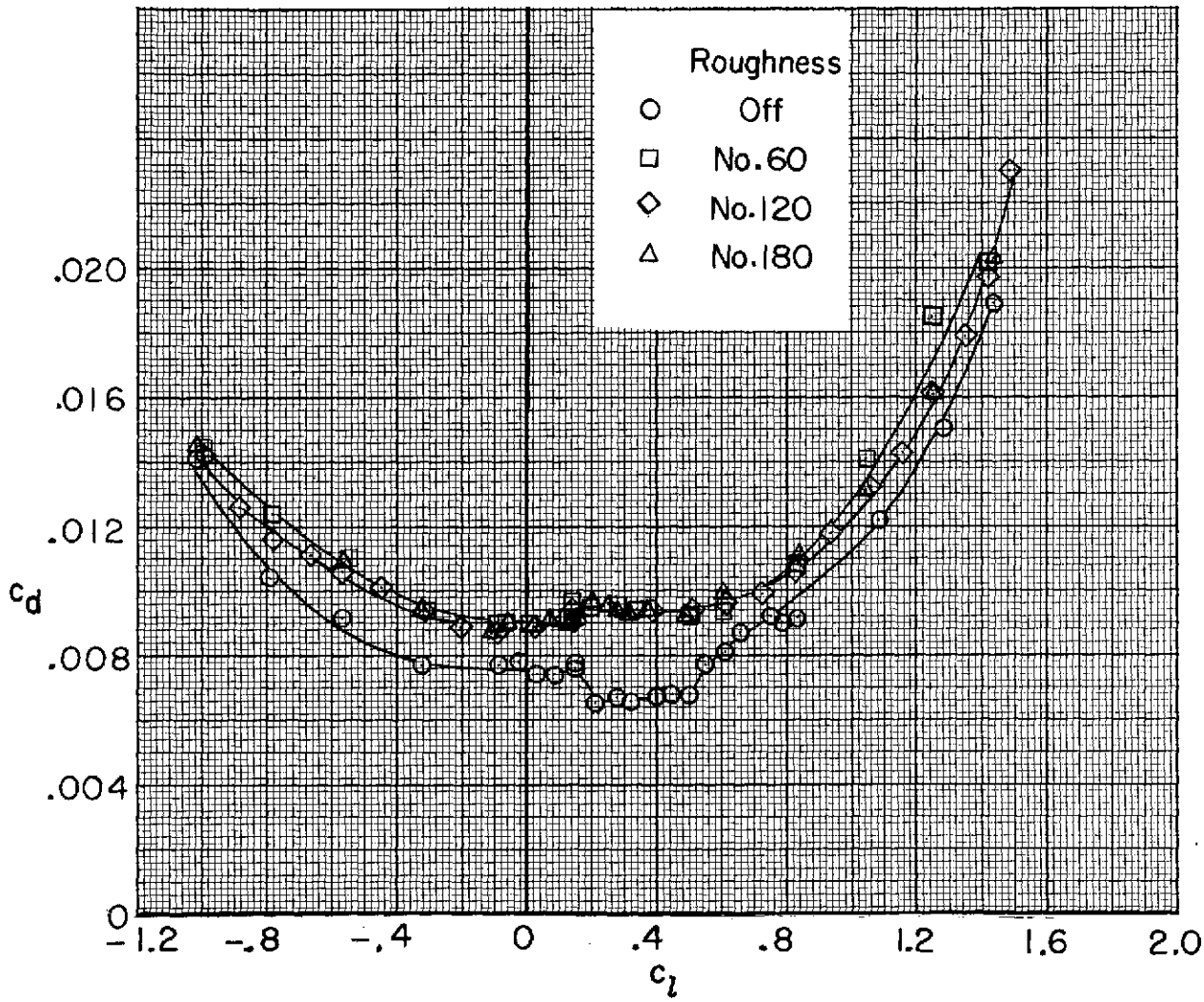

(b) Drag polars.

Figure 7.- Concluded.

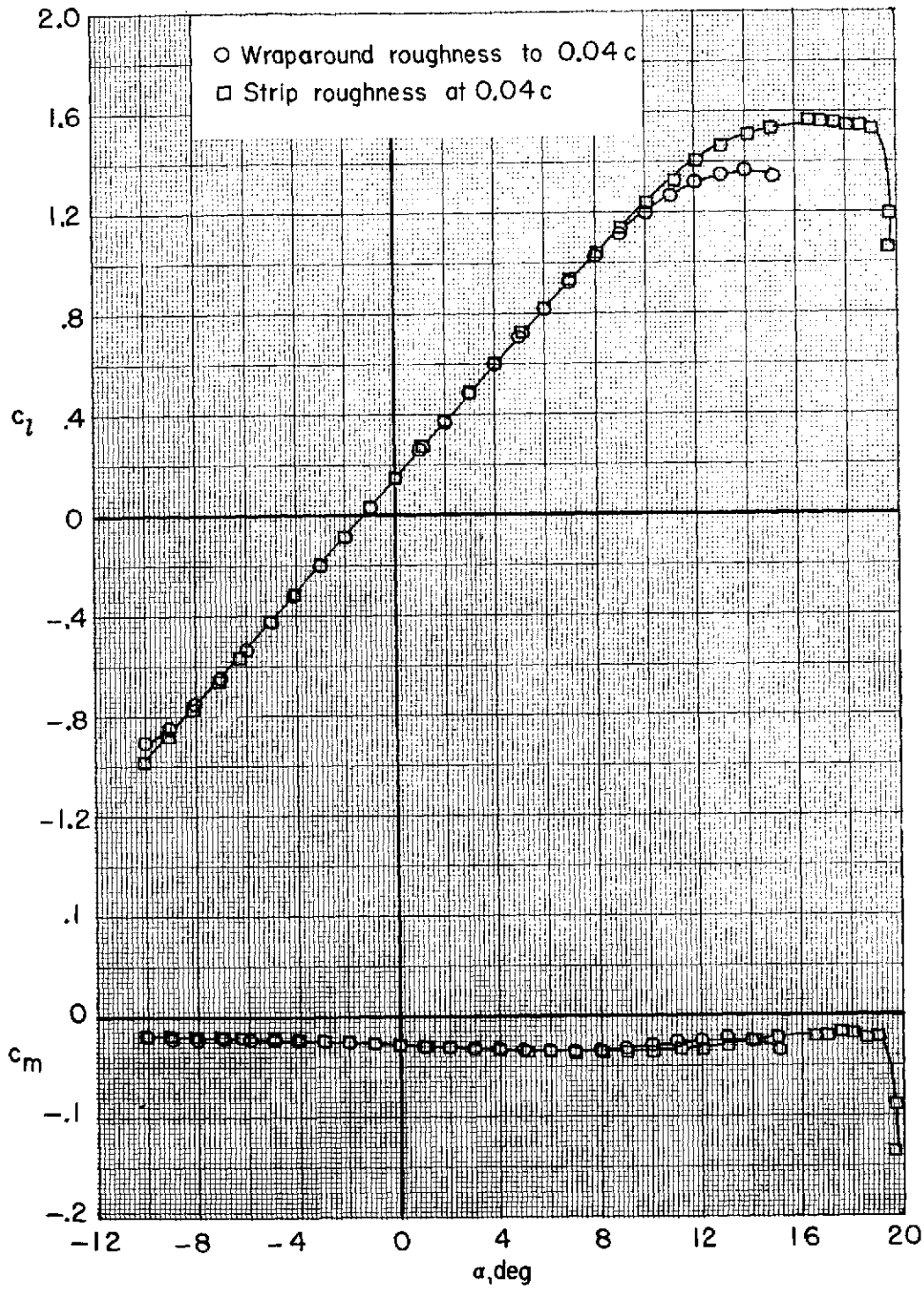

(a) Lift and moment data.

Figure 8.- Effect of the strip and wraparound roughness on section characteristics. M = 0.15; R = 5.9×10^6; no. 60 grit.

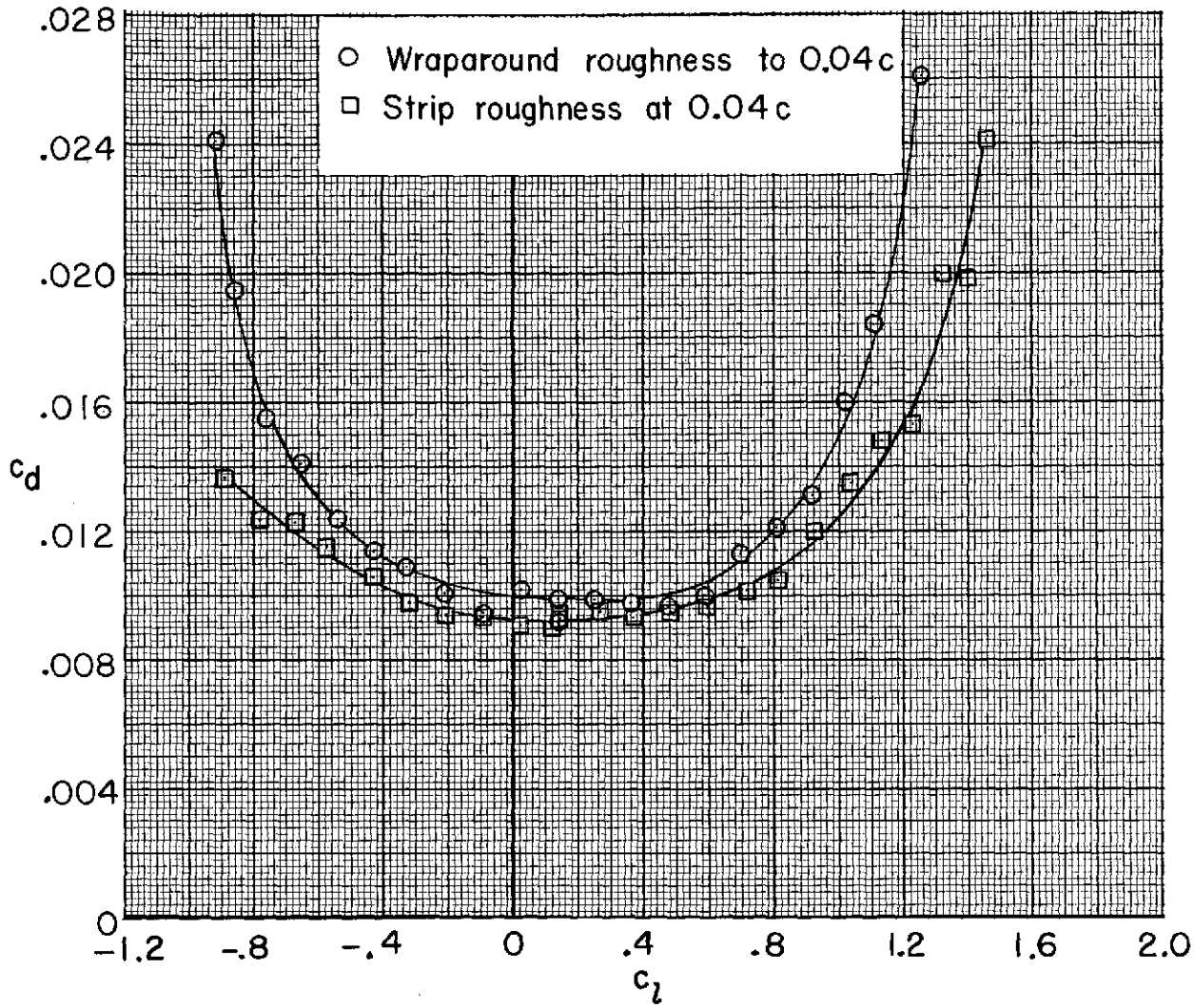

(b) Drag polars.

Figure 8.- Concluded.

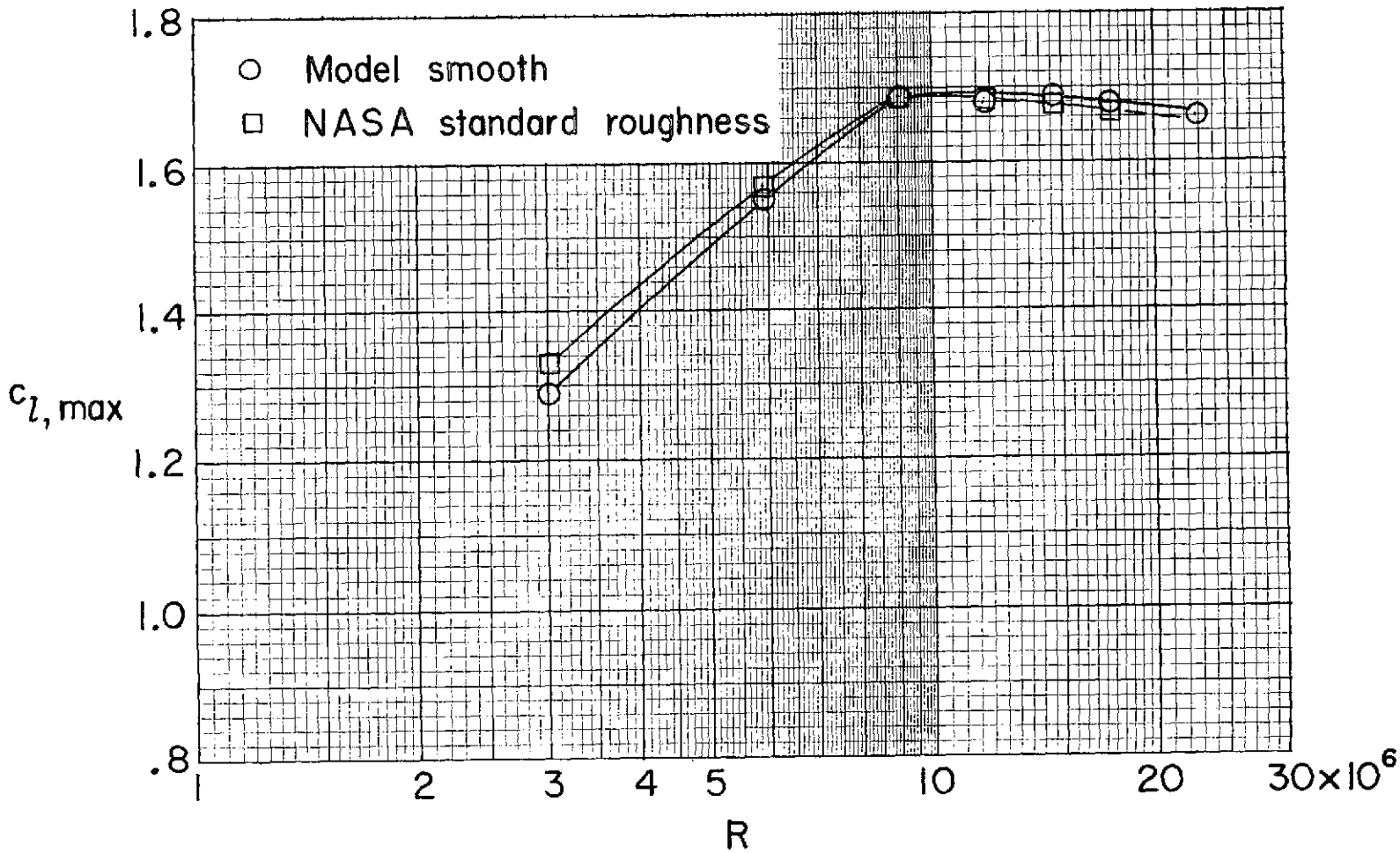

Figure 9.- Variation of maximum lift coefficient with Reynolds number. M = 0.22.

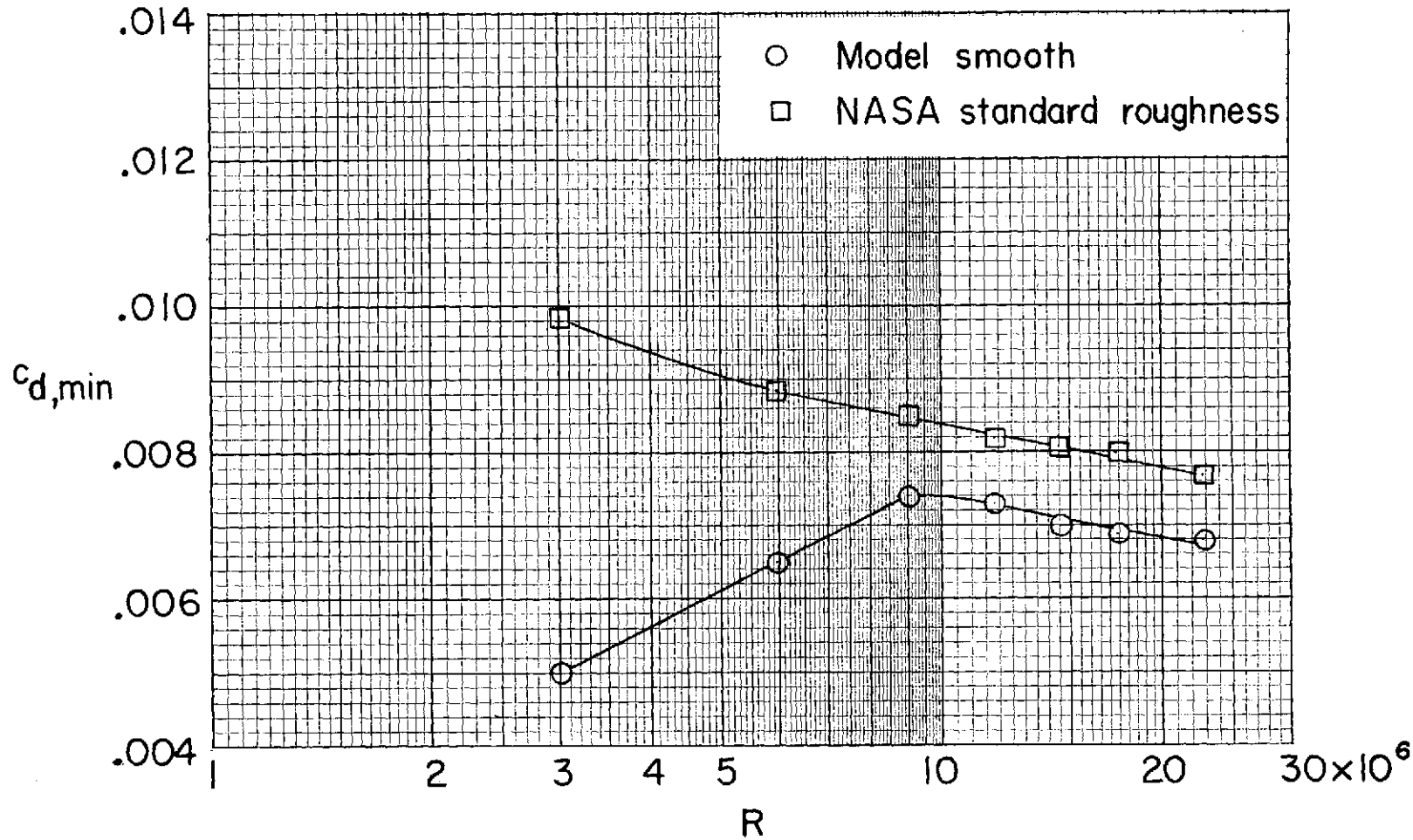

Figure 10.- Variation of minimum drag coefficient with Reynolds number. M = 0.22.

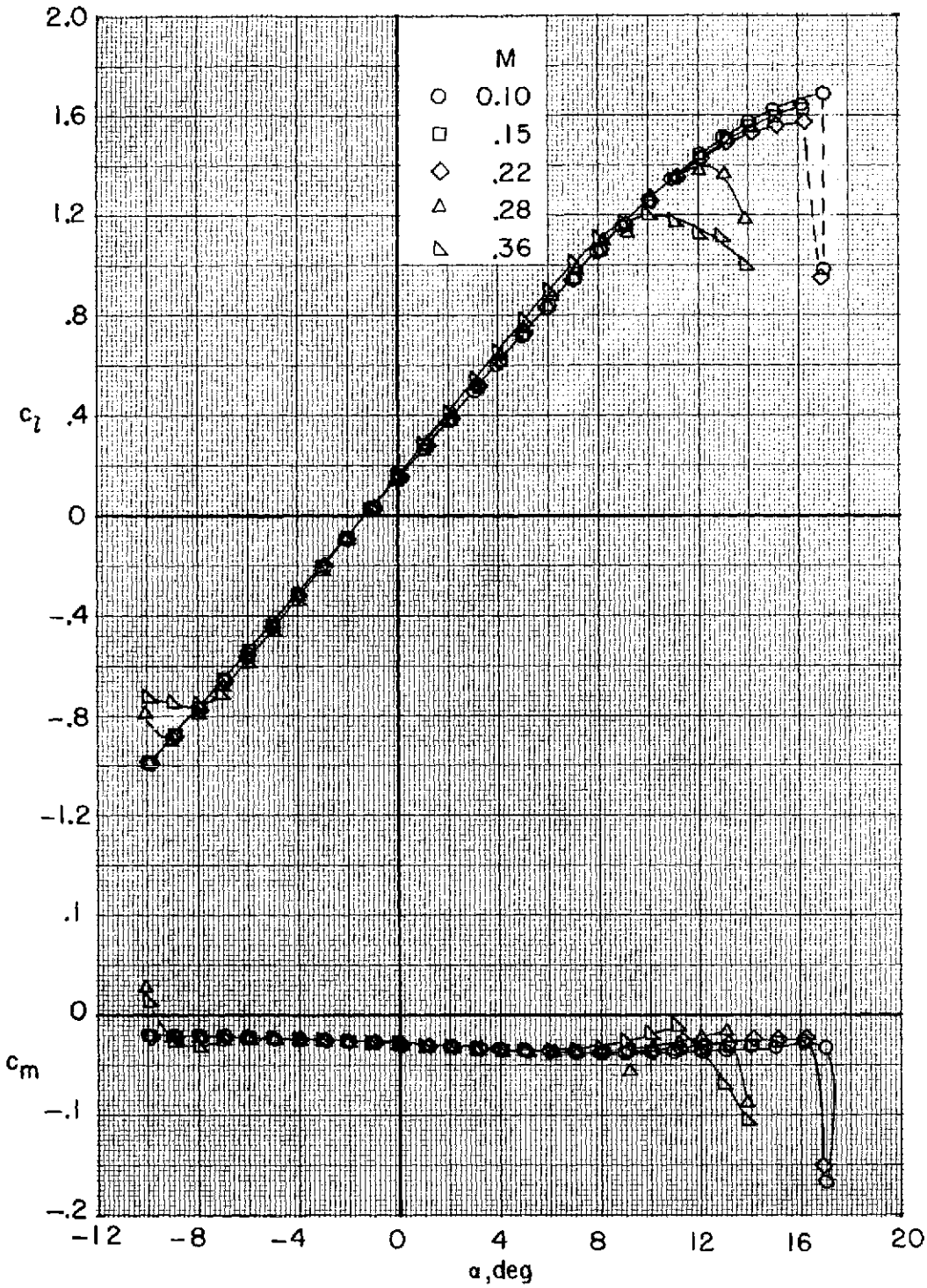

(a) Lift and moment data.

Figure 11.- Effect of Mach number on section characteristics and chordwise pressure distributions. $R = 5.9 \times 10^6$; transition fixed at $x/c = 0.05$.

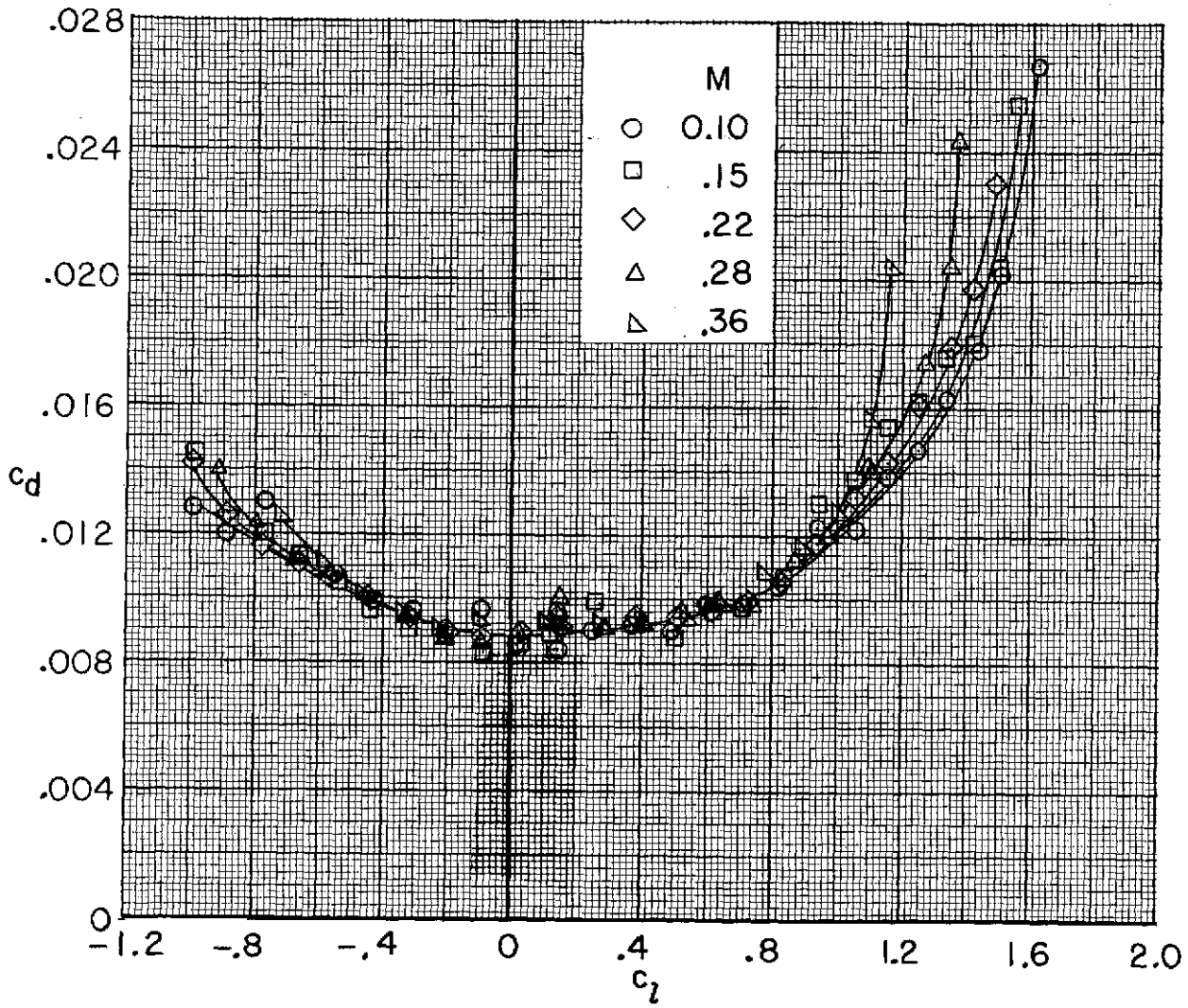

(b) Drag polars.

Figure 11.- Continued.

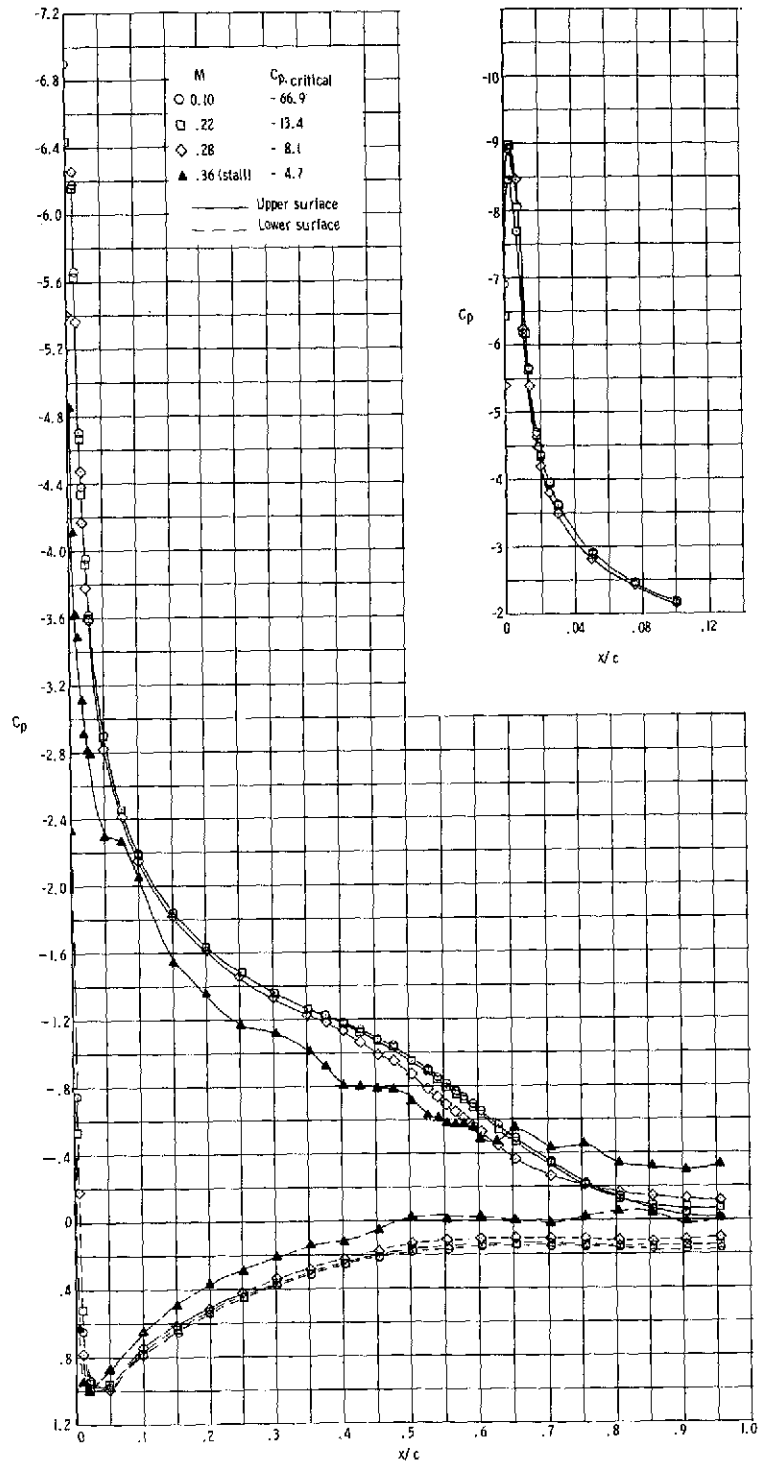

(c) Chordwise pressure distributions; $\alpha = 12^{o}$.

Figure 11.- Concluded.

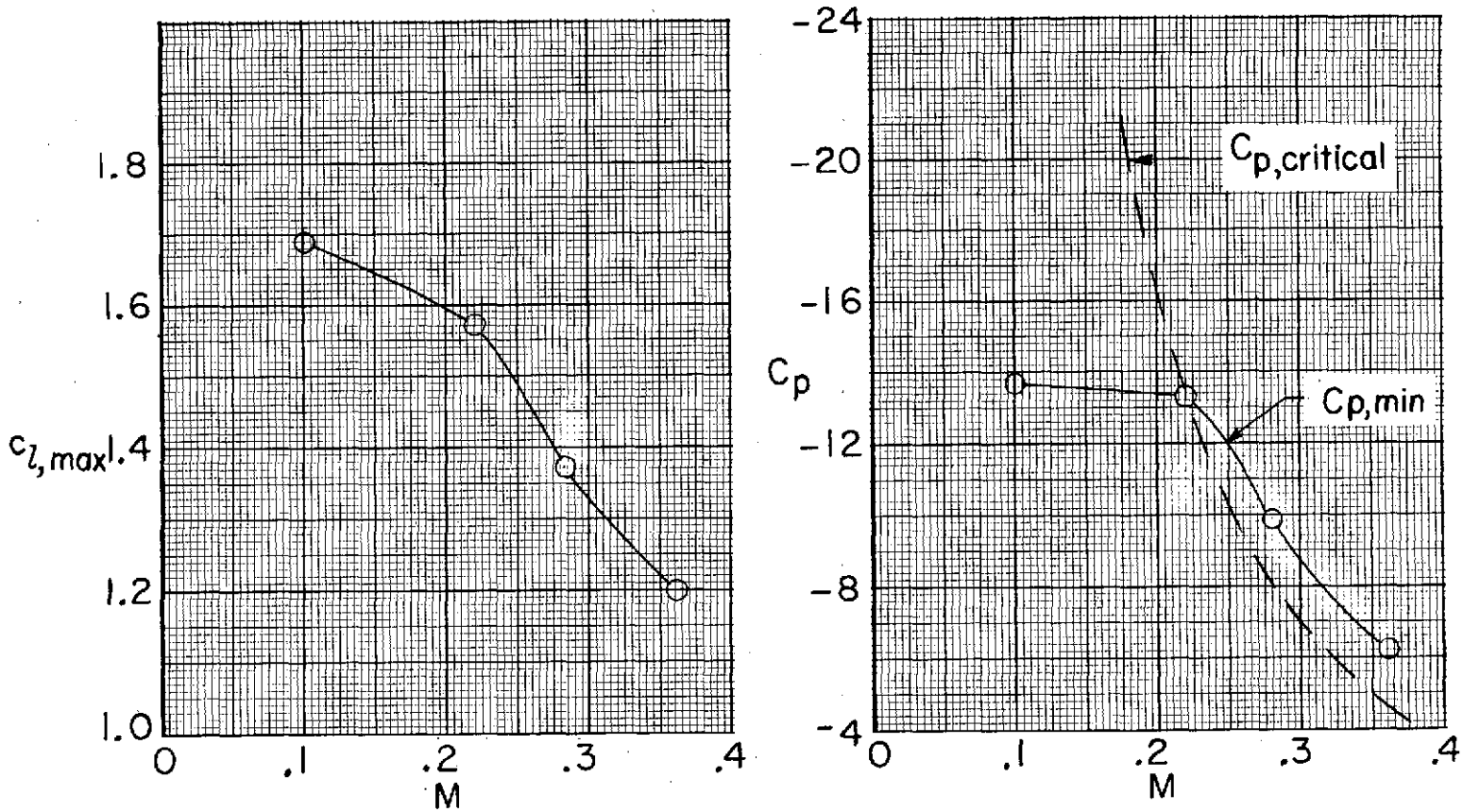

Figure 12.- Variation of maximum lift coefficient and airfoil minimum upper surface pressure coefficient with Mach number. $R = 5.9 \times 10^6$; transition fixed at $x/c = 0.05$.

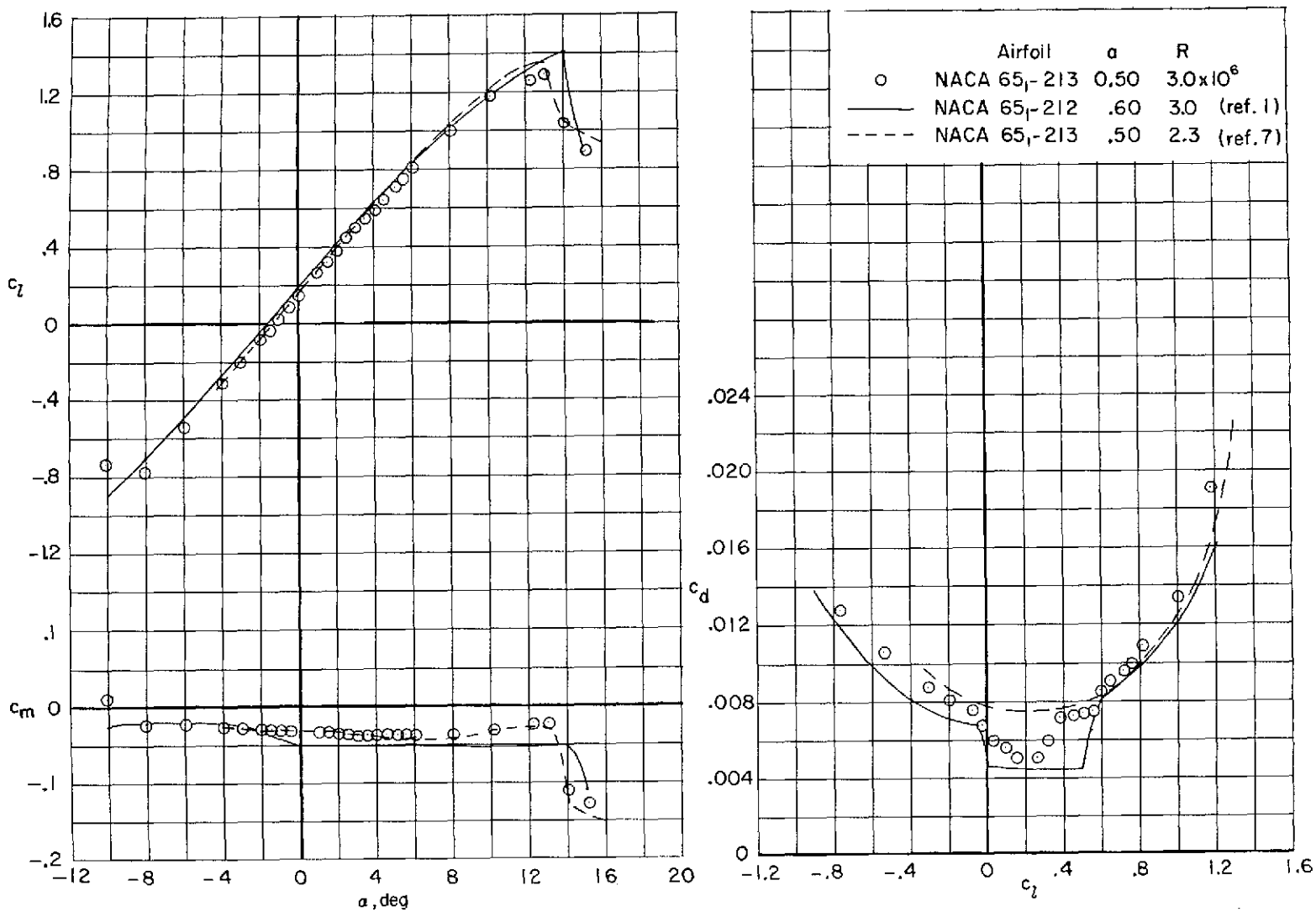

(a) $R = 2.3 \times 10^6$ and 3.0×10^6.

Figure 13.- Comparison of section characteristics for NACA 65_1-212 (a = 0.60) and 65_1-213 (a = 0.50) airfoils. Models smooth; $M \leq 0.22$.

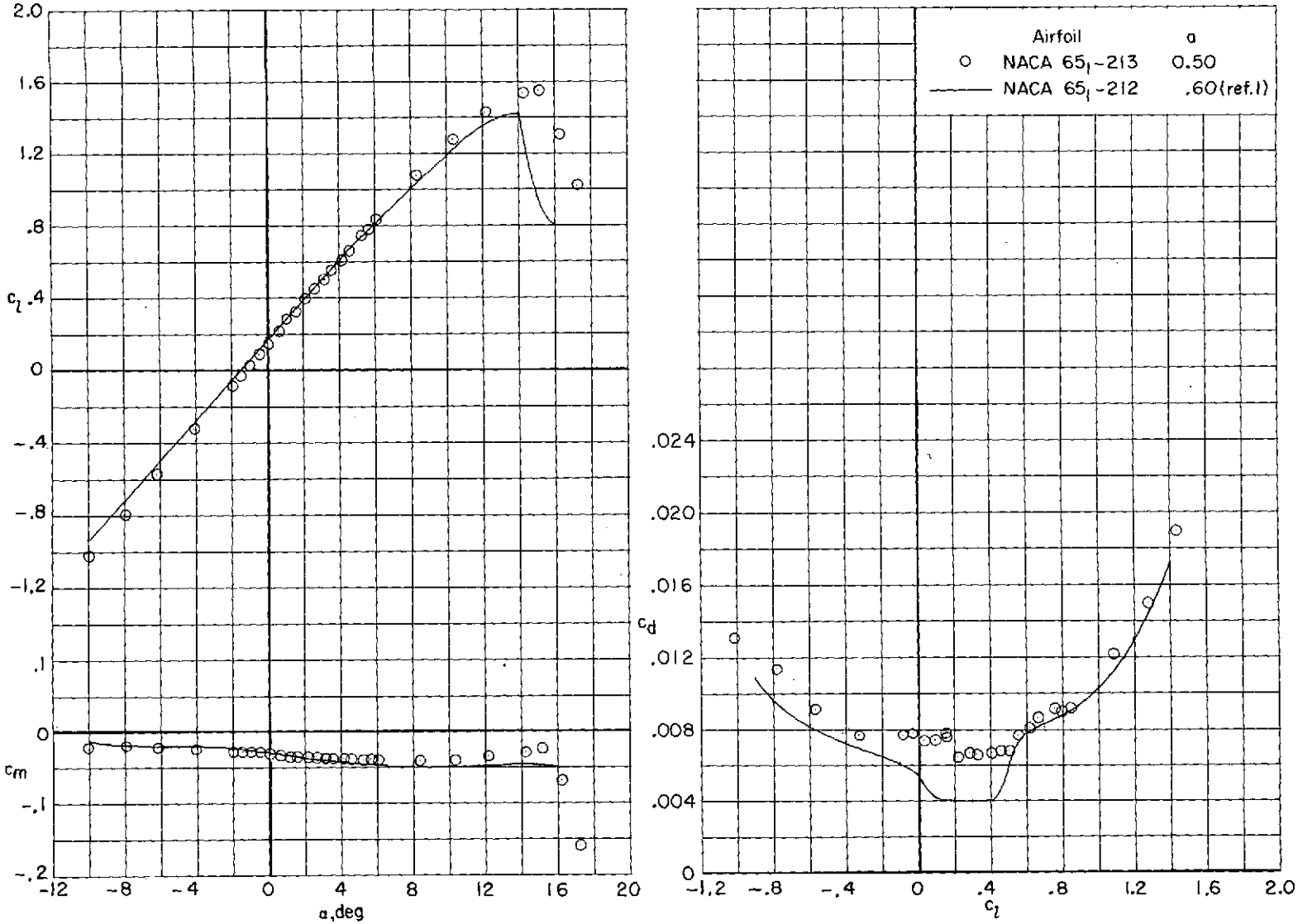

(b) $R \approx 6.0 \times 10^6$.

Figure 13.- Concluded.

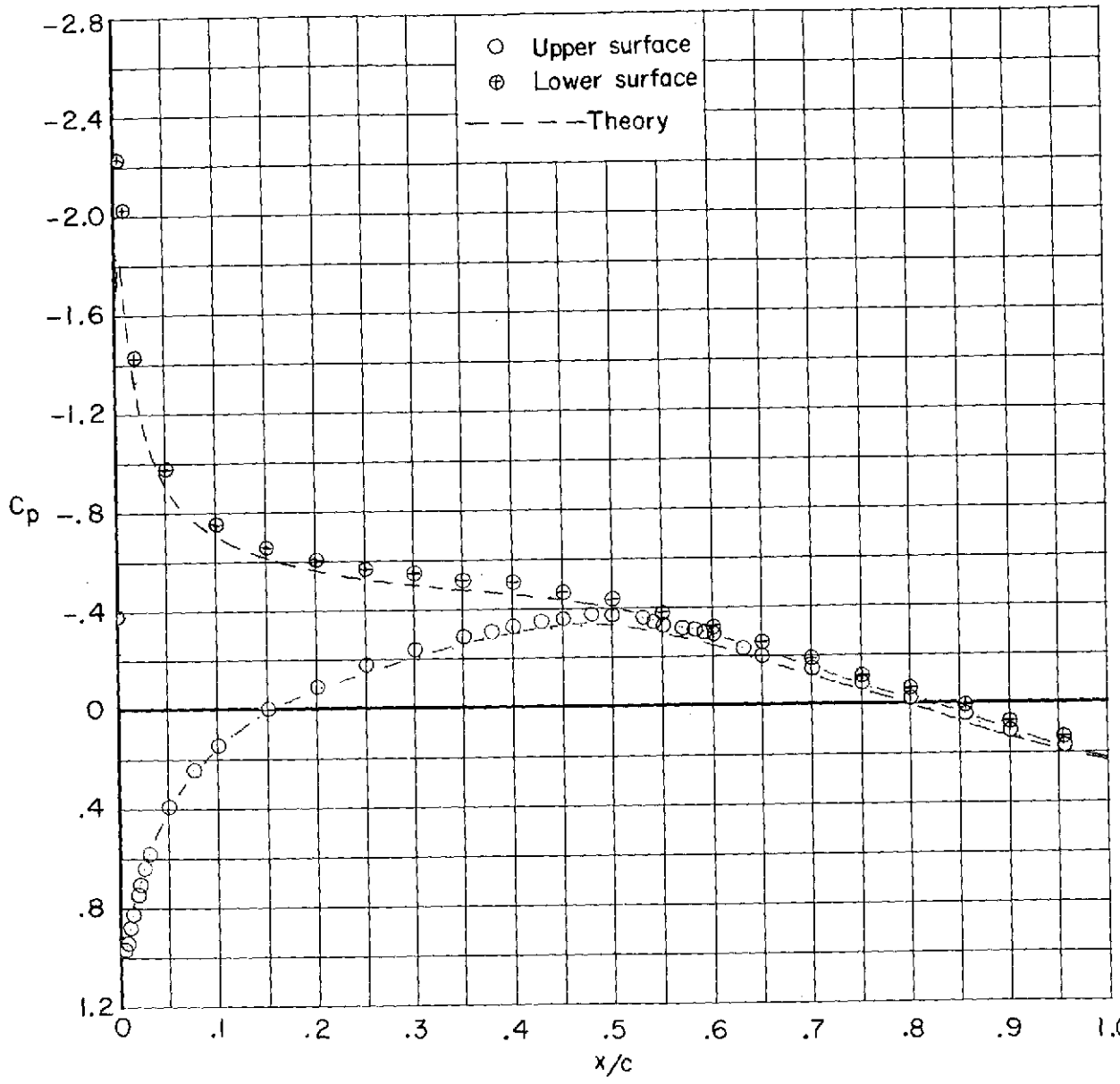

(a) $\alpha = -4.1^{o}$.

Figure 14.- Comparison of experimental and theoretical chordwise pressure distributions. M = 0.22; R = 5.9×10^{6}; model smooth.

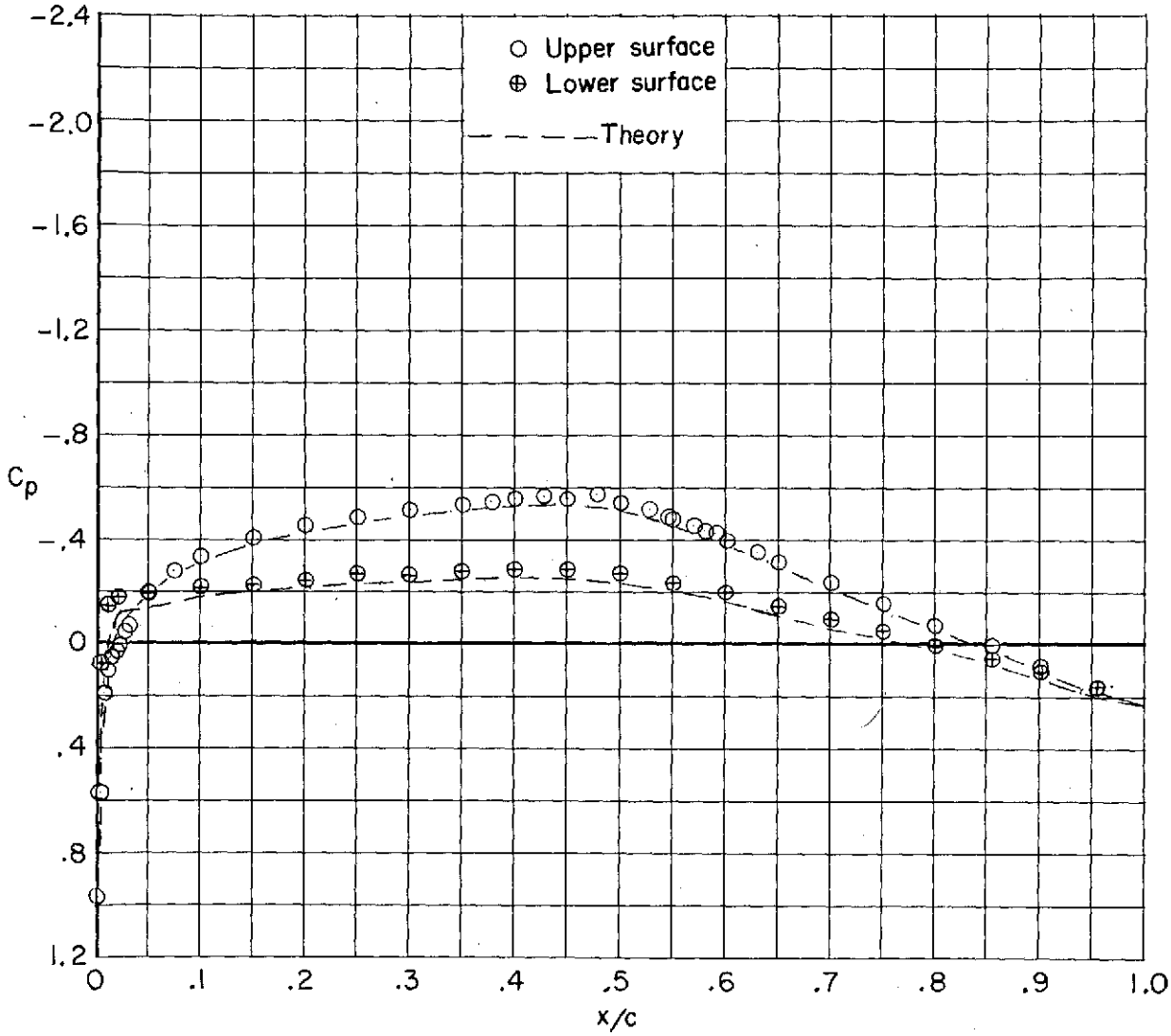

(b) $\alpha = 0.0^{o}$.

Figure 14.- Continued.

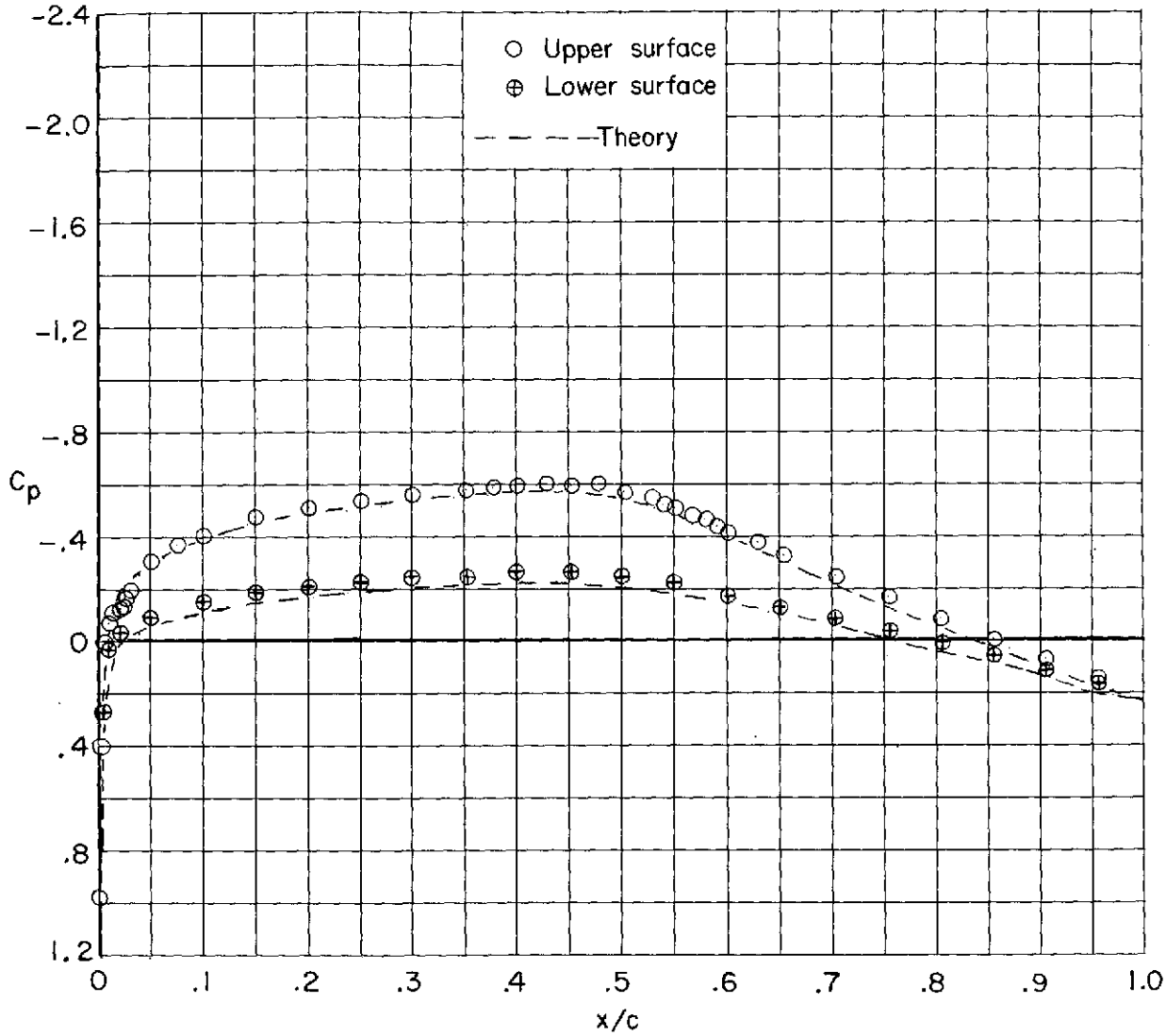

(c) $\alpha = 0.60^{\circ}$.

Figure 14.- Continued.

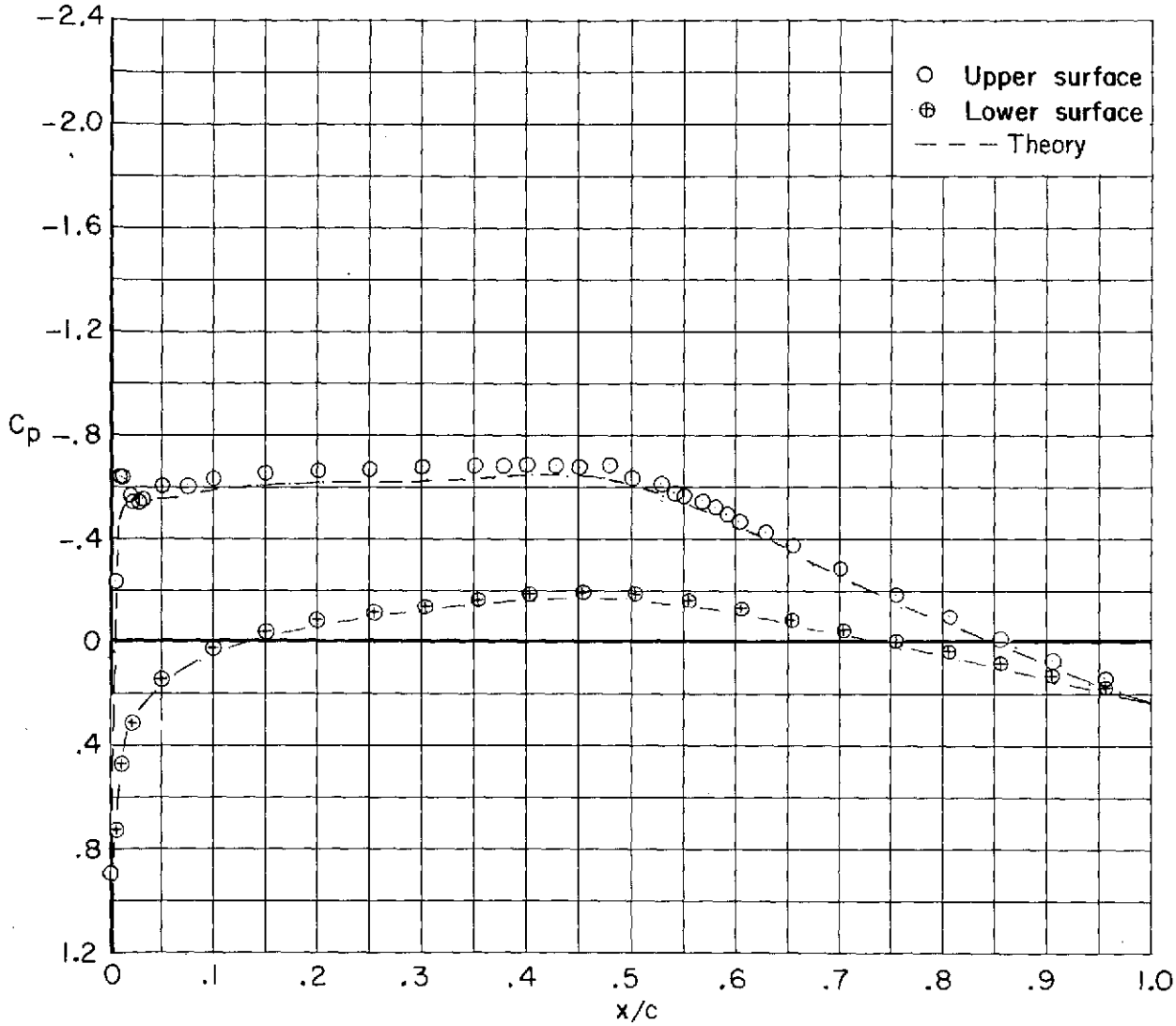

(d) $\alpha = 2.1^{\circ}$.

Figure 14.- Continued.

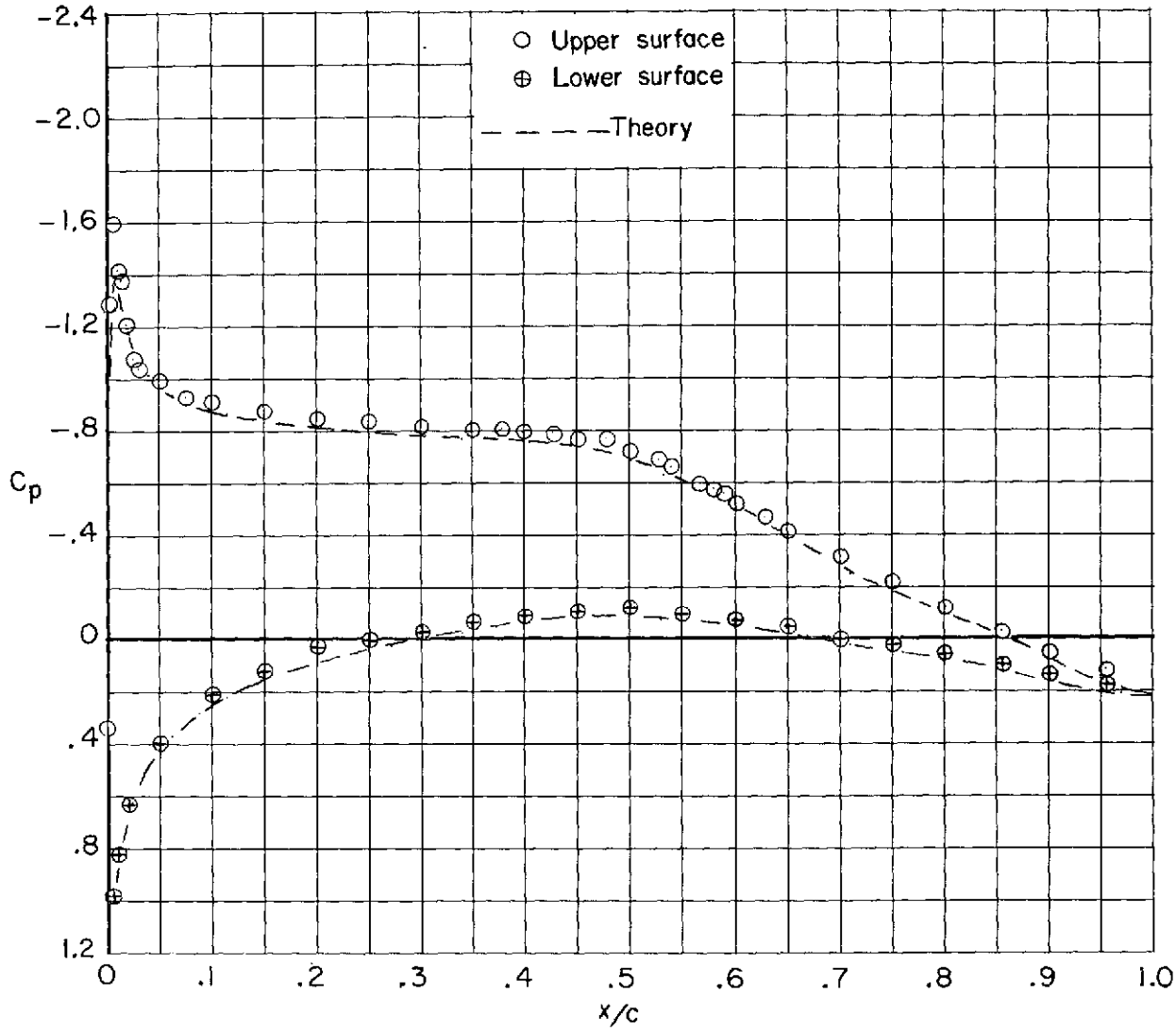

(e) $\alpha = 4.1^{o}$.

Figure 14.- Continued.

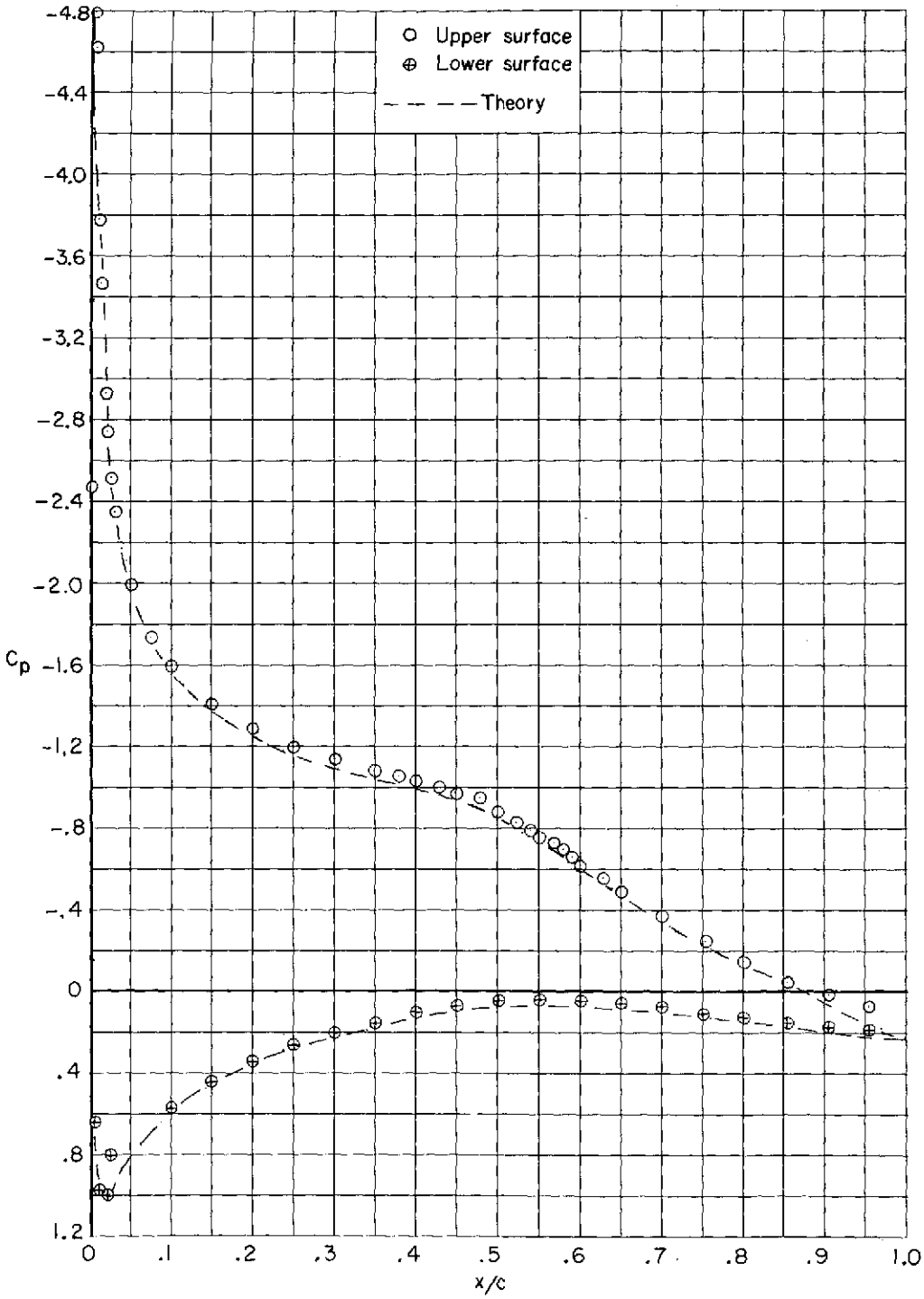

(f) $\alpha = 8.3^{\circ}$.

Figure 14.- Continued.

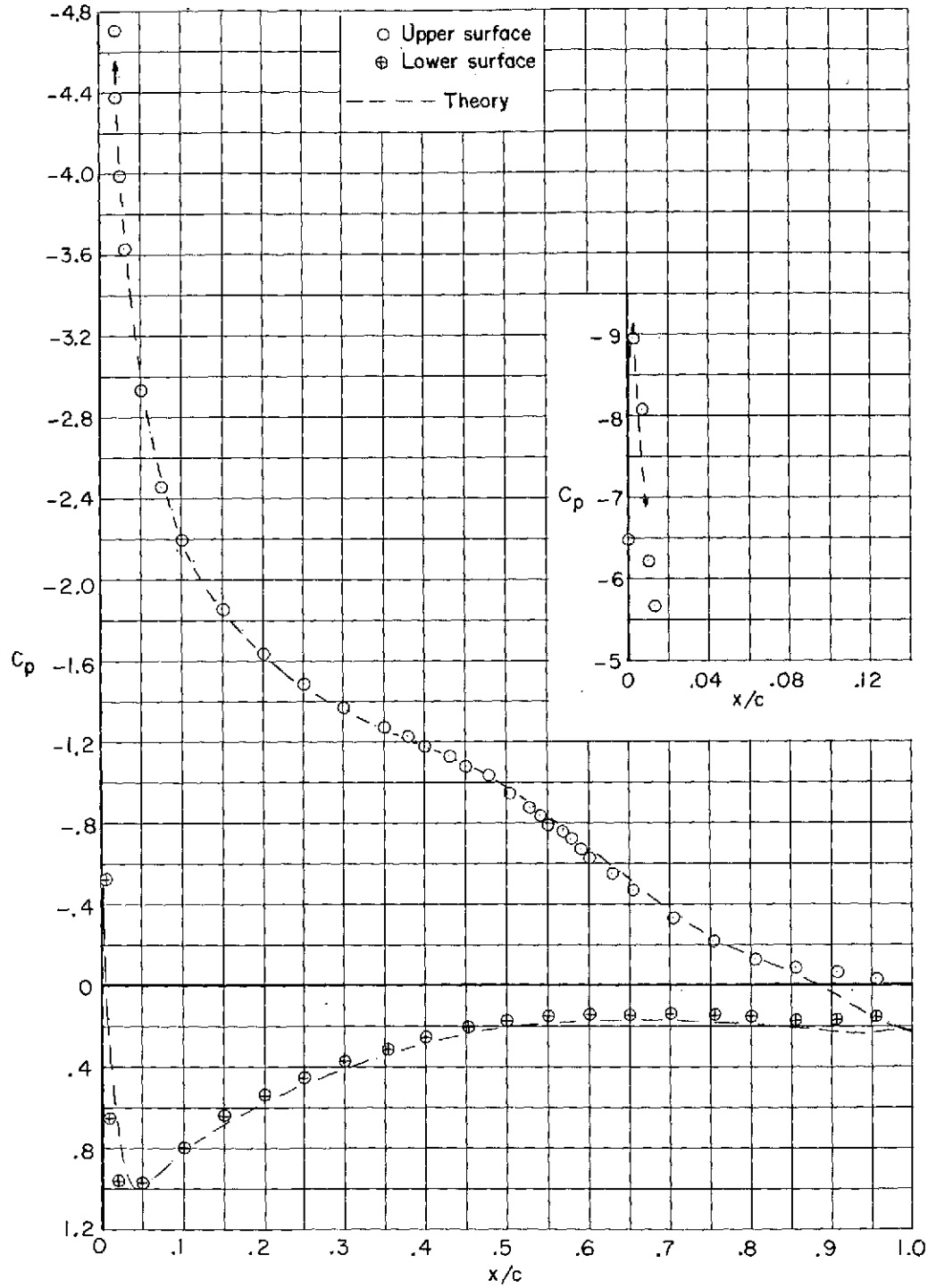

(g) $\alpha = 12.1^{\circ}$.

Figure 14.- Continued.

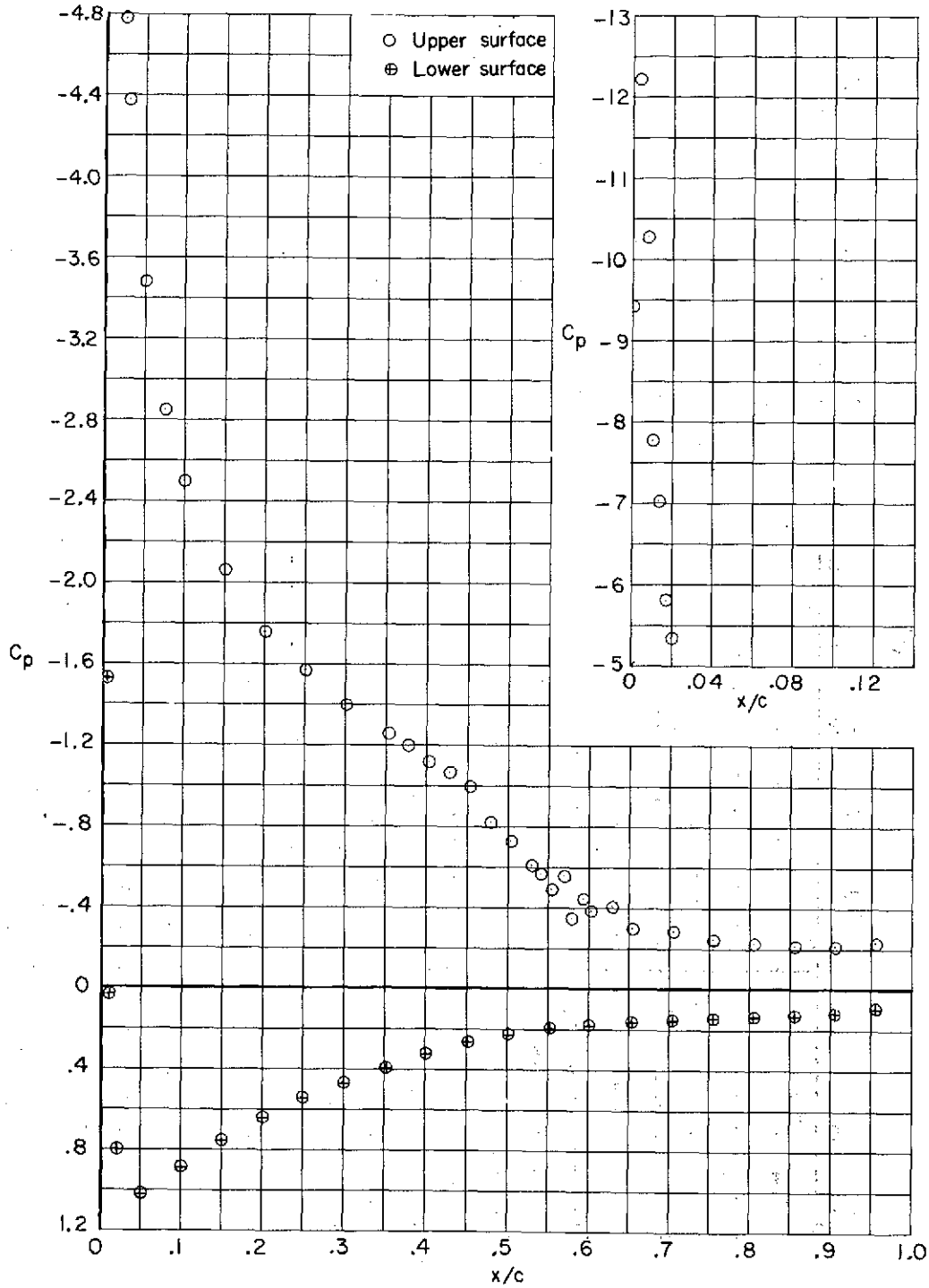

(h) $\alpha = 15.1^{\circ}$.

Figure 14.- Continued.

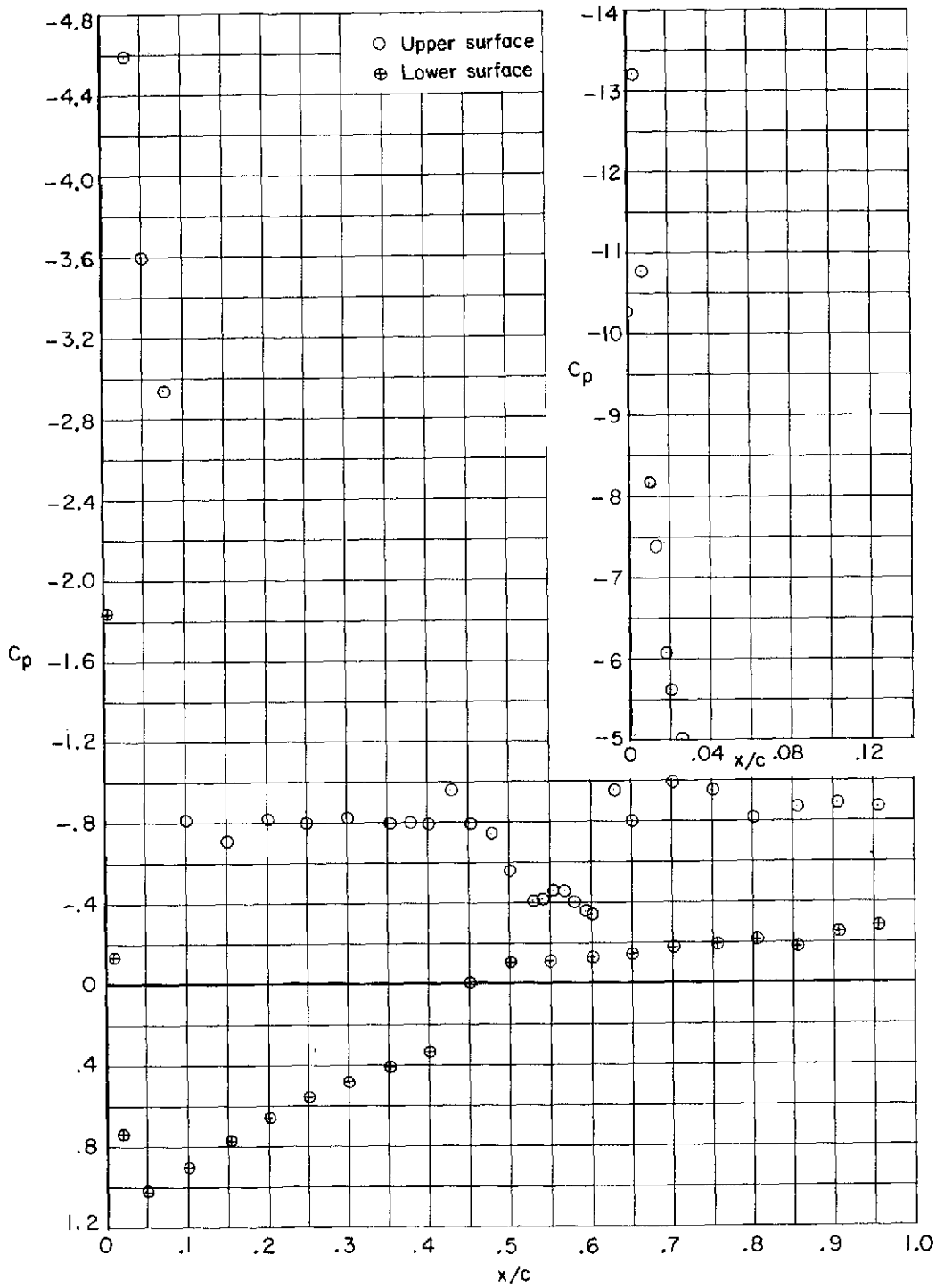

(i) $\alpha = 16.2^{\circ}$.

Figure 14.- Concluded.

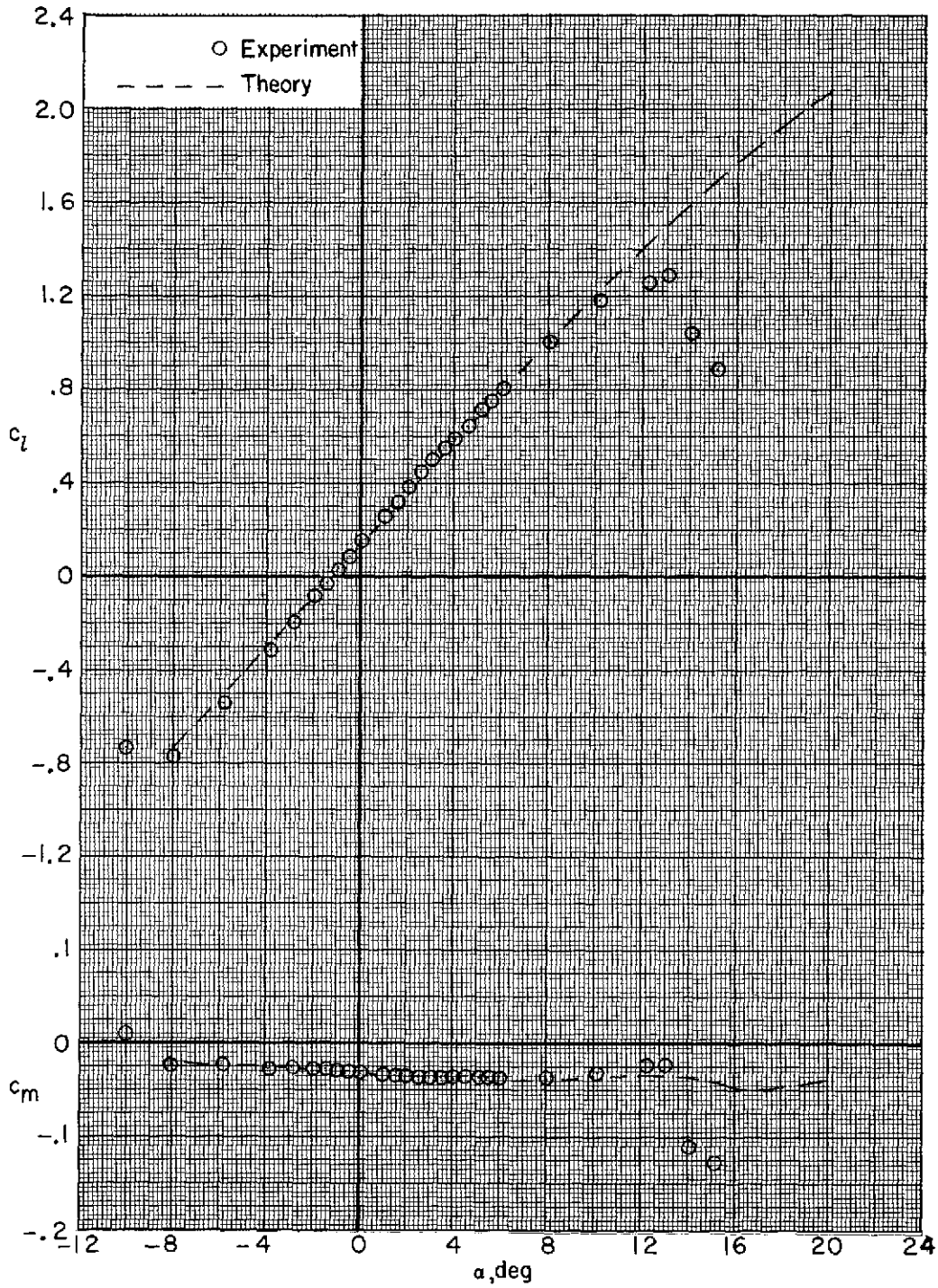

(a) $R = 3.0 \times 10^6$; model smooth.

Figure 15.- Comparison of experimental and theoretical section characteristics. M = 0.22.

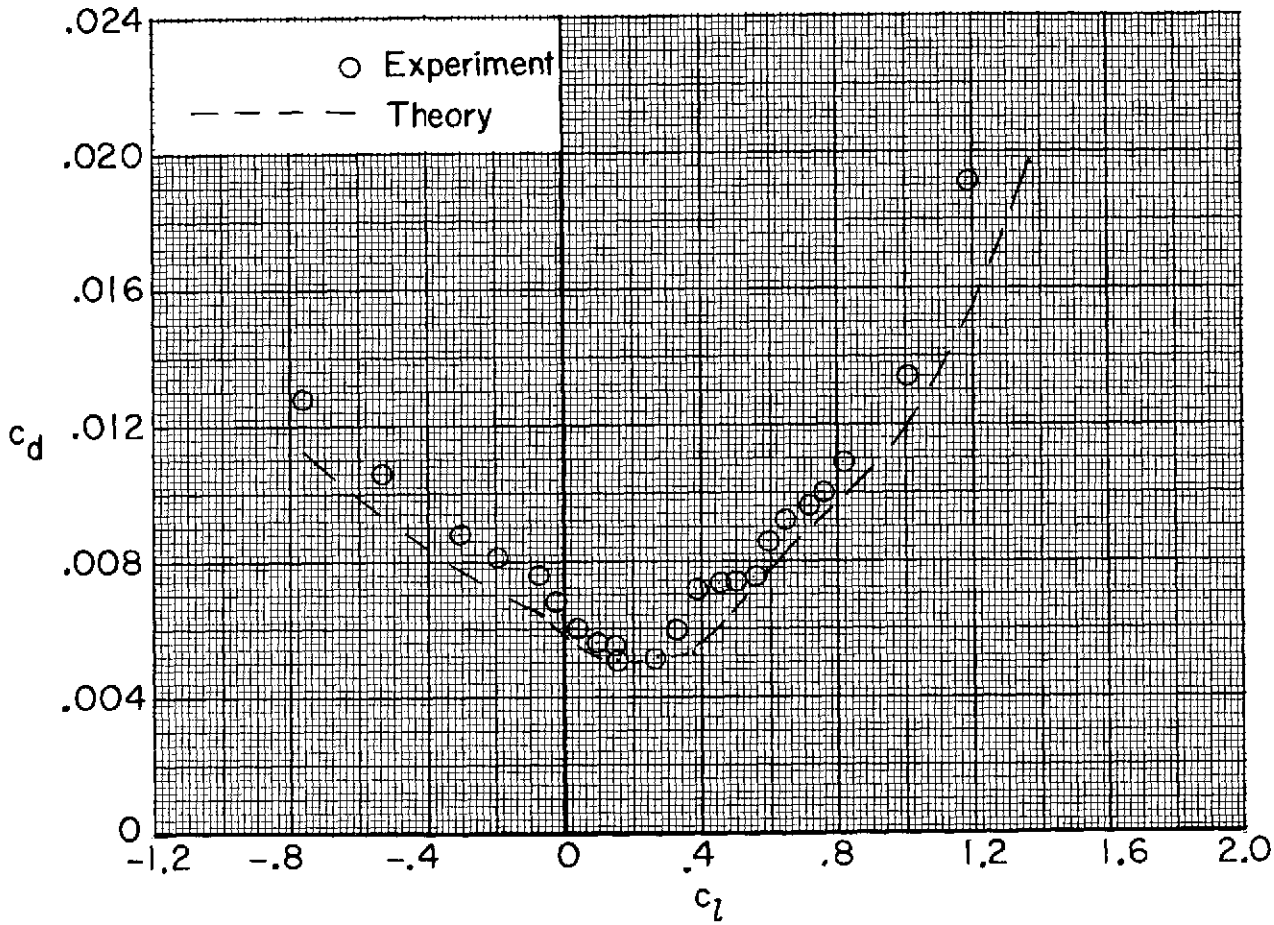

(a) $R = 3.0 \times 10^6$. Concluded.

Figure 15.- Continued.

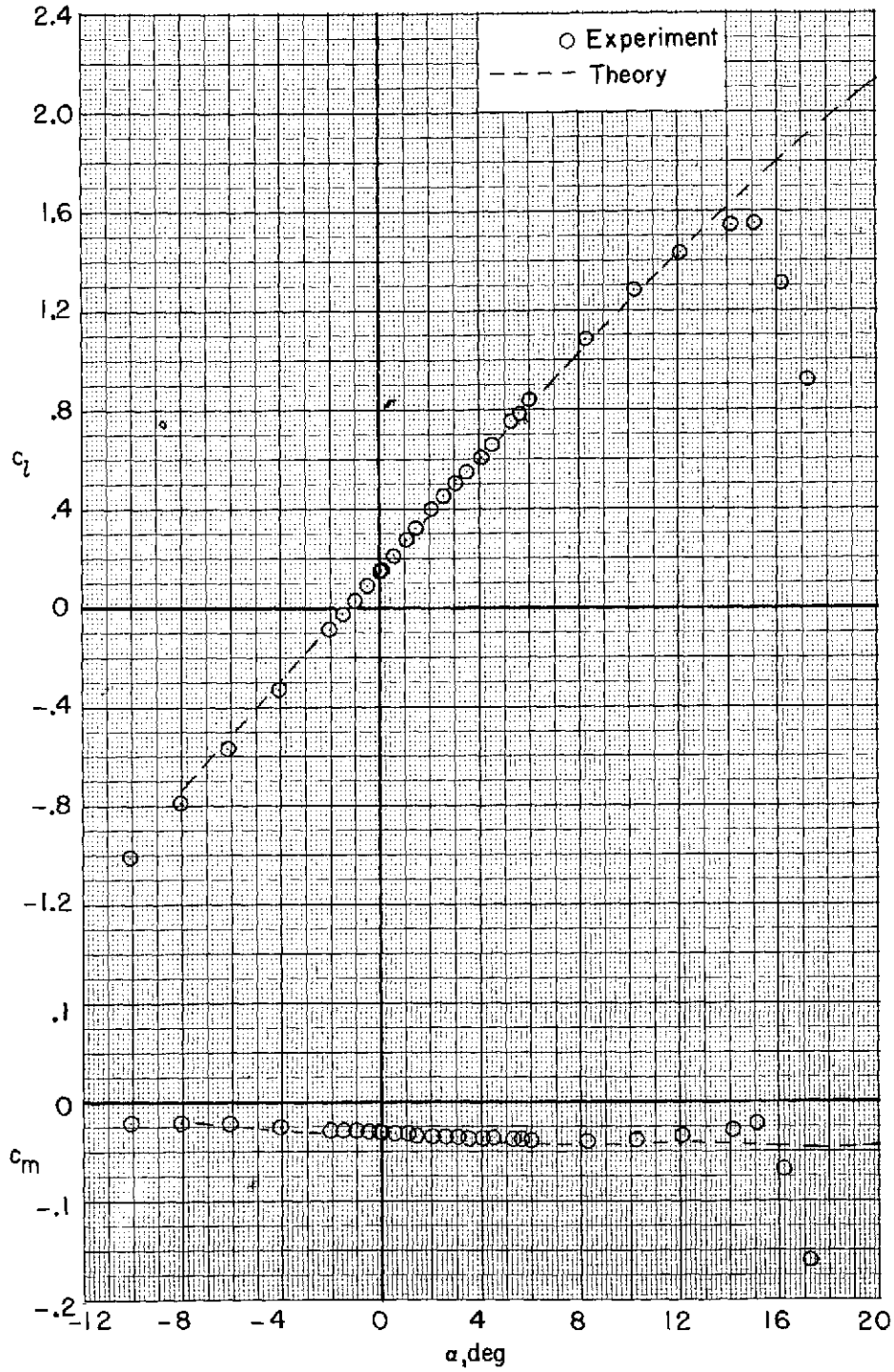

(b) $R = 5.9 \times 10^6$; model smooth.

Figure 15.- Continued.

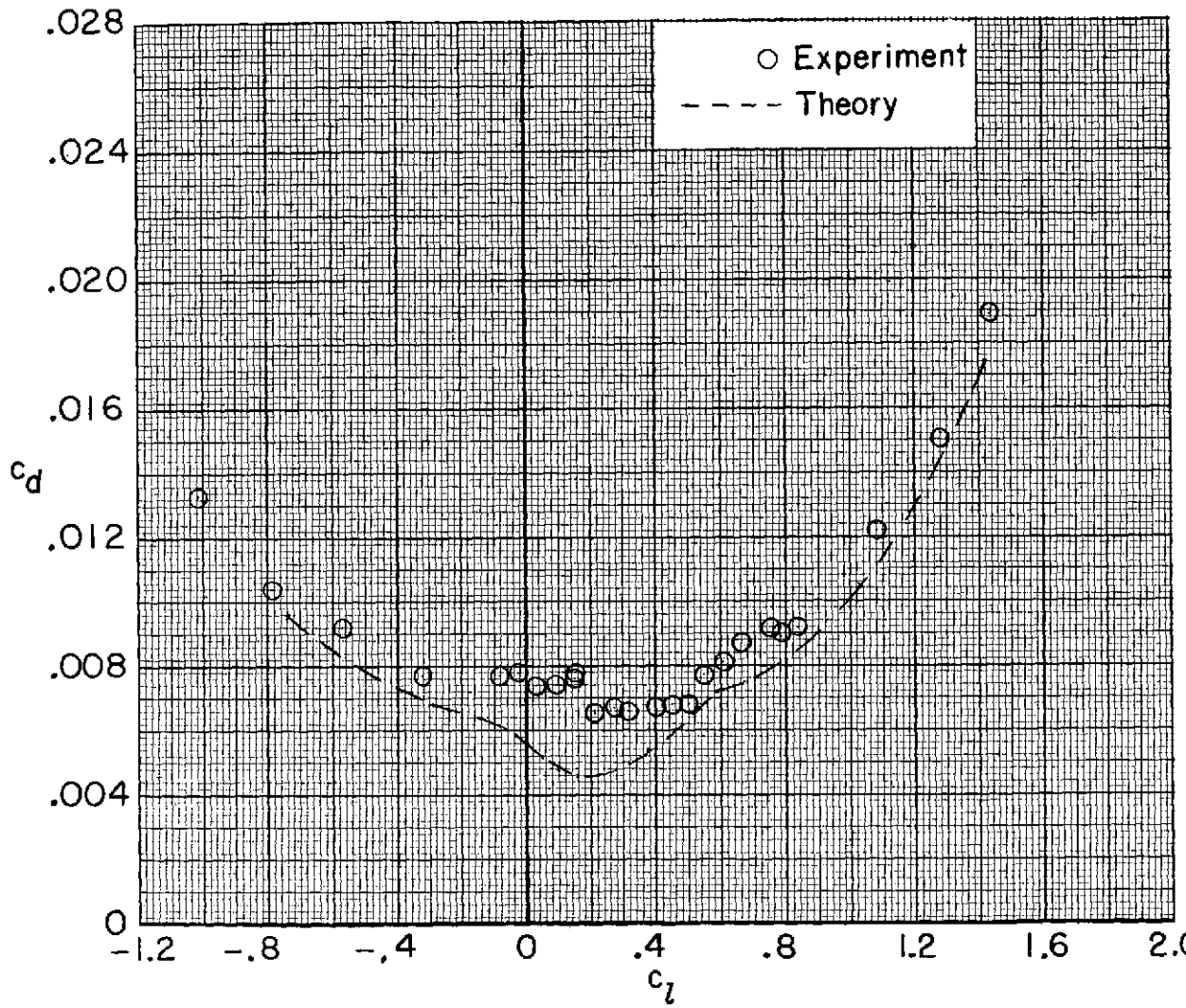

(b) $R = 5.9 \times 10^6$. Concluded.

Figure 15.- Continued.

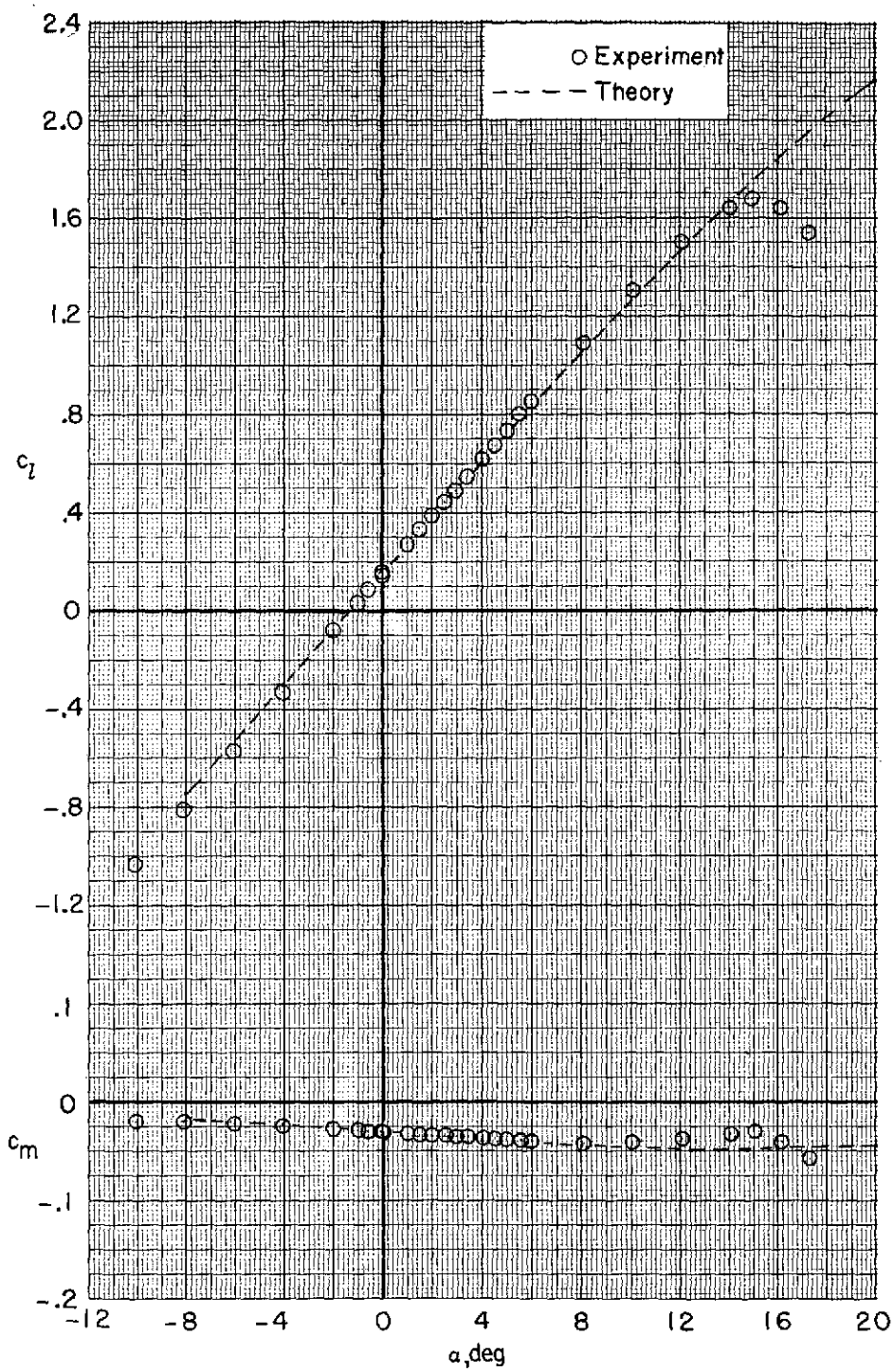

(c) R = 11.8×10^6; model smooth.

Figure 15.- Continued.

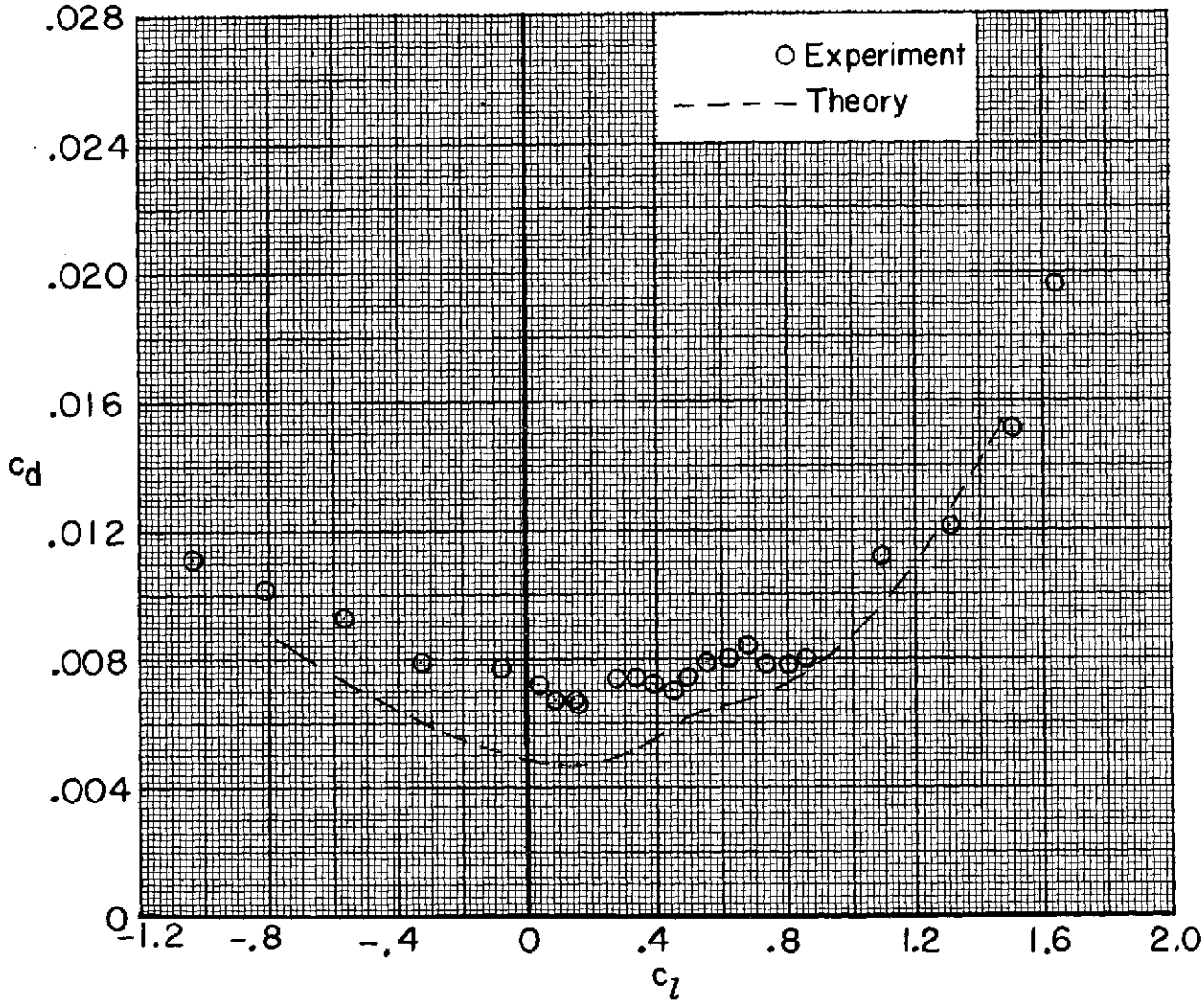

(c) R = 11.8×10^6. Concluded.

Figure 15.- Continued.

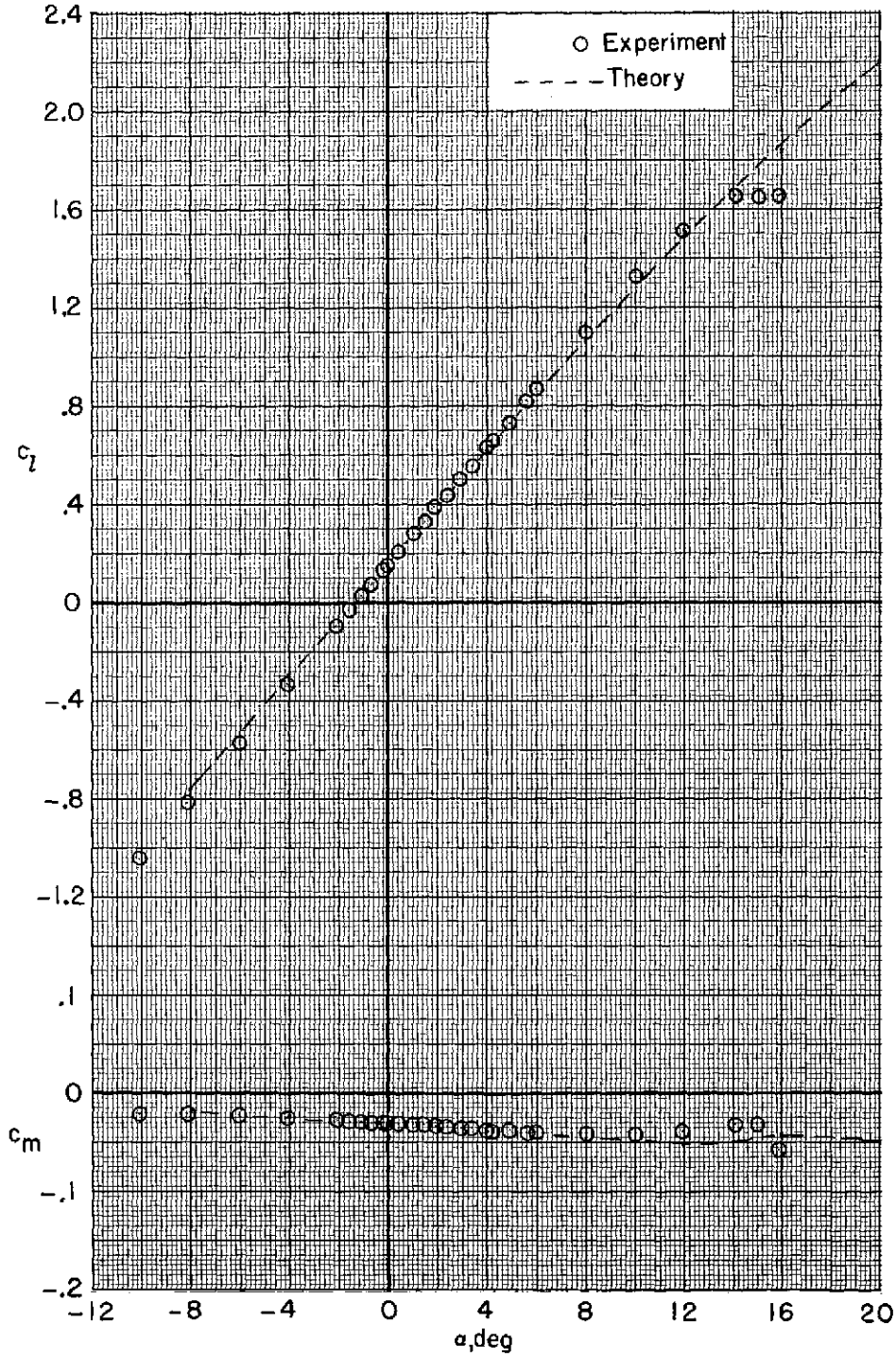

(d) $R = 22.8 \times 10^6$; model smooth.

Figure 15.- Continued.

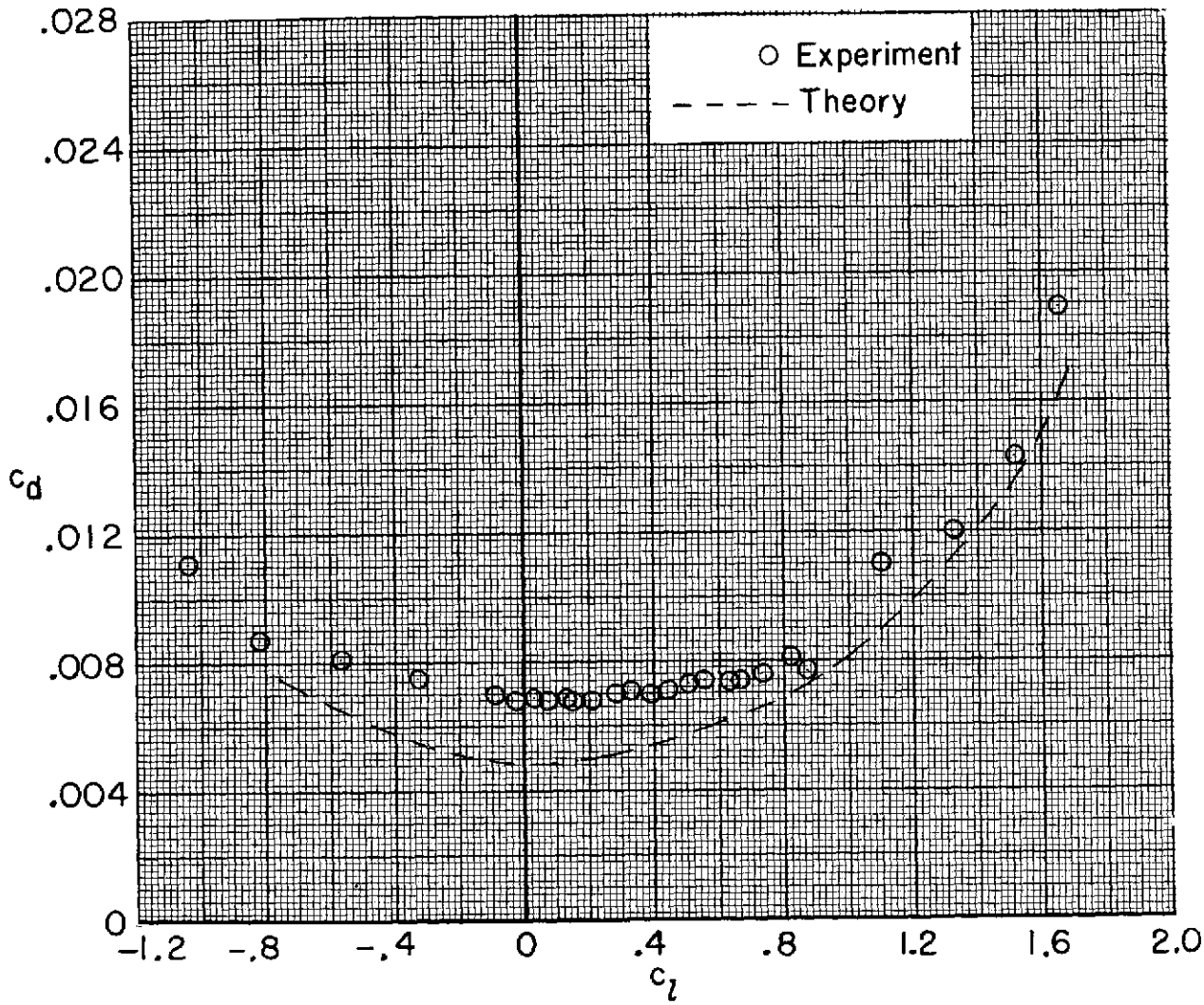

(d) $R = 22.8 \times 10^6$. Concluded.

Figure 15.- Continued.

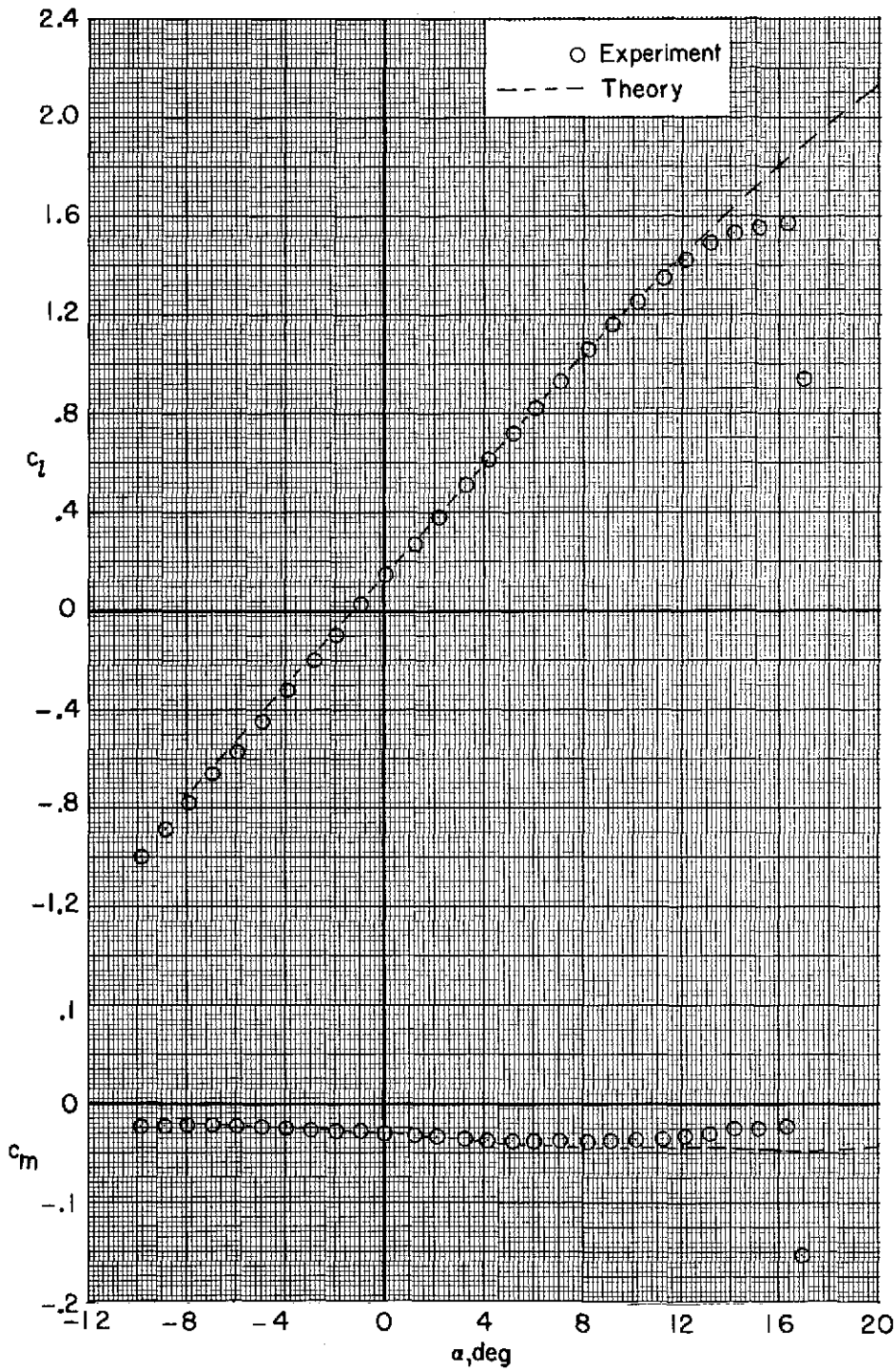

(e) $R = 5.9 \times 10^6$; transition fixed at $x/c = 0.05$.

Figure 15.- Continued.

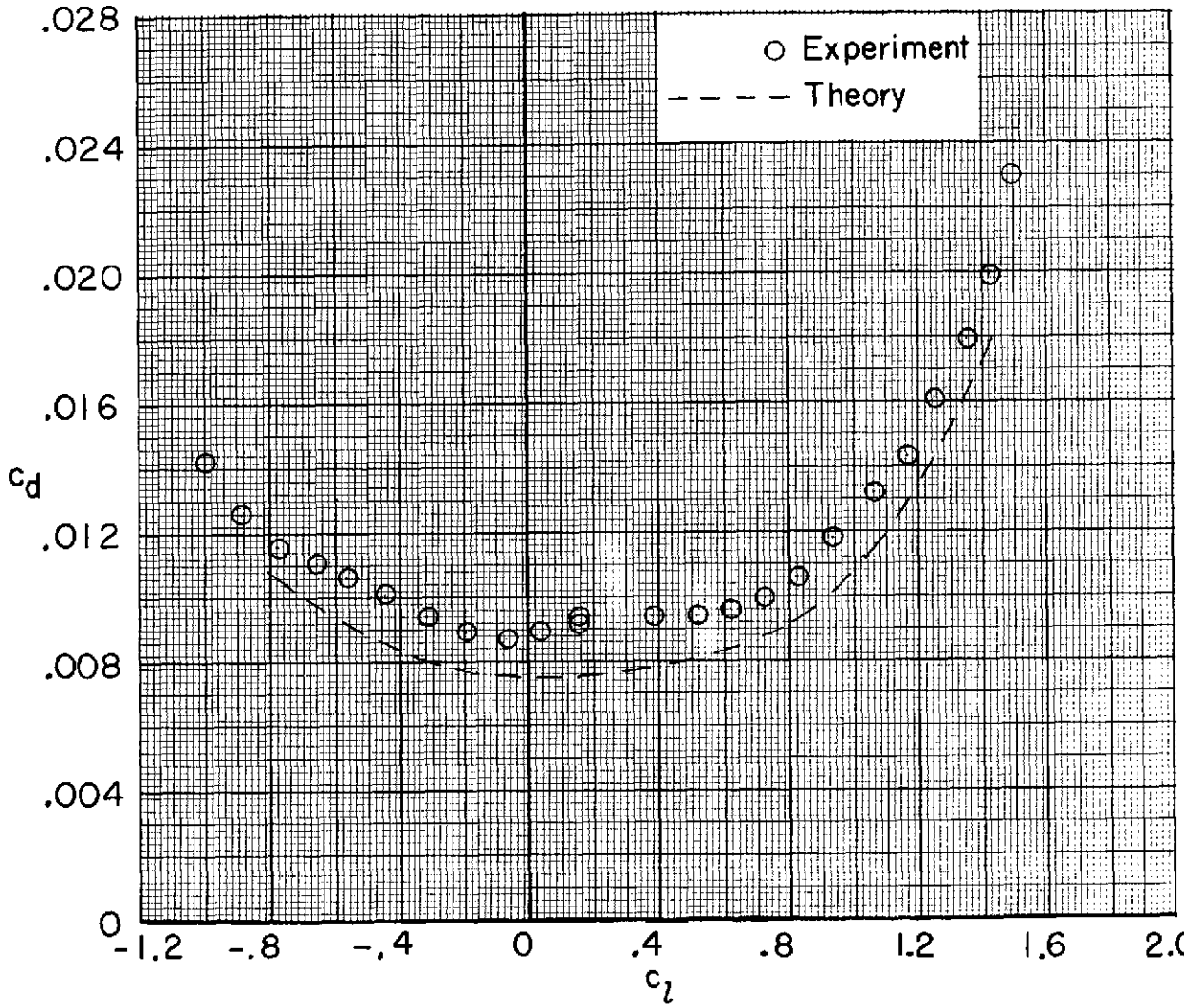

(e) $R = 5.9 \times 10^6$. Concluded.

Figure 15.- Concluded.

L-72-3634

Figure 16.- Calibration probe mounted in wind tunnel.

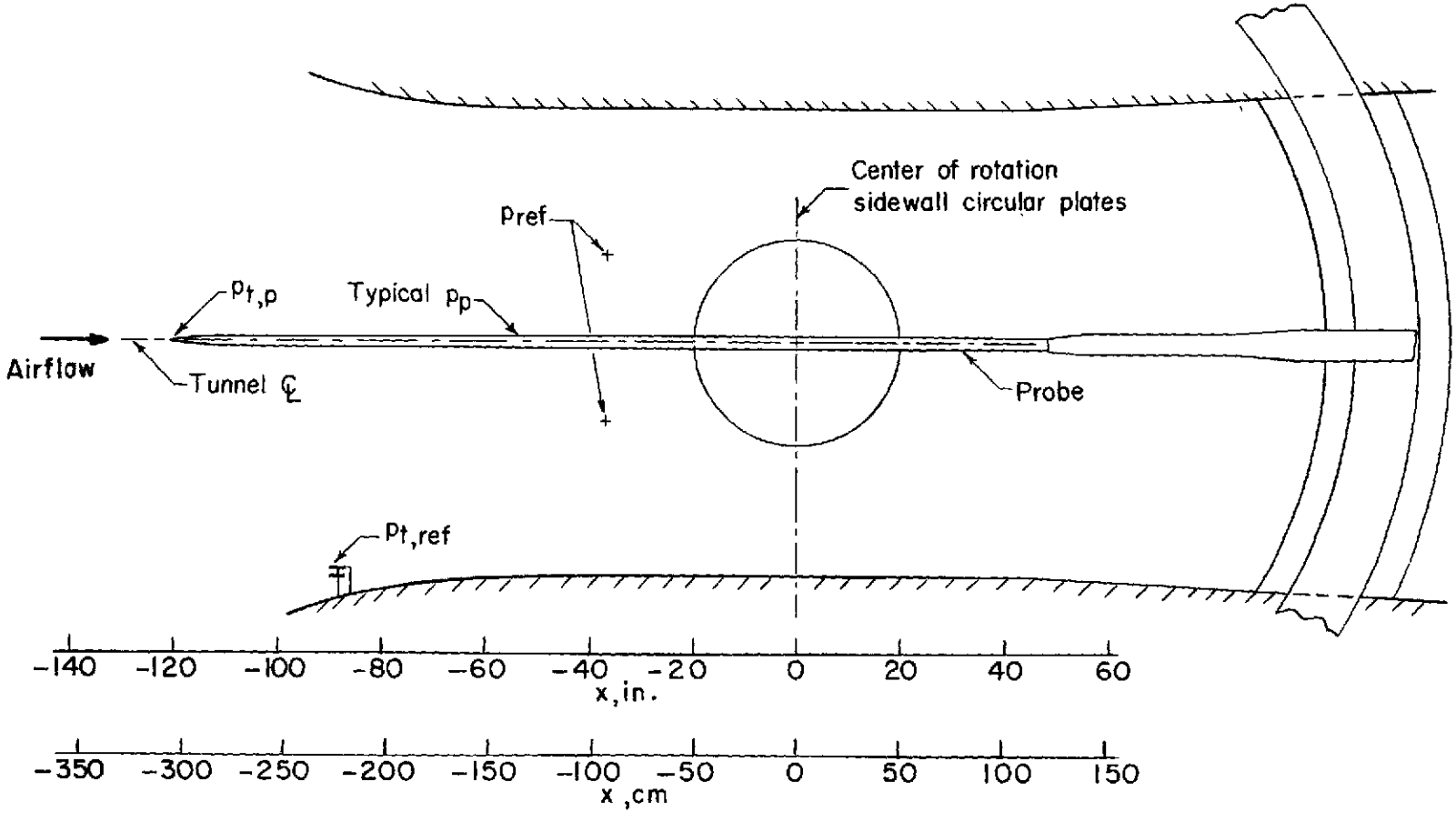

Figure 17.- General calibration arrangement.

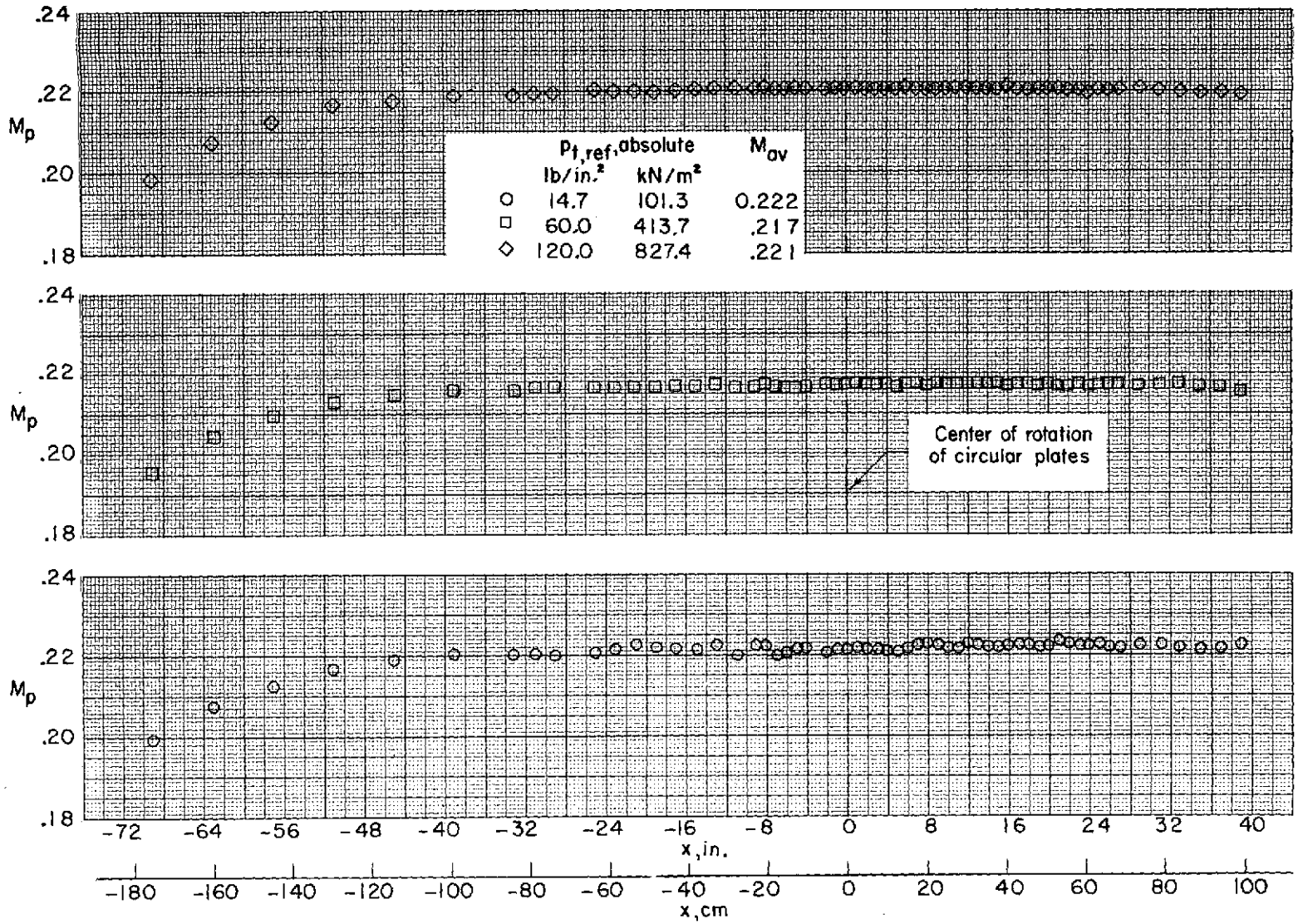

Figure 18.- Typical probe Mach number distribution along longitudinal center line of tunnel.

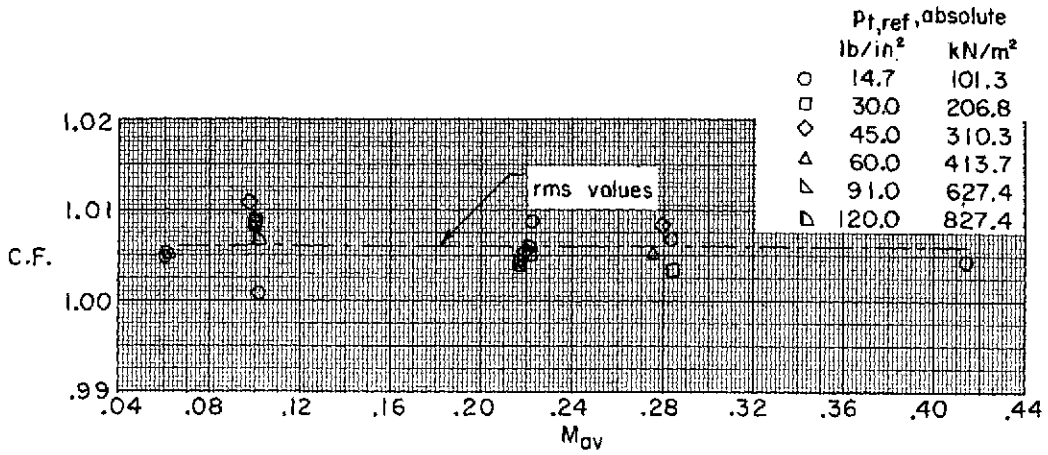

(a) Calibration factor (C.F.) as a function of M_{av}.

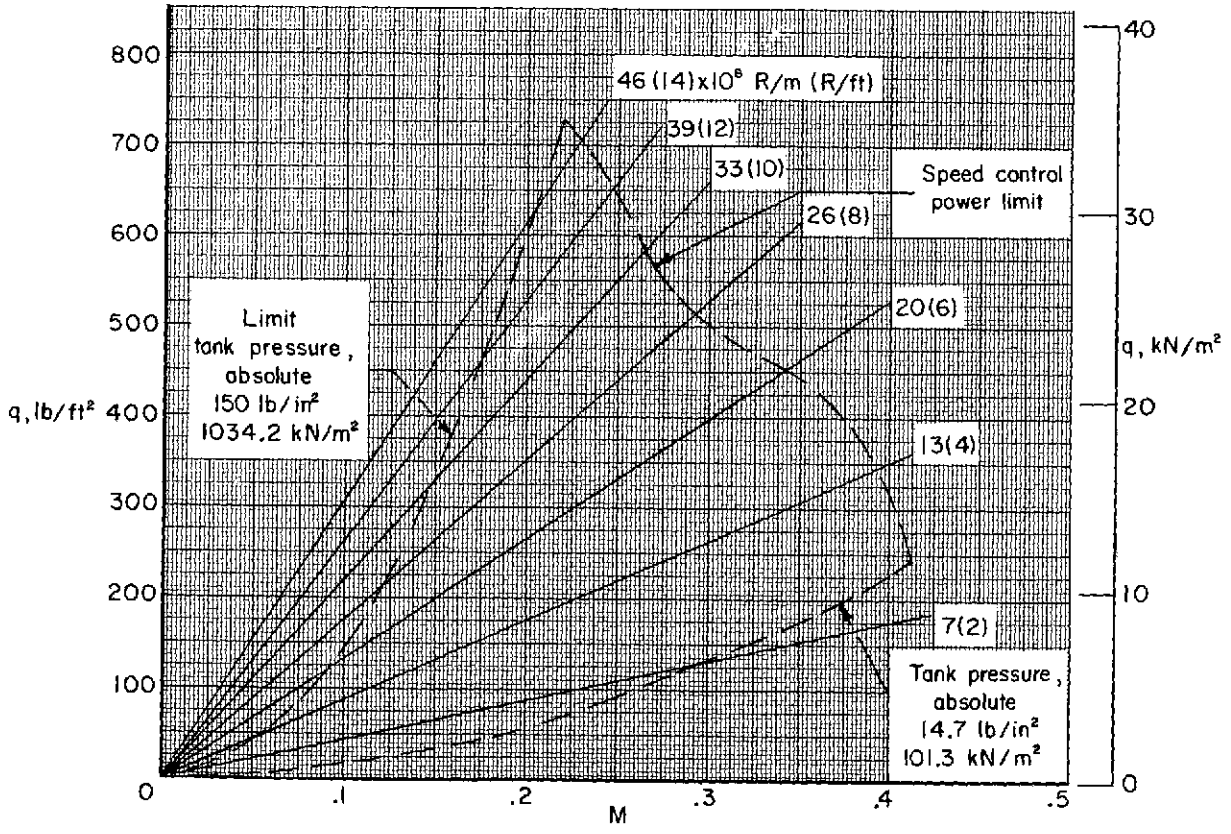

(b) Variation of q with M for constant values of Reynolds number.

Figure 19.- Calibration factor and operational characteristics of Langley low-turbulence pressure tunnel.